IOWA STATE UNIVERSITY
Digital Repository

Retrospective Theses and Dissertations

Iowa State University Capstones, Theses and Dissertations

1974

Combined forced and free laminar convection in horizontal tubes

Samy Morad Morcos
Iowa State University

Follow this and additional works at: https://lib.dr.iastate.edu/rtd

 Part of the Mechanical Engineering Commons

Recommended Citation
Morcos, Samy Morad, "Combined forced and free laminar convection in horizontal tubes " (1974). *Retrospective Theses and Dissertations*. 5996.
https://lib.dr.iastate.edu/rtd/5996

This Dissertation is brought to you for free and open access by the Iowa State University Capstones, Theses and Dissertations at Iowa State University Digital Repository. It has been accepted for inclusion in Retrospective Theses and Dissertations by an authorized administrator of Iowa State University Digital Repository. For more information, please contact digirep@iastate.edu.

www.manaraa.com

INFORMATION TO USERS

This material was produced from a microfilm copy of the original document. While the most advanced technological means to photograph and reproduce this document have been used, the quality is heavily dependent upon the quality of the original submitted.

The following explanation of techniques is provided to help you understand markings or patterns which may appear on this reproduction.

1. The sign or "target" for pages apparently lacking from the document photographed is "Missing Page(s)". If it was possible to obtain the missing page(s) or section, they are spliced into the film along with adjacent pages. This may have necessitated cutting thru an image and duplicating adjacent pages to insure you complete continuity.

2. When an image on the film is obliterated with a large round black mark, it is an indication that the photographer suspected that the copy may have moved during exposure and thus cause a blurred image. You will find a good image of the page in the adjacent frame.

3. When a map, drawing or chart, etc., was part of the material being photographed the photographer followed a definite method in "sectioning" the material. It is customary to begin photoing at the upper left hand corner of a large sheet and to continue photoing from left to right in equal sections with a small overlap. If necessary, sectioning is continued again — beginning below the first row and continuing on until complete.

4. The majority of users indicate that the textual content is of greatest value, however, a somewhat higher quality reproduction could be made from "photographs" if essential to the understanding of the dissertation. Silver prints of "photographs" may be ordered at additional charge by writing the Order Department, giving the catalog number, title, author and specific pages you wish reproduced.

5. PLEASE NOTE: Some pages may have indistinct print. Filmed as received.

Xerox University Microfilms
300 North Zeeb Road
Ann Arbor, Michigan 48106

74-15,436

MORCOS, Samy Morad, 1945-
COMBINED FORCED AND FREE LAMINAR CONVECTION IN HORIZONTAL TUBES.

Iowa State University, Ph.D., 1974
Engineering, mechanical

University Microfilms, A XEROX Company, Ann Arbor, Michigan

THIS DISSERTATION HAS BEEN MICROFILMED EXACTLY AS RECEIVED.

Combined forced and free laminar convection in horizontal tubes

by

Samy Morad Morcos

A Dissertation Submitted to the
Graduate Faculty in Partial Fulfillment of
The Requirements for the Degree of
DOCTOR OF PHILOSOPHY

Major: Mechanical Engineering

Approved:

Signature was redacted for privacy.

In Charge of Major Work

Signature was redacted for privacy.

For the Major Department

Signature was redacted for privacy.

For the Graduate College

Iowa State University
Ames, Iowa

1974

TABLE OF CONTENTS

		Page
	NOMENCLATURE	viii
	ACKNOWLEDGMENTS	xii
I.	INTRODUCTION	1
	A. Laminar Flow Heat Transfer with Forced and Free Convection	1
	B. Literature Survey	4
	1. Heat transfer	4
	a. Analytical studies	5
	b. Experimental studies	10
	2. Pressure drop	13
	C. Scope of Investigation	18
II.	EXPERIMENTAL APPARATUS	20
	A. Test Loop	20
	B. Test Sections	25
	1. Glass tube	25
	2. Metal tube	28
III.	EXPERIMENTAL PROCEDURE	35
	A. General Loop Operation	35
	B. Operating Procedure	36
	1. Heat transfer	36
	2. Pressure drop	38
	C. Data Reduction	39
	1. Heat transfer	39
	2. Pressure drop	40
	D. Circumferential Heat Flux Distribution	41
	1. Glass tube	43
	2. Metal tube	47

		Page
	3. Calculated wall temperature and heat flux distributions	48
IV.	RESULTS AND DISCUSSION	57
	A. Heat Transfer	57
	1. Experimental results	57
	2. Correlation of data	65
	B. Pressure Drop	77
V.	CONCLUSIONS AND RECOMMENDATIONS	85
VI.	APPENDIX A: WORKING FLUID PROPERTIES	88
	A. Distilled Water	88
	1. Density	88
	2. Isobaric thermal expansion coefficient	89
	3. Enthalpy	89
	4. Viscosity	90
	5. Thermal conductivity	91
	6. Prandtl number	91
	B. Ethylene Glycol	92
	1. Density	92
	2. Isobaric thermal expansion coefficient	93
	3. Enthalpy	93
	4. Viscosity	94
	5. Thermal conductivity	95
	6. Prandtl number	95
VII.	APPENDIX B: CALIBRATION OF FLOWMETER	96
	A. Distilled Water	96
	B. Ethylene Glycol	99
VIII.	APPENDIX C: DUMMY LOAD CHARACTERISTICS	101
IX.	APPENDIX D: HEAT LOSS	104
X.	APPENDIX E: CIRCUMFERENTIAL HEAT FLUX DISTRIBUTION	107
	A. Glass Tube	107
	B. Metal Tube	113

		Page
XI.	APPENDIX F: SAMPLE CALCULATIONS	116
	A. Heat Transfer	116
	B. Pressure Drop	123
XII.	APPENDIX G: TABULATION OF EXPERIMENTAL RESULTS	139
XIII.	BIBLIOGRAPHY	148

LIST OF TABLES

Number	Title	Page
1	Inside tube wall temperatures as obtained by one-dimensional and two-dimensional procedures	50
2	Flowmeter calibration data for distilled water	97
3	Flowmeter calibration data for ethylene glycol	99
4	Dimensional and property information for calculations of metal tube heat loss	104
5	Heat transfer results for water with glass tube	139
6	Heat transfer results for water with metal tube	140
7	Heat transfer results for ethylene glycol with glass tube	141
8	Heat transfer results for ethylene glycol with metal tube	142
9	Isothermal pressure drop results for water with glass tube	143
10	Isothermal pressure drop results for ethylene glycol with glass tube	144
11	Isothermal pressure drop results for ethylene glycol with metal tube	145
12	Nonisothermal pressure drop results for ethylene glycol with glass tube	146
13	Nonisothermal pressure drop results for ethylene glycol with metal tube	147

LIST OF FIGURES

Number	Title	Page
1	Comparison of available analytical heat transfer predictions	9
2	Comparison of available experimental heat transfer data	14
3	Comparison of available analytical pressure drop predictions	17
4	Schematic layout of test loop	21
5	Photograph of experimental apparatus	22
6	Electrical connection diagram for glass tube	27
7	Guard shield and wall thermocouple installations	29
8	Power clamp and expansion joint for metal tube	31
9	Combined characteristics of dc generator and dummy load	33
10	Circumferential variation of inside wall temperature, heat flux, and Nusselt number for water with glass tube — Run: 4	51
11	Circumferential variation of inside wall temperature, heat flux, and Nusselt number for water with glass tube — Run: 31	52
12	Circumferential variation of inside wall temperature, heat flux, and Nusselt number for ethylene glycol with metal tube — Run: 4	53
13	Circumferential variation of inside wall temperature, heat flux, and Nusselt number for ethylene glycol with metal tube — Run: 25	54
14	Nusselt number as a function of reduced length for water with glass tube	59
15	Nusselt number as a function of reduced length for ethylene glycol with metal tube	60
16	Fully-developed heat transfer data for water with different tubes	61

Number	Title	Page
17	Fully-developed heat transfer data for ethylene glycol with different tubes	62
18	Comparison of present heat transfer data for water with results from previous investigations	64
19	Viscosity correction factor applied to metal tube with different fluids	67
20	Heat transfer data evaluated at film temperature for glass tube with different fluids	69
21	Heat transfer data evaluated at film temperature for metal tube with different fluids	70
22	Correlation of water and ethylene glycol data including Prandtl number effect for different tubes	71
23	Steady-state energy balance for a tube wall element	72
24	Final correlation of heat transfer data	74
25	Comparison of present heat transfer correlation with data from previous investigations	76
26	Isothermal friction factor for water with glass tube	78
27	Friction factor data for ethylene glycol with glass tube	80
28	Friction factor data for ethylene glycol with metal tube	81
29	Comparison of friction factor data for ethylene glycol with results from previous investigations	83
30	Calibration curve for flowmeter with water	98
31	Calibration curve for flowmeter with ethylene glycol	100
32	Computer printout of a typical heat transfer run	127
33	Computer printout of a typical pressure drop run	138

NOMENCLATURE

Latin symbols

A	cross sectional area
A_0, a_0, B_0, b_0, C_0, c_0, D_0, d_0, etc.	arbitrary constants used in solution of differential equations in Appendix E
c_p	specific heat
d_1	inside tube diameter
d_2	outside tube diameter
e	thermocouple reading
FM	nondimensional Monel float reading, Eq. (B.4)
FMR	flow meter reading
FP	nondimensional Pyrex float reading, Eq. (B.2)
$F(\theta)$	outside tube wall temperature distribution, Eq. (3.3)
f	Darcy friction factor, $2g_c\, d_1\, \Delta p/(L\, \rho\, u^2)$
$f(\theta)$	nondimensional outside tube wall temperature, Eq. (E.23)
Gr	Grashof number, $g\, \beta\, \rho^2\, d_1^3\, (\bar{T}_{w,i} - T_b) / \mu^2$
g	acceleration due to gravity
g_c	gravitational constant in Newton's law
h	circumferential average heat transfer coefficient, $\bar{q}_i'' / (\bar{T}_{w,i} - T_b)$
h_{nc}	natural convection heat transfer coefficient
$h(\theta)$	local heat transfer coeeficient, $q_i''/(T_{w,i} - T_b)$
I	electric current
i	enthalphy
k	fluid thermal conductivity

k_w	tube wall thermal conductivity
L	length along tube axis
L_S	tube length from onset of heating to measuring section
L_T	total heated length of test section
m	harmonic index
$\dot{m}$	mass flow rate
Nu	circumferential average Nusselt number, hd_1/k
Nu (θ)	local Nusselt number, $h(\theta)\, d_1/k$
n	outer normal direction to tube wall; harmonic index
Pr	Prandtl number, $c_p\, \mu/k$
Pw	tube wall parameter, $h\, d_1^2/(k_w\, t)$
Pw^*	modified tube wall parameter, $k\, d_1/(k_w\, t)$
p	static pressure
Δp	pressure drop
q	rate of heat transfer
q_c	reduced outside heat flux, Eq. (3.8)
q'	rate of heat transfer per unit tube length
q'_ℓ	rate of heat loss per unit length
q"	local heat flux
$\bar{q}$"	circumferential average heat flux
q"'	rate of volumetric heat generation
q^*	reduced rate of volumetric heat generation, Eq. (3.17)
R	nondimensional radial distance, r/r_2
R_c	power cable resistence
R_d	dummy load resistence
R_ℓ	total load resistence

R_t	test section resistence
Ra	Rayleigh number, Gr Pr
Re	Reynolds number, $4\dot{m}/(\pi d_1 \mu)$
r	radial distance measured from center of tube
r_1	inside tube radius
r_2	outside tube radius
s	coordinate along tube periphery
s^*	nondimensional coordinate along tube periphery, s/d_1
T	local fluid temperature
T_b	bulk or mixed-mean fluid temperature
T_w	local wall temperature
$\bar{T}_w$	circumferential average wall temperature
ΔT_w	temperature drop across tube wall
T_∞	ambient temperature
t	tube wall thickness
u	mean axial velocity
V_S	voltage across shunt
V_T	voltage across test section
v	specific volume
X	reduced length, $L_S/(d_1 \text{ Re Pr})$
Δx	differential indicating fluid head

Greek symbols

α_j	coefficient of the nondimensional outside tube wall temperature distribution f (θ), Eq. (3.9)

β	isobaric thermal expansion coefficient, $-\frac{1}{\rho}\left(\frac{\partial \rho}{\partial T}\right)_p$
θ	angle measured clockwise from the top of the tube; reduced temperature (Appendix A)
μ	dynamic viscosity
ν	separation constant, Eq. (E.8)
ρ	density
ρ_e	electric resistivity
τ_w	nondimensional local tube wall temperature, Eq. (3.6)
τ^*_w	reduced nondimensional local tube wall temperature, Eq. (E.33)
ϕ	a function of R only, Eq. (E.7)
ψ	a function of θ only, Eq. (E.7)

Subscripts

b	evaluated at bulk fluid temperature
f	evaluated at fluid film temperature, $(\bar{T}_{w,i} + T_b) / 2$
h	across heated section
i	inside; inlet
m	maximum; harmonic
n	harmonic
o	outside; outlet; isothermal
t	total
w	evaluated at tube wall temperature

ACKNOWLEDGMENTS

The author wishes to express his sincere appreciation to Dr. Arthur E. Bergles, his thesis advisor, for his many helpful suggestions and guidance throughout the work. He contributed freely of his time and abilities to direct this study to its successful conclusion.

Thanks are extended to Professor Henry M. Black, Dr. Jerry L. Hall, Dr. Richard H. Pletcher, and Dr. Donald F. Young for their helpful suggestions, which contributed to the final form of the thesis.

The author is grateful for the financial support provided by the Department of Mechanical Engineering and the Engineering Research Institute. Major portions of this work were supported by the National Science Foundation under grant GK-36851.

General thanks are extended to staff and colleagues at the Georgia Institute of Technology for assistance during early stages of doctoral work. Support for the present program by Mr. Leon Girard of the Engineering Research Institute Machine Shop and Mr. Clifford O. Osam of the Mechanical Engineering staff is acknowledged with thanks.

I. INTRODUCTION

A. Laminar Flow Heat Transfer with Forced and Free Convection

Laminar flow heat transfer in tubes is encountered in a wide variety of engineering situations. It is estimated that more than $100 million are involved in laminar flow heat exchangers associated with viscous liquids in general chemical and food industries. In another area, the design of compact heat exchangers, where a consideration of both the heat transfer and pumping power is involved, applications of laminar heat transfer will yield high-performance surfaces, particularly in gas-flow heat exchangers. Similarly, optimization of space base and space shuttle heat rejection and cooling systems usually results in operation in the laminar heat transfer regime due to the size of the flow passage and the nature of coolant fluids. Applications may also be extended to the biomedical fields. In order to reduce the hazards of surgery when transfusions are required, blood is heated before being given to the patient; yet, due to the physical nature of the red cells and the plasma, the blood flow has to be laminar. Finally, in various heat transfer equipment designed primarily for turbulent flow, off-design operation may result in laminar flow conditions. When laminar heat transfer occurs, it usually represents the dominant thermal resistance in a heat exchanger.

In his discussion of the heat transfer activity in the present decade, Sabersky [1] emphasized that even though such heat exchangers have been and are now being used widely, there is a lack of understanding of many details of the laminar flow and heat transfer mechanisms. The

difficulties with laminar flow are associated with the fact that fluids which in practice are in this flow regime often have properties which are highly dependent on temperature. Both Sabersky [1] and Porter [2] see a need to predict the commonly occurring laminar heat transfer conditions with much greater accuracy in the future in order to meet the demands of modern technology. In such demands, two aspects of the heat transfer problem have to be considered:

1. Situations where a heat exchanger is provided mainly to remove or supply heat as a part of the economic and thermodynamic balance of the process.
2. Those cases where the heat exchanger is a crucial aspect of the process; for instance, in a chemical reactor where temperature distributions must be maintained to attain optimum conversion, or in situations where product degradation is possible due to adverse temperature conditions either within the bulk liquid or at contacting surfaces.

In any convective heat transfer process within a gravitational force field, density differences arising from differences in temperature are responsible for natural convection effects. For a pure forced convection flow associated with a large Reynolds number, the natural convection effects may be neglected. If, on the other hand, the buoyant force resulting from density differences is relatively large, as exemplified by a large Grashof number, the effects of forced convection are negligible. However, in most practical situations both forced and free convection modes are present. An indication of the relative magnitude of the two

effects may be obtained from a study of the nondimensional parameters which appear in the governing conservation equations.

In situations where natural convection effects are pronounced, the orientation of the tube axis becomes important, the two limiting alignments being vertical and horizontal. In vertical tubes the velocities produced by buoyant forces are parallel to the direction of the forced motion. Since rotational symmetry is retained, it is straightforward to solve the equations of motion and energy analytically with both free and forced convection, as was done by Hallman [3] for upward and downward flow. However, in the case of horizontal tubes, the buoyant and inertia forces are perpendicular to each other, which results in the loss of rotational symmetry. The fluid motion is, therefore, much more difficult to analyze. As the tube is heated, the fluid near the wall is warmer and, therefore, lighter than the bulk fluid at the core. As a consequence, two upward currents flow along the side walls, and, by continuity, the heavier fluid near the center of the tube flows downward. This sets up two vortices which are symmetrical about a vertical meridional plane. The superposition of the forced flow and these two natural convection vortices results in the formation of two symmetrical spiraling motions. As a result of the combined forced and free convection flow, the heat transfer coefficient and the friction factor are well above the constant property predictions.

Two idealized boundary conditions are generally considered for laminar heat transfer associated with a circular tube: uniform wall temperature and uniform wall heat flux. With uniform wall heat flux, a wall-minus-fluid temperature difference exists throughout the tube and,

therefore, the secondary motion continues along the tube axis. For a sufficiently long tube, a fully-developed condition is reached in which the change of the heat transfer coefficients is primarily due to variation in the fluid bulk temperature levels. This is quite different from the uniform wall temperature boundary condition, in which case the secondary motion develops to a maximum intensity and then diminishes to zero as the temperature difference decreases.

For pure forced convection, both the fully-developed and the thermally developing analyses are given by the classical Graetz analysis [4] for uniform wall temperature and by the analysis of Siegel et al. [5], for example, for uniform wall heat flux. It is observed, however, that experimental data exhibit substantial deviations (up to a factor of ten) from the above analytical predictions, which is in large part due to the inadequacy of the the constant property assumptions. Accordingly, recent analytical and experimental work has been directed toward accounting for the large discrepancies between experimental data the analytical predictions, by considering the effect of combined forced and free convection.

B. Literature Survey

1. Heat transfer

The problem of combined forced and free laminar convection in tubes under various boundary conditions and different geometrical orientations has been the subject of numerous investigations. Since the present work is concerned with the problem of combined forced and free laminar convection in horizontal tubes with uniform wall heat flux, the review of the

current state of knowledge will be restricted to this situation.

a. Analytical studies Several attempts have been made to determine the effect of secondary motion on a fully-developed laminar flow analytically, using series solutions. Morton [6] was the first to develop such a procedure and used Nu Gr/4 as a perturbation parameter. He assumed a constant axial pressure gradient and determined the coefficients of expansion to second-order perturbations. Iqbal and Stachiewicz [7] and Iqbal [8] obtained solutions for velocity and temperature distributions in terms of power series of Ra Nu/(4 Re Pr), where the axial pressure gradient was assumed to be constant. Faris and Viskanta [9] solved the governing equations using $Gr/(4\ Re^2)$ as a perturbation parameter. They also considered the axial pressure gradient to be constant, and pointed out that this is a valid assumption except for very low Reynolds numbers ($Re \ll 25$). Both Iqbal and Stachiewicz and Faris and Viskanta indicated that Nu depends on Re, which is contrary to what is expected for a fully-developed laminar flow.

In all of these perturbation analyses, the tube wall temperature was assumed to be constant around the periphery. Under this assumption, wall temperature varies linearly downstream as a consequence of the uniform wall heat flux and constant heat transfer coefficient. A common feature of all these perturbation techniques is that the solutions are applicable only for small Rayleigh numbers, and give extremely high estimates of the heat transfer coefficients for practical values of $Ra > 3 \times 10^3$.

The boundary layer analysis is another practical analytical approach to the problem. For large Rayleigh numbers, the flow in the tube can be

divided into two portions: a flow in a thin layer near the tube wall, and a flow outside this boundary layer, called the core. Separate consideration of the thin layer and the core allows the use of two sets of conservation equations which are easier to deal with than the set of conservation equations for the entire flow region. In the thin layer, where strong velocity and temperature gradients exist, boundary layer approximations can be used. For the core flow, velocity and temperature fields are mainly affected by the secondary flow, and the viscosity and thermal conductivity may be disregarded. The main difficulty with this approach is that the velocity and temperature at the outer edge of the boundary layer are not given a priori but are dependent on the flow and temperature fields in the boundary layer itself.

Mikesell [10] attempted a boundary layer solution and found that $Nu = K_1\ Ra^{0.25}$, where K_1 is a pure number of order unity when Pr is quite large and $(Nu\ Gr/Pr\ Re^2)\ (Pr/Gr)^{0.25}$ is small. A more recent and complete boundary layer solution developed by Siegwarth et al. [11] agreed well with limited ethylene glycol data for large Rayleigh numbers. Siegwarth et al. pointed out that the effect of the temperature field on the flow depends strongly on the value of the Prandtl number; for Pr = 1 the secondary motion produces a boundary layer behavior in the primary flow similar to that for the temperature field, while for $Pr \to \infty$ the secondary flow has no effect on the primary flow. They also presented an approximate solution for the case of large Prandtl numbers with a negligible axial density gradient, which led to the following result:

$$Nu = 0.56\ Ra^{0.25} \tag{1.1}$$

The integral boundary layer solution of Mori and Futagami [12], which is restricted to a Prandtl number of about unity, is in comparatively good agreement with their data for air. They obtained the following expressions for the Nusselt number as a function of the Prandtl and Rayleigh numbers:

$$Nu = 0.503\ Ra^{0.25}, \quad \text{for} \quad Pr = 0.72 \tag{1.2}$$

$$Nu = 0.57\ Ra^{0.25}, \quad \text{for} \quad Pr = 1 \tag{1.3}$$

It is interesting to note that the correlation curve obtained by Siegwarth et al. [11] for $Pr \to \infty$ predicts nearly the same results as those obtained by Mori and Futagami for $Pr = 1$.

In order to bridge the gap between perturbation analyses and boundary layer solutions, Hwang and Cheng [13] and Cheng et al. [14] developed a boundary vorticity method for analyzing secondary flow problems. Their method determines the vorticity function at the boundary numerically and has the advantage that two second-order partial differential equations are solved instead of a single fourth-order biharmonic equation. Their numerical solution, presented as Nu versus Ra, reveals that Nu for a Pr of about unity approaches the asymptotic solution for the case of $Pr \to \infty$. In other words, a simple correlation for Nu as a function of Ra exists for a wide range of Prandtl numbers. This agrees with the results Siegwarth et al. [11] presented for $Pr \to \infty$ and with the analysis of Mori and Futagami [12] for $Pr = 1$. However, the curve obtained by Mori and Futagami [12] for the case of $Pr = 0.72$ contradicts the boundary vorticity numerical solution, even though it agrees quite well with the limited

available data for air.

Using finite-difference techniques, Newell and Bergles [15] obtained solutions for two limiting wall boundary conditions: zero wall thermal conductivity "ZC," which results in a uniform circumferential heat flux, and infinite wall thermal condictivity "IC," which results in a uniform temperature around the tube circumference. In their analysis, a water density formulation was utilized; it is expected, therefore, that the results are most applicable for water. The convergence rate of the iterative technique was slow, and long computing times were required.

Siegwarth and Hanratty [16] used finite-difference techniques to solve the time-dependent partial differential equations which represent the vorticity, the stream function, and the temperature. They obtained the secondary flow patterns and the temperature and axial velocity fields, but did not develop a predictive equation for the Nusselt number.

A composite plot of the available analytical results for circular tubes with uniform heat flux is presented in Fig. 1. All the upper curves represent solutions for the case of uniform circumferential wall temperature and can be considered upper-bound solutions. Taken as a group, the perturbation, boundary vorticity, and boundary layer models describe a pieced-together curve which is in fair agreement with the complete finite-difference solution of Newell and Bergles [15] for low, medium, and high Rayleigh numbers, respectively. However, the finite-difference technique appears to be the only approach that gives an accurate prediction of the heat transfer coefficient over the full range of Rayleigh numbers. The only limitations of the finite-difference methods are the large computer

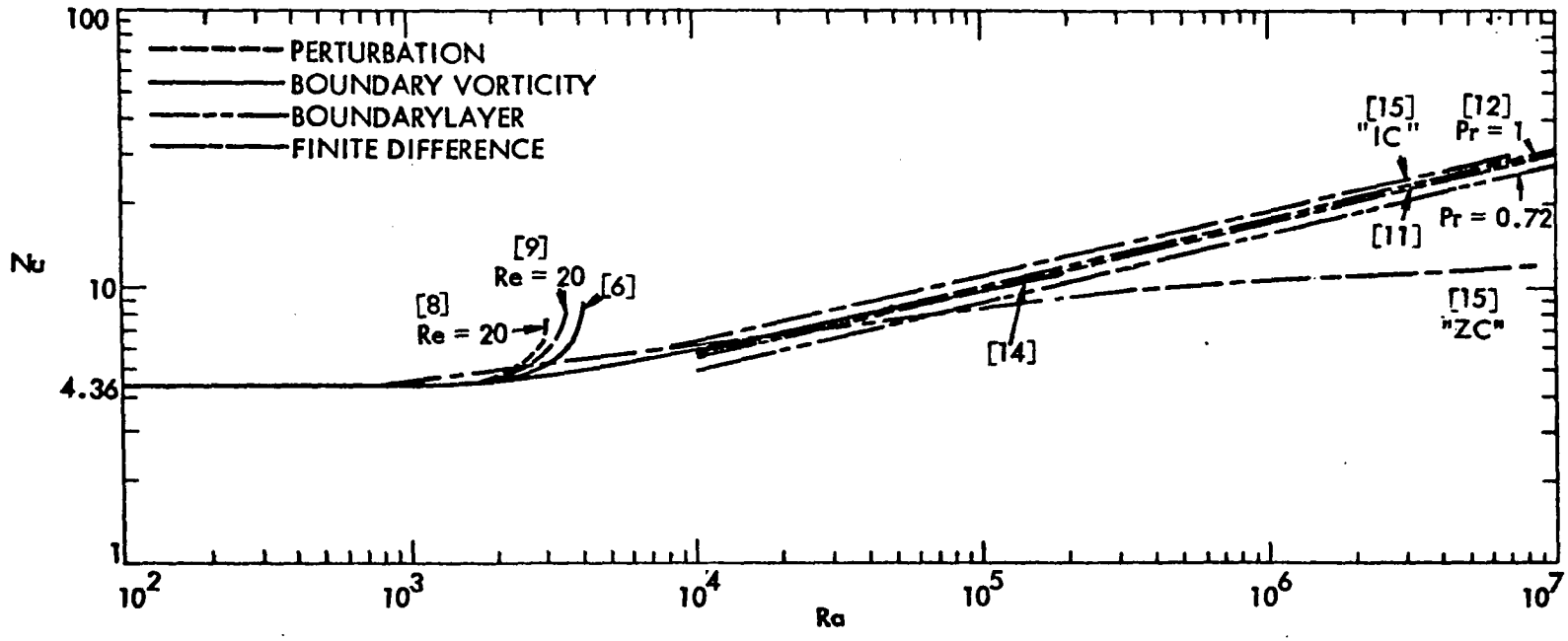

Fig. 1. Comparison of available analytical heat transfer predictions

storage and long running times required. The lower curve of Newell and Bergles [15] shown in Fig. 1 represents the only available solution for the case of zero wall thermal conductivity "ZC" which is much lower than the upper-bound solutions. For the real case of a nonzero finite wall thermal conductivity, in which neither the heat flux nor the wall temperature will be uniform circumferentially, the actual data are expected to lie within the bounds delineated by uniform circumferential wall temperature and zero wall thermal conductivity solutions. Since the tube wall is coupled with the fluid for this real case, an analytical solution is virtually impossible.

b. Experimental studies Experimental data are rather abundant for various fluids. Ede [17] was among the first to put on record experimental work showing the natural convection effects for horizontal tubes. Water was used with electrically-heated aluminum-brass pipes with inside diameters ranging from 0.5-2.0 in. and wall thicknesses up to 0.279 in. Ede's results exhibit large scatter and are approximately represented by the equation

$$Nu = 4.36\ (1 + 0.06\ Gr^{0.3}) \qquad (1.4)$$

McComas and Eckert [18] investigated the effect of free convection on laminar flow of air in an electrically heated 1/2-in. i.d. Nichrome V tube with a 0.007-in. wall thickness. They reported that Nu increased as the ratio of Gr to Re increased, but they did not establish any correlation equation.

Mori et al. [19] measured velocity and temperature distributions for laminar air flow with large Rayleigh numbers using a 1.4-in. i.d. brass

tube with a 0.047-in. wall thickness. Heat was applied by means of nicrome wires wound around the tube at a constant pitch. The Nusselt number was calculated from the temperature distribution, and the correlation for experimental data for Pr = 0.72 is given by

$$Nu = 0.61 \left[1.8 + \left(\frac{Gr\ Nu}{4} \right)^{0.2} \right] \tag{1.5}$$

Petukhov and Polyakov [20, 21] and Petukhov et al. [22] conducted a comprehensive investigation of local heat transfer for the laminar flow of water. A stainless steel tube with a 0.743-in. i.d. and a 0.014-in. wall thickness was electrically heated. Numerous thermocouples were attached to the tube wall at various locations along the heated section and along the perimeter. A considerable variation in the circumferential wall temperature was reported. The data seem to be in good agreement with those of Mori et al. [19] for air. Their correlation of the experimental data for the Nusselt number is given by the interpolation equation

$$\frac{Nu}{Nu_o} = \left[1 + \left(\frac{Ra}{Ra_o} \right)^4 \right]^{0.045} \tag{1.6}$$

where Ra_o was determined from the condition that Nu does not differ by more than 5 percent from Nu_o.

Shannon and Depew [23, 24] studied experimentally the influence of free convection on forced laminar flow of water and ethylene glycol in an electrically heated stainless steel tube with a 0.305-in. i.d. and a 0.035-in. wall thickness. They presented their results in the form

$Nu - Nu_o$ versus $Ra^{0.25}/Nu_o$ and indicated that natural convection is unimportant for $Ra^{0.25}/Nu_o < 2$. The data for water deviate considerably from those for ethylene glycol, with sizeable scatter for both. Surprisingly enough, the boundary layer analysis of Mori and Futagami [12] for $Pr \cong 1$ seems to be closer to the data for glycol than those for water; the authors claim that water has some unusual behavior which causes it to deviate.

The experimental data presented by Siegwarth et al. [11] seems to be in good agreement with their boundary layer approximation for large Prandtl numbers. Their test section was an electrically heated, 2.5-in. i.d. aluminum pipe with a 1-in. wall thickness. The results lend support both to the work of Mori and Futagami [12] regarding the boundary layer behavior of the flow close to the wall for large Rayleigh numbers, and to the work by Siegwarth et al. [11] regarding the small effect of the secondary flow on axial velocity distribution for large Prandtl numbers.

Recently, Hussain and McComas [25] presented experimental data for air flowing in a 1-in. i.d. Nichrome V tube with a 0.014-in. wall thickness. Significant peripheral temperature variations (as much as 13 ^{o}F) occurred at large Rayleigh numbers. The data showed an unusual dependence on the Reynolds number; for $Re < 1200$, the Nusselt number far from the entrance was below the pure forced flow prediction while for large Re, Nu was generally higher than for the pure forced flow.

Lichtarowicz [26] examined the effect of free convection on the fully developed laminar flow of air in a 1/2-in. i.d. stainless steel tube with a 0.06-in. thickness. The data were taken at very low heat fluxes with Rayleigh numbers between 3×10^2 and 10^3. His experimental data, though

misplotted, were much lower than those of McComas and Eckert [18] but showed a good agreement with Morton's analysis [6].

Bergles and Simonds [27] reported the only available experimental data for an electrically heated glass tube used in an attempt to corroborate the "ZC" lower-bound analytical soltuion for fully developed secondary flow. Water was used in a 0.433-in. i.d. Pyrex E-C tube with a 0.053-in. thick wall which supported a large circumferential temperature gradient. The data showed a considerable scatter and evident deviation from the "ZC" boundary condition solution of Newell and Bergles [15].

A composite plot of available experimental data is presented in Fig. 2. The substantial disagreement among various investigators of a given fluid, as well as among investigators of each of the three different fluids, is quite clear.

The foregoing analytical and experimental studies point out the need for more advances in the state-of-the-art of this important case of fully-developed laminar flow in horizontal tubes with uniform wall heat flux. The extensive analytical studies have led only to bounding solutions, while the experimental results are widely scattered within the range of these solutions. A better understanding of this basic heat transfer process would not only lead to more accurate design specifications, but would also indicate how improved performance could be achieved.

2. Pressure drop

It was reported, in the few analytical investigations available, that the friction factor for a fully-developed laminar flow in a horizontal tube increases with the increasing intensity of the secondary flow. Morton [6] was the first to report an expression for the friction factor

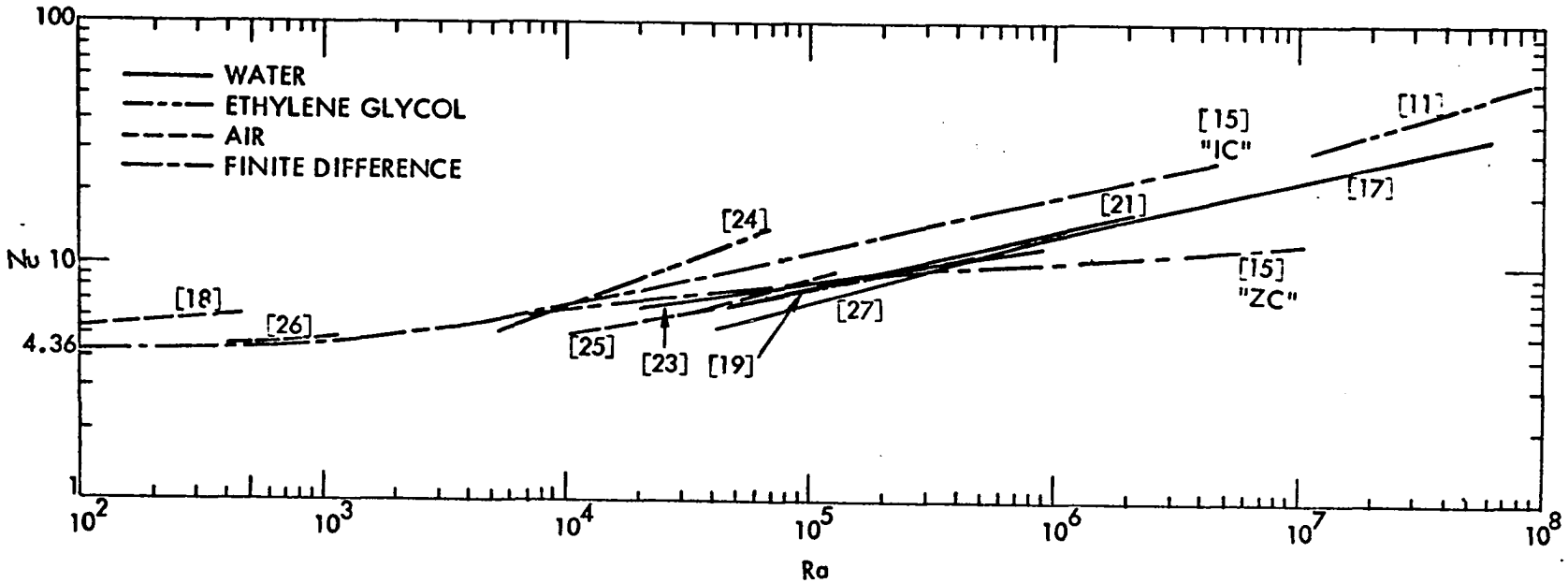

Fig. 2. Comparison of available experimental heat transfer data

in terms of the perturbation parameter Gr Nu/4. Del Casal and Gill [28] extended Morton's analysis to account for axial pressure gradient variations. Using a slightly different perturbation parameter, $Gr\ Nu/(2\ Pr\ Re^2)$, they developed a friction factor equation which was similar to Morton's but included an additional interaction term. They showed their new interaction term to be significant for values of $Pr\ Re^2 < 100$. However, their values of f/f_o, contrary to Morton's results, depend on Re. Iqbal and Stachiewicz [29], assuming density to vary linearly with temperature, utilized perturbation techniques to obtain an expression for the friction factor.

In their boundary layer approximation, Mori and Futagami [12] developed an expression for the friction factor which is expected to be valid at high Rayleigh numbers and for Prandtl numbers of about unity. They showed that as the Prandtl number increased the friction factor decreased as a result of the velocity boundary layer thickness increase.

Using the boundary vorticity method, Hwang and Cheng [13] presented their numerical solution as a plot of $(fRe)/(fRe)_o$ versus Nu Gr/4 for various values of Pr. The effect of the Prandtl number was similar to that predicted by Mori and Futagami [12].

Newell and Bergles [15], with their finite difference techniques, obtained the friction factor for the "ZC" and "IC" boundary conditions. They accounted for Prandtl number variations by correlating their results as $(f - f_o)/f_o$ versus $[\ (Nu - Nu_o)/Nu_o]/\exp\ (Pr/7)$.

The only experimental results available appear to be those of Hussain and McComas [25] for air. Their results were approximately 40 percent

higher than the isothermal results over a Reynolds number range from 600 to 3000. No correlation of the experimental results was given.

A comparison of the available analytical predictions of the friction factor is presented in Fig. 3. The disagreement between the different investigators is, once more, quite clear. The perturbation solutions are adequate only for very small rates of heating and give unrealistically high estimates of the friction factor for Rayleigh numbers greater than 10^3. Figure 3 also serves to show the range of applicability of the boundary vorticity method and the boundary layer approximation in terms of Ra. For the range of Ra between 10^4 and 10^5, a sizeable discrepancy exists between the two predictions. However, it appears that at higher values of Ra the two predictions approach each other. As for the predictions of Newell and Bergles [15], there is still a large difference between the "IC" and "ZC" boundary conditions, and it would be expected that actual data would lie between these two limiting solutions. However, their prediction for the "IC" boundary condition seems to agree with the general trend of the results presented by Mori and Futagami [12] for $Ra > 10^5$, while the prediction for the "ZC" boundary condition is in fair agreement with the boundary vorticity solution [13] for $Ra < 10^5$.

The fact that there are no dependable experimental data on the effect of combined forced and free convection on pressure drop makes it hard to judge the validity of the foregoing analytical predictions. This is partly understandable, since accurate measurements of the extremely low pressure drop variations are quite difficult.

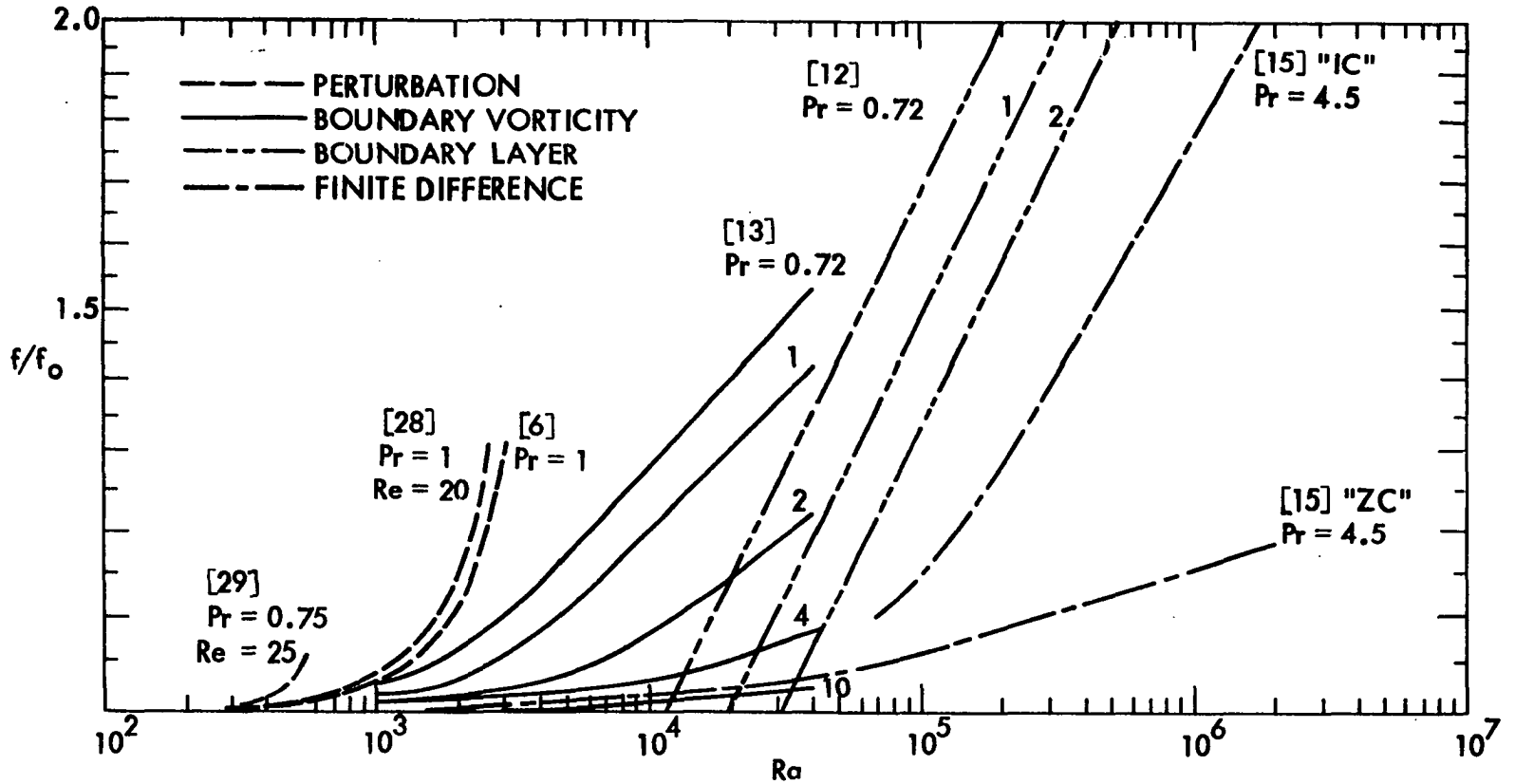

Fig. 3. Comparison of available analytical pressure drop predictions

C. Scope of Investigation

The present study was initiated in order to obtain an accurate prediction of the heat transfer coefficient and the pressure drop for combined forced and free laminar convection in horizontal circular tubes. This orientation is involved in the majority of practical applications. The experiments were concerned with a uniform wall heat flux which is approximated in many engineering situations, for example, electric resistance heating, nuclear heating, gas turbine regenerators, and counterflow heat exchangers with equal thermal capacity rates.

The flow was hydrodynamically fully developed at the onset of heating. As indicated by the work of Petukhov and Polyakov [21] and Bergles and Simonds [27], the developing length for the combined forced and free convection flow is much shorter than that required in the absence of free convection effects. For instance, with a moderate heating rate corresponding to $Ra = 5 \times 10^5$, the developing length for pure forced flow is more than 60 times longer than that required in the presence of the secondary flow. Moreover, increasing Rayleigh number values result in a decrease in the thermal entrance length. Major attention in the present work was, therefore, focused on a study of the fully developed case.

The literature review reveals that accurate predictions of the heat transfer coefficient for the case of fully developed laminar flow in horizontal tubes with uniform heat flux are not yet available. Moreover, Sabersky [1] pointed out that pertinent heat exchanger design information is often not easily available to the designer or is not in a form which would make it easy to apply. It seems that further analysis at the

present time has the serious limitation of the necessity for very large expenditures of computer time in order to account for variation of transport properties and for the coupling between the fluid and the tube wall. Therefore, the goal of this study is to seek a primarily experimental solution to the problem using the existing analytical solutions for guidance. The experimental work is directed toward a better understanding of the different variables and dimensionless groups which affect the heat transfer coefficient so that a more accurate prediction can be achieved for different fluids and tube materials. This is particularly important not only for more precise heat exchanger design but also for a better evaluation of augmentative techniques for laminar heat transfer where the increase in the heat transfer coefficient is of the same order of magnitude as the scatter in the existing correlations for normal conditions.

II. EXPERIMENTAL APPARATUS

A. Test Loop

The test facility used in this investigation was designed and constructed specifically for this program in the ISU Heat Transfer Laboratory. The facility was designed to allow maximum flexibility in testing different fluids and test sections.

A schematic layout of the test loop is shown in Fig. 4; Fig. 5 shows a view of the experimental apparatus. It is a closed loop, low pressure system with all piping made of 1/2-in. nominal copper tube, type L-Hard. The working fluid was circulated with an Oberdorfer Model 1GCC centrifugal pump driven by a 1/6 hp, 3450 rpm motor. A one gallon Greer accumulator, charged with nitrogen to an initial pressure of 15 psig, was installed at the pump outlet to dampen any pressure fluctuations. The small, high speed pump and the accumulator ensured a flow with a low turbulence level. After passing the accumulator, the flow splits into a test-section line and a bypass line for flow control.

In the test-section line, fluid passed through a filter, a flowmeter, and a preheater; it then flowed through the test section and merged with the fluid from the bypass line. After passing through a heat exchanger, the fluid returned to the pump. The flowmeter used was Model 1307, Size 7 Brooks rotameter with two spherical floats. A Pyrex float that could measure a maximum of 0.17 gpm of water and a Monel float with a maximum flow of 0.39 gpm of water were both calibrated for water and ethylene glycol (Appendix B). The preheater included a Chromalox type MT-115A

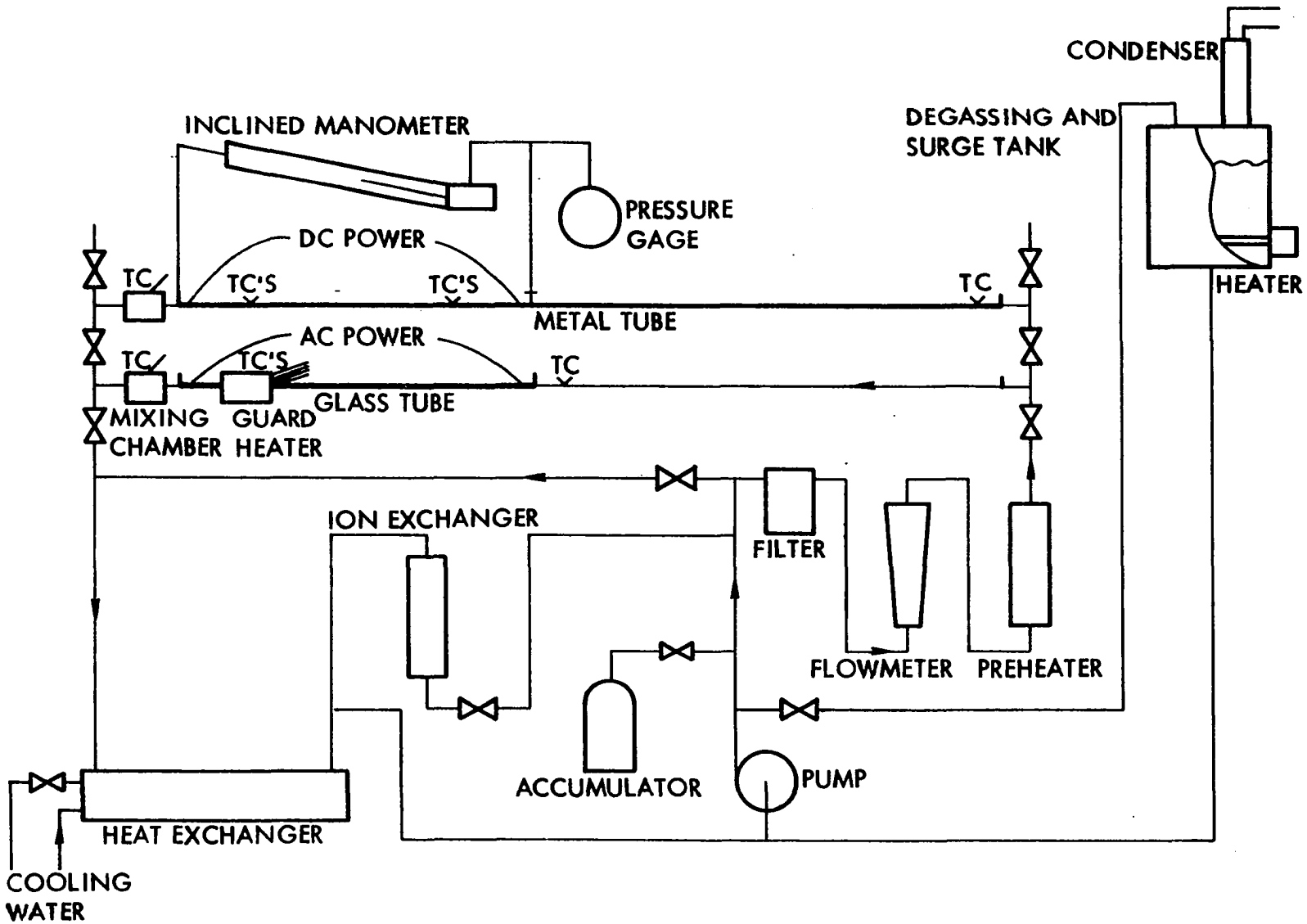

Fig. 4. Schematic layout of test loop

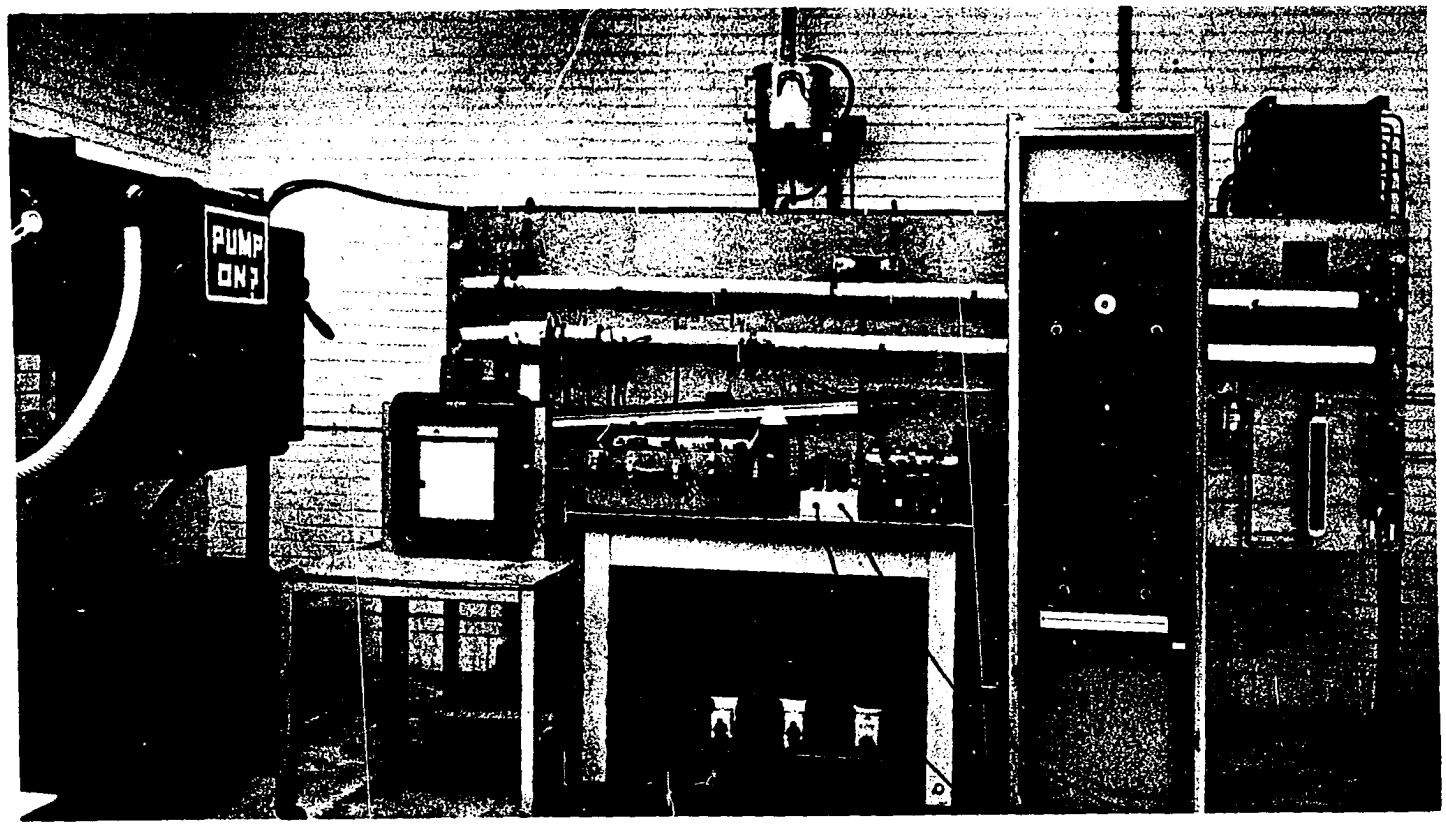

Fig. 5. Photograph of experimental apparatus

immersion heater whose power could be varied from 0 to 1.5 kw by means of a variac.

The test facility included two horizontal test sections, with a provision for adding additional sections. The first test section was an electrically-conductive glass tube; the second was a thin-wall stainless steel tube. The specifications for these test sections will be presented later. Two Jamesbury ball valves, one placed upstream and one downstream of the test section, were used to roughly adjust the flow rate and control the pressure level in the heated section. The flow rate was more precisely controlled by a Whitey Model 1RM4 needle valve, installed upstream of the test section. Additional ball valves were installed in the test section line to permit independent testing of each tube. An inlet section of about 6.5 ft was used to develop the flow hydrodynamically before it entered the heated section. A mixing chamber was placed at the test section outlet in an attempt to get an accurate indication of the outlet temperature. The ends of the test section were electrically insulated from the rest of the loop by means of short pieces of Buna N pressure hose.

The heat exchanger used was a four-pass, Model 302-05, American Standard BCF exchanger in which the working fluid flowed in the outer annulus and the cooling water flowed in the inner tubes. Due to seasonal temperature variations, the minimum fluid inlet temperature to the test section was 50 ^{o}F in winter and 70 ^{o}F in summer.

In order to minimize the dissolved gas in the system, a 5 gallon stainless steel degassing tank, which also served as a surge tank, was

provided. A 3 kw Chromalox immersion heater, type MT-230A, was installed at the bottom of the tank to systematically raise the loop fluid temperature in order to expel any dissolved air. The loop was also equipped with a Barnstead Type HN, mixed-bed demineralizer to prevent fouling of the heated tubes when distilled water was used.

The inlet fluid temperature was measured by a thermocouple probe installed directly in the fluid stream just prior to the heated section. The bulk temperature of the exit fluid was measured by a thermocouple probe placed in the mixing chamber. All fluid and tube wall temperatures were measured by 30-gage copper-constantan thermocouples fabricated from the same reel of Leeds and Northrup duplex wire. All thermocouples were monitored on a multi-point Speedomax temperature recorder. They were also connected, through a 10-point selector switch, to a common ice bath and a Leeds and Northrup No. 8662 precision potentiometer with 0.005 mv resolution.

The inlet pressure to the test section was measured with an 8.5-in. Helicoid test gage having a specified accuracy of 0.25 percent of full scale. Pressure taps, with a 0.02-in. diameter, were located 1 in. away from both side of the heated test sections. The inside of the tube was hand-reamed to remove any burrs resulting from drilling of the tap holes. The pressure drop across the test section was measured with a Meriam Model 40HE35 inclined manometer. The range of the manometer was 4 in., with 50-in. long scale, which resulted in a 0.005 in. resolution. Meriam blue fluid (1.75 specific gravity) and mercury were used as indicating fluids for the inclined manometer.

B. Test Sections

1. Glass tube

The first test section was constructed from a Pyrex Brand, E-C coated glass tube manufactured by Corning Glass Company. The glass tube is externally coated with an optically-transparent, electrically-conductive tin-oxide layer. Heat is generated quite uniformly by passing an electric current through the thin resistive coating. This tubing represents the closest possible approximation to the uniform wall heat flux boundary condition with zero circumferential wall thermal conductivity "ZC". A similar glass tube was first used by Bergles and Simonds [27] with no real operating problems.

Measurements near both ends of the tube indicated an inside diameter of 0.419 in. and a wall thickness of 0.048 in. The length of the heated section was 44.5 in., thus providing a heating section with a L_T/d_1 ratio of 106. A 75-in. long stainless steel tube with a 0.412-in. i.d. was used as velocity approach length. The ends of the two tubes were butted together to form hydrodynamically smooth joints by means of Veeco vacuum couplings.

The glass tube was divided into three sections by four 1/2-in. wide silver bands, which were 1.5 in. away from either end of the tube to allow for easy connections to inlet and outlet sections. The electric resistance of each section was about 150 ohms. Electric power connections to the tube were such that one, two, or three sections could be heated. This provided a simple procedure for obtaining the heat transfer coefficient for various tube lengths without moving the thermocouples to

different axial locations. Figure 6 shows the electric connection diagram for the three sections of the glass tube, which were powered by a 220 volt ac power supply controlled by a General Radio Model W20HG2 adjustable autotransformer. A variable rheostat was placed in each of two sections of the glass tube to compensate for any slight difference in the electric resistance of the three sections. A Western Model 310 wattmeter with a resolution of 0.5 watt was used to measure the electric power supplied. Calibration of the wattmeter by the Electronic Shop of the Engineering Research Institute showed an accuracy of 0.5 percent of full scale. Provision was made for using the same wattmeter to independently measure the electric power supplied to each section of the glass tube so that systematic errors resulting from any discrepancy in calibration would be minimized.

The outside wall temperatures were measured at an axial location 41.5 in. downstream from the onset of heating. This axial location will be designated as the measuring section. Four thermocouples were placed 90^{o} apart, circumferentially, at the measuring section to record the outer tube wall temperature profile. Moreover, the vacuum couplings at both ends of the glass tube permitted the rotation of the tube during each run so that an accurate circumferential wall temperature profile could be obtained. Due to electrical pick-up it was necessary to electrically insulate the thermocouple beads from the wall with 0.003-in. thick strips of insulation paper whose thermal conductivity was 0.0642 Btu/hr-ft-^{o}F.

In order to insure that the thermocouples were located in an adiabatic region, a guard shield surrounded the thermocouples at the

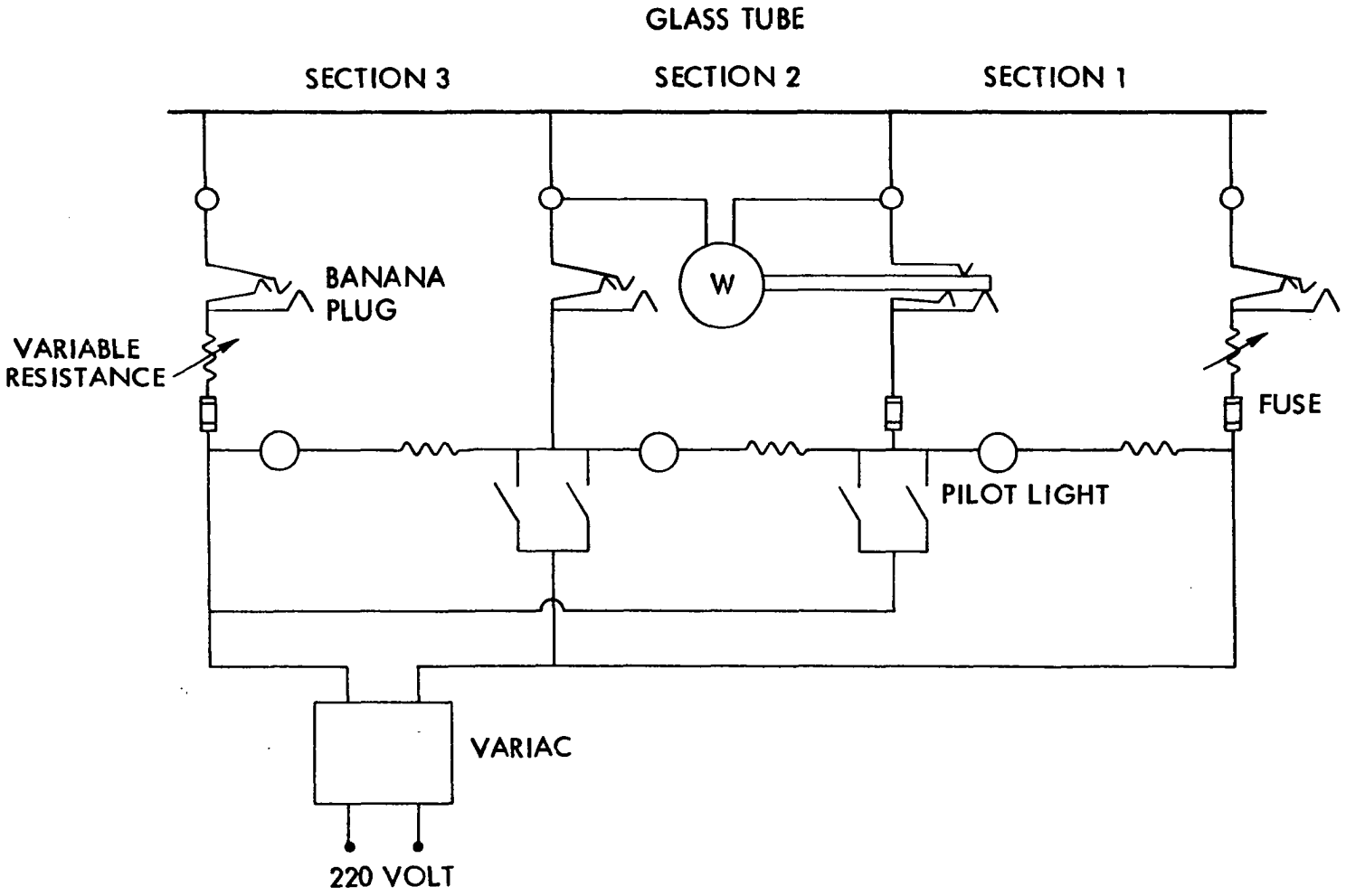

Fig. 6. Electrical connection diagram for glass tube

measuring section. The guard shield, shown in Fig. 7, was constructed from a 2-in. diameter, 6-in. long aluminum tube which was slit nearly through, longitudinally, into four separate sections. After the aluminum tube was insulated with Scotch No. 27 glass cloth electric tape, each section was wrapped with nichrome heater wire connected to four separate variacs. Four thermocouples were then attached to the inside wall of the guard shield opposite the corresponding tube wall thermocouples. In this way, the inner wall termperature of the guard shield segments could be independently adjusted to approximate the outer tube wall temperature profile. The guard shield assembly was completed by drawing the eight thermocouples out through the Micarta end supports and filling the aluminum tube with glass fiber insulation. The entire glass tube was heavily insulated with a 1-in. thick glass fiber insulating tube.

2. Metal tube

The second test section was constructed from a 304 stainless steel tube with an overall length of 10.7 ft. Heat was applied to the last 4 ft of the tube; the remainder of the tube was used to develop the flow hydrodynamically prior to its entering the heated section. The inside tube diameter and wall thickness, as checked near both ends, were 0.401 in. and 0.02 in., respectively. The inside diameter was chosen to resemble that of the glass tube. The wall thickness was a compromise between provision of the minimum thickness required for maximum electric resistance and provision of sufficient mechanical strength and circumferential conductance. The circumferential conductance of the metal tube was about ten times that of the glass tube, which was an adequate variation to test the influence of this parameter.

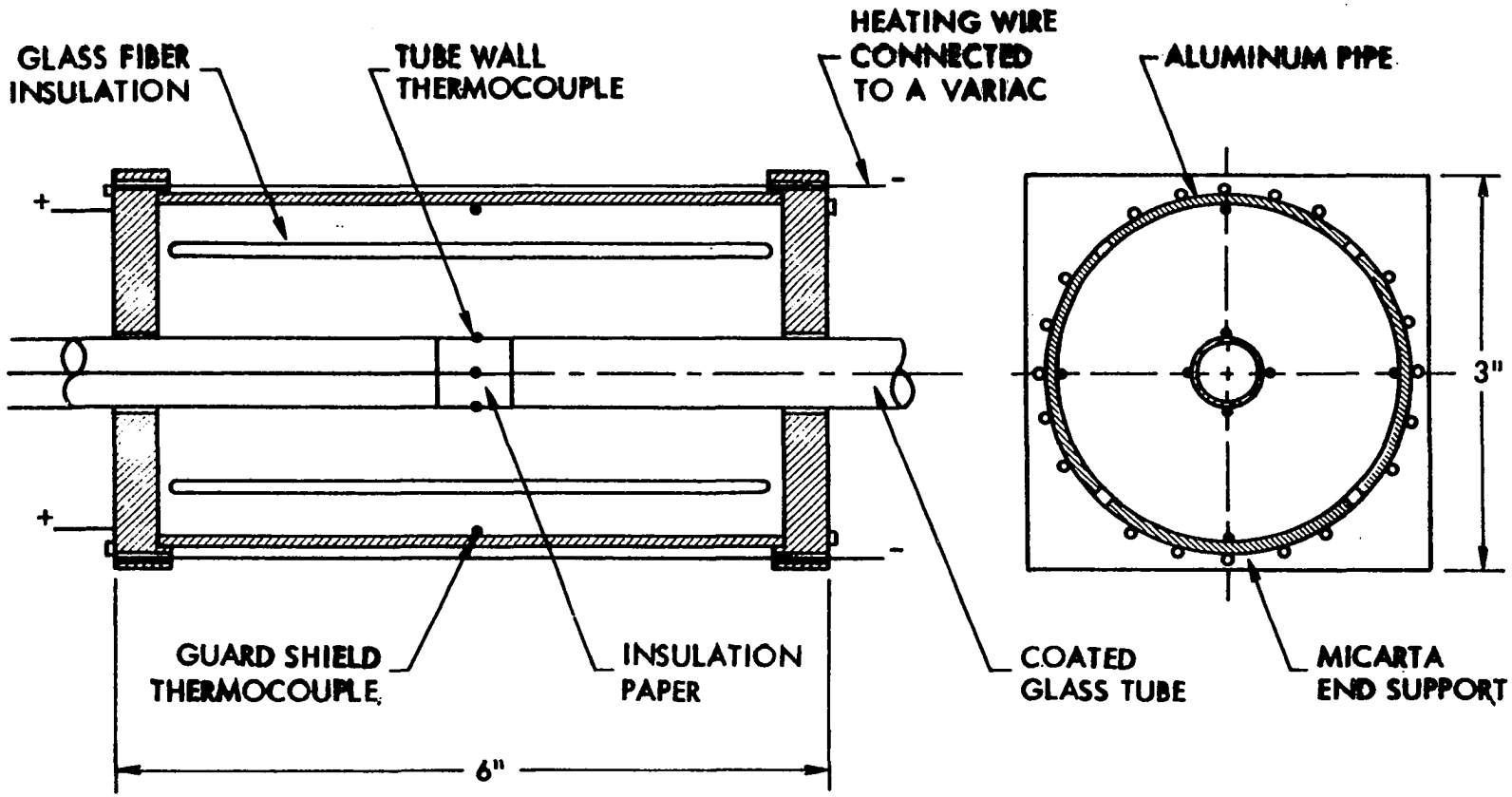

Fig. 7. Guard shield and wall thermocouple installations

The test section was heated by a dc current passed directly through the tube wall. An electric power supply, adapted from components available in the Mechanical Engineering Department, was installed for this program. It consisted of a 25-kw dc compound-wound generator driven by an induction motor. The generator was rated at 125 v and 200 amp while running at 1755 rpm. Power connections to the test section were made with about 40 ft of No. 3/0 THW copper cable. Aluminum clamps were used to connect the power cables to two brass bushings soldered on each end of the heated test section. Thermal expansions were compensated for by allowing free displacement of one end of the tube through a flexible joint connection to the power clamp. Details of the flexible joint and the power clamp connection are given in Fig. 8.

It was mandatory that the system be able to provide both sufficient electric power for the high heat flux runs and a power level selection capability so that the range of Rayleigh numbers of physical interest could be generated. However, the total resistance of the heated test section and the power cables was so small that it was feared this load might act as a short circuit unless additional resistance was added. Therefore, a dummy load was connected in series with the test section in order to boost the resistance. The dummy load was constructed from eighteen power resistors, each having an electric resistance of 7.1 ohm and a maximum current carrying capacity of 12 amp. The power resistors were arranged in three rows, each row having six resistors connected in parallel. Provision was made to connect one, two, or three parallel rows in series with the test section to obtain step variations in the dummy load characteristics. Changes in the shunt field rheostat of the compound-

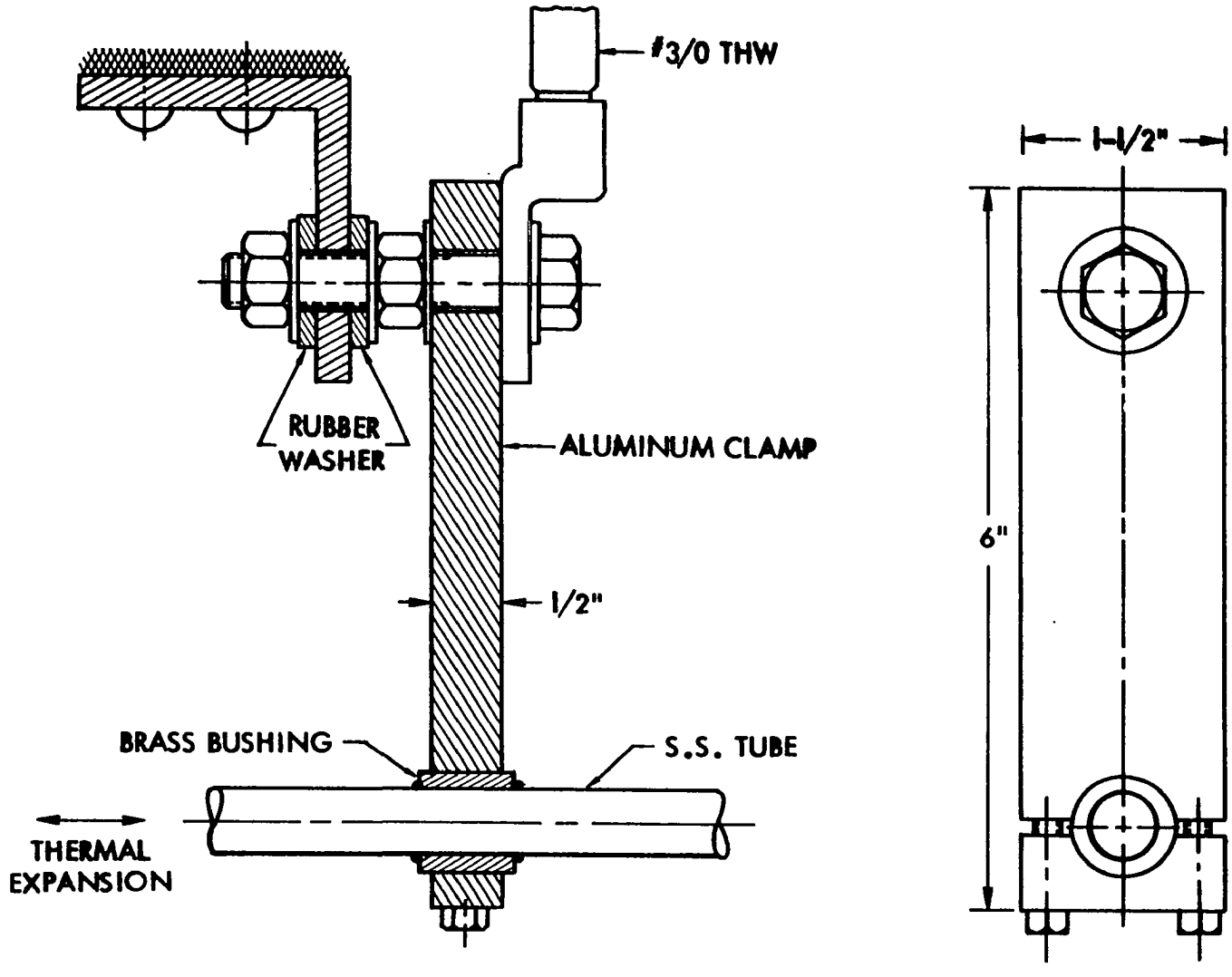

Fig. 8. Power clamp and expansion joint for metal tube

wound generator brought about variations in its load curve which made it possible to continuously select any heat flux level within the range of interest. Details of the calculations of the dummy load are given in Appendix C; the combined characteristics of both the dc generator and the dummy load are shown in Fig. 9.

The power input to the test section was determined by measuring the current and the total voltage drop across the heated section. This method was felt to be superior to any measurement method involving the resistance of the tube, since a sufficiently accurate resistance-temperature relation is difficult to obtain. A DigiTec Model 204 dc digital voltmeter was connected across the heated section to measure the voltage drop. It was estimated that the accuracy of the voltmeter was within $\pm$ 1 percent, and its resolution was 0.005 v. The current was measured by a calibrated Esterline Angus shunt (240 amp/100 mv) connected in series with the test section. The voltage across the shunt resistance was monitored with a Leeds and Northrup 8690 potentiometer with a resolution of 0.02 mv.

The outside wall temperature was measured at two axial locations, 11 in. and 44 in. from the onset of heating point. Four thermocouples were placed 90° apart, circumferentially, at each axial location and were electrically insulated from the tube with thin strips of insulating paper. The tube was then heavily insulated with 1-in. thick glass fiber insulation. The Veeco vacuum couplings at either end of the test section allowed the tube to be rotated about its axis so as to obtain an accurate circumferential wall temperature profile.

As mentioned above, the circumferential conductance of the metal tube was much larger than that of the glass tube. Appreciable

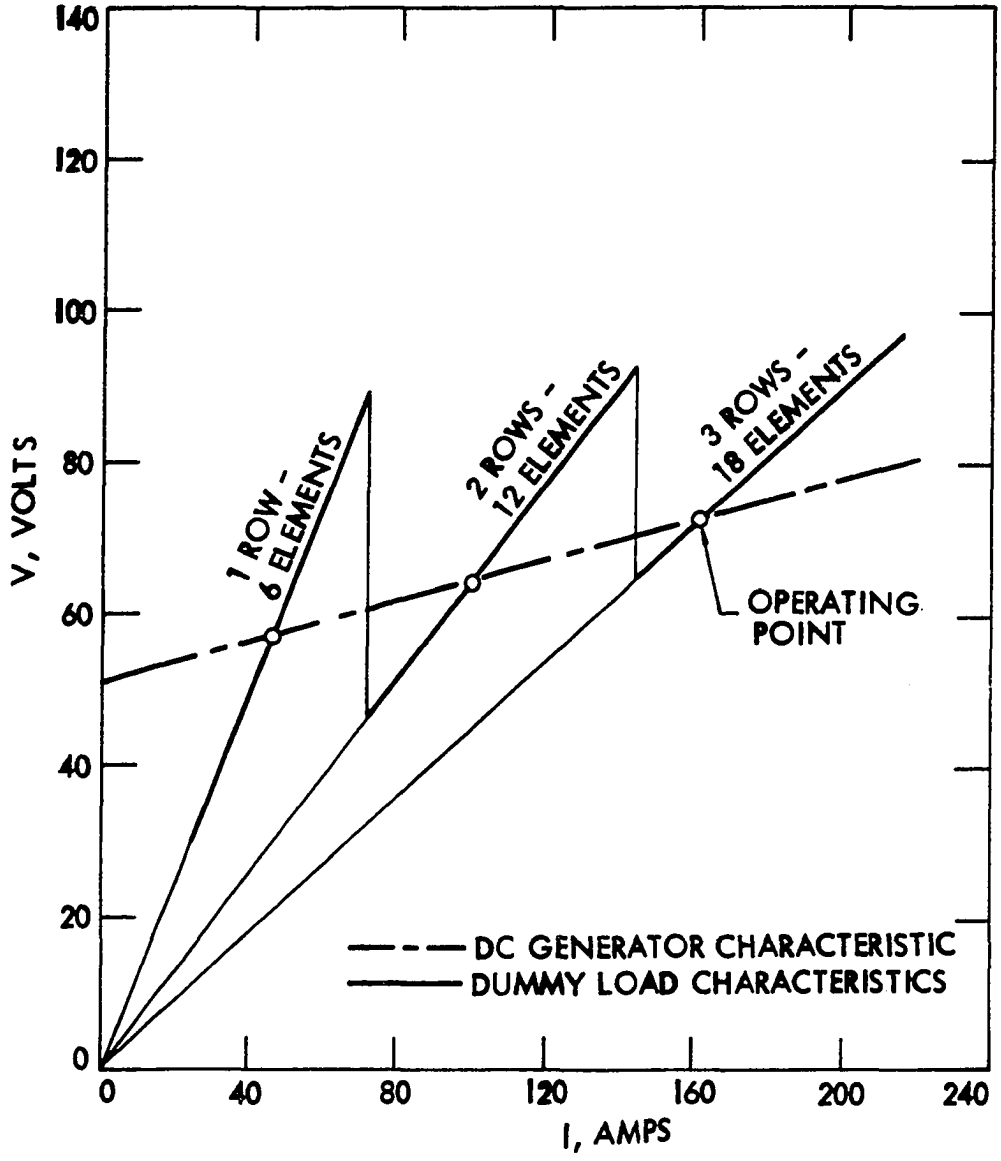

Fig. 9. Combined characteristics of dc generator and dummy load

circumferential heat flow was, therefore, expected to lead to more uniform wall temperatures at any axial location. In addition, the temperature drop across the metal tube wall was very much smaller than that across the glass tube, which resulted in a lower outside wall temperature level for the metal tube. It was, therefore, decided not to employ any elaborate guard shield but rather to depend on the heavy insulation.

III. EXPERIMENTAL PROCEDURE

A. General Loop Operation

Distilled water was the first working fluid to be used because of its availability and wide application. Selection criteria for a second fluid required that it would not only provide a substantial variation in Prandtl number but would also extend the range of Rayleigh numbers to lower values than those obtained when using water. Several fluids were considered, and ethylene glycol was found to be the most suitable. It extends the range of the Rayleigh number and has a Prandtl number value as much as 30 times that of water. The physical properties of both fluids, as a function of temperature, are given in Appendix A.

The loop was first filled with distilled water from the top of the degassing tank, and air was bled from all high points of the system. The water in the degassing tank was then brought to a boil while the loop water was circulated with the heat exchanger cooling water on. Degassing was accomplished by bleeding a portion of the loop water into the top of the vigorously boiling degassing tank. A small condenser on the top of the degassing tank allowed the gases to escape while condensing back most of the water vapor. This was continued for about 20 hours before initial data-taking. From time to time throughout the experiments the whole process was repeated, and the water was occasionally replaced. This procedure was sufficient to maintain the dissolved gas content at such a low level that no gas evolution

was observed in the visual section during the course of the experiments. Gas bubbles would significantly alter the laminar flow and heat transfer characteristics.

After the water data for both the glass and metal test sections were completed, the water was thoroughly flushed out with compressed air. Since ethylene glycol is completely miscible with water, the loop was charged with dry nitrogen to eliminate any moisture in the air. A water aspirator was used to create enough suction while the loop was being filled with ethylene glycol from the degassing tank. The gas content of the glycol in the loop, as indicated by a Seaten-Wilson Model AD-4003B Aire-Ometer, was below 18 cc/liter. Such low gas content, together with the fact that no gas bubbles were observed in the glass tube test section, eliminated any need for degassing when using ethylene glycol.

B. Operating Procedure

1. Heat transfer

The testing generally proceeded by increasing the power input to the test section while maintaining a constant flow rate and inlet temperature. The fluid flow rate and pressure level were controlled by the two ball valves at either end of the test section and by the needle valve at the test section inlet. The fluid inlet temperature was controlled by adjusting the heat exchanger cooling water and varying the preheater power supply.

The ac power input to the glass tube test section was set by the adjustable autotransformer. When more than one section was heated, the variable rheostat was used to compensate for any differences in the electric resistance of the sections so that a uniform average wall heat flux could be maintained along the tube. This adjustment was necessary for each run since the tube resistance changed with temperature. For the metal tube, the dc power input was controlled by matching the dummy-load characteristics with the compound-wound generator load curve. At low power levels, the power setting would remain essentially constant while steady-state conditions were being attained. However, at relatively high power levels, the power setting had a tendency to drift and oscillate. In these cases, a continuous adjustment of the shunt field rheostat of the generator was made to keep the generator output fairly constant, and the average reading was always recorded.

The outer wall temperatures were recorded with the four thermocouples placed at 0, 90, 180, and 270 degrees at the measuring section. The heated section was rotated 45 degrees and the readings of the four thermocouples were then recorded. In this manner, the eight temperature measurements and the condition of symmetry around a vertical meridional plane were used to accurately determine the circumferential wall temperature profile. In the case of the glass tube test section, the power input to each segment of the guard shield was adjusted by the four independent variacs until the guard shield thermocouples yielded almost the same value as the corresponding tube wall thermocouples. At relatively high heat flux runs, it was not possible to support the

same temperature variation in the guard shield segments as was established in the glass tube wall. In such cases it was only possible to maintain an agreement between the thermocouples at each individual segment.

The equipment was allowed to operate at least 45 minutes before taking each data set so that steady-state conditions could be established. Continuous monitoring of the system temperatures during this period, on the multipoint temperature recorder, indicated when equilibrium was achieved. Once equilibrium was reached, the signals for test section flow rate, inlet and outlet fluid temperatures, outer wall temperatures, and eletric power input were recorded.

2. Pressure drop

Isothermal pressure drop data were obtained by varying the fluid inlet temperature (using the preheater and the heat exchanger) for different flow rates. The overall test section pressure drop was measured by the inclined differential manometer. Due to the extremely low pressure drop and the relatively large time constant of the measuring system, it was necessary to wait as much as one hour before recording the differential head of the indicating fluid.

The procedure used for obtaining the nonisothermal pressure drop data was essentially the same as that followed in the heat transfer runs. The only difference was that the outer tube wall temperature was not recorded. Instead, the mean wall temperature was calculated from the heat transfer results as described in the next section.

C. Data Reduction

1. Heat transfer

As mentioned above, both test sections were insulated with 1 in. of heavy density glass fiber insulation. This insulation limited the heat loss to the surroundings to about 1.5 percent of the total power input. The heat loss calculations are presented in Appendix D.

The local bulk temperature at the measuring section was computed from inlet temperature, flow rate, and actual power input. For all the data runs, the thermal power input was calculated and compared with the measured electric power input. In most cases the error, expressed as a percentage of the measured electric power, was about 7 percent. However, the discrepance at low Reynolds numbers was as high as 13 percent, due to insufficient agitation of the fluid in the mixing chamber. Therefore, the actual power input to the test section was considered to be the measured electric power as corrected for heat loss.

The tube wall temperature drop was obtained by solving the steady-state one-dimensional heat conduction equation. This correction, applied uniformly around the circumference, ranged from 2 to 40°F for the glass tube and was always less than 1°F for the metal tube. It was recognized that the actual heat flux to the liquid was circumferentially nonuniform. As demonstrated in a subsequent section, however, the above procedure is entirely adequate. The circumferential average wall temperature was computed from the eight inner wall temperature readings by numerical integration.

The average heat transfer coefficient was calculated by using the heat flux based on the inside tube surface area, average inner wall temperature, and calculated bulk fluid temperature at the measuring section. The usual definitions of the Reynolds and Nusselt numbers are based on the inside tube diameter. The Grashof number is defined in terms of the local average wall to bulk fluid temperature difference and the inside tube diameter. All properties were evaluated at the local bulk fluid temperature.

A Fortran IV program (listed in Appendix F) was written to facilitate the data reduction. The program was run on the IBM/360 computer at the Iowa State University Computation Center. Sample calculations and a printout of a representative run are included in Appendix F. The final heat transfer results for water and ethylene glycol with both the glass and metal test sections are tabulated in Appendix G.

2. Pressure drop

For isothermal pressure drop runs, inlet fluid temperature was used to evaluate all physical properties. The indicating fluid differential head was used to calculate the pressure drop across the test section. The friction factor was then calculated according to the following relation:

$$\Delta p = \frac{g}{g_c} \frac{f \rho L}{d} \frac{\rho u^2}{2g} \qquad (3.1)$$

For the pressure drop data for the heating runs, only the inlet fluid temperature, flow rate, and power input were recorded. As pointed out previously, the developing length for the combined forced and free laminar convection flow is much shorter than that required in the case of pure forced convection flow. Therefore, all physical properties were evaluated at the fluid bulk temperature at a section half way along the heated section. The average tube wall temperature was obtained through multiple iterations, using the already established relation between the Nusselt and Rayleigh numbers.

Sample calculations for a typical nonisothermal pressure drop run, and a listing of the computer program used to facilitate the data reduction are given in Appendix F; a summary of the entire pressure drop results is given in Appendix G.

D. Circumferential Heat Flux Distribution

As mentioned earlier, the fluid motion is dependent on the type of heating and the characteristics of the tube wall. The two limiting tube wall situations of interest with electric heating are very large and very small circumferential wall conductance. With the first case, the tube wall temperature tends to be circumferentially uniform, the heat input per unit length being constant. For the latter case, the heat flux tends to be uniform in both the circumferential and axial directions. However, in physically realizable situations represented by the two present test sections, the wall thermal conductivity has a nonzero, finite value, such that neither the heat flux nor the wall temperature are uniform circumferentially.

The major task in the data reduction is to determine the circumferential variation of the heat flux and the inside wall temperature for both the glass and metal tubes. These quantities can be deduced from the outside wall temperature measurements and the known total heat input.

Numerous studies have been concerned with the influence of variable circumferential heat flux for laminar and turbulent flow in tubes. For instance, Sparrow and Lin [30] and Rapier [31] presented an analysis of a fully-developed turbulent flow in a circular tube with uniform heat input per unit length and variable circumferential wall temperature. Reynolds [32,33] considered essentially the same problem for both laminar and turbulent flows. Recently, Luikov et al. [34] applied perturbation techniques to the problem of fully-developed combined forced and free laminar convection in horizontal tubes with prescribed circumferentially varying wall heat flux. This is of particular interest in situations where the tube is externally heated or cooled by forced-convection cross flow, by free convection, by film condensation, or by thermal radiation from a nonuniform environment.

These investigations have been concerned almost exclusively with cases in which either the inside wall temperature or the wall heat flux are arbitrarily prescribed. In practice, however, the prescribed quantity is the input heat rate per unit length, and the circumferential heat flux and temperature distributions represent dependent variables. It is therefore necessary to obtain the temperature and heat flux distributions by solving the so-called conjugated problem. For this

type of problem, the energy equations for the entire wall-fluid system and those for the hydrodynamics are solved together, and the traditional limiting thermal boundary conditions are not necessary.

Luikov et al. [35] presented solution methods for the conjugated problem of laminar flow inside circular tube. They reduced the problem to a singular integral equation for the unknown temperature of the surface but did not consider the effect of free convection. Additional inclusion of the buoyant effects, when the velocity field is coupled with the temperature field, would further complicate the analysis. This explains why no analysis is presently available for the conjugated problem of combined forced and free laminar convection in horizontal tubes. The only practical way to approach such problems is to obtain the heat flux and temperature distributions around the inside tube surface from the measured outside wall temperature and total heat flux.

In order to determine the desired heat flux and temperature distributions, it is necessary to solve the two-dimensional conduction equation for the tube wall, taking into account both radial and tangential heat transfer. At this point, it is convenient to deal separately with the glass and metal tubes because, due to the nature of the heat generation, they have different boundary conditions at the outer surface of the tube.

1. Glass tube

Since the glass tube is externally coated with a thin layer of tin oxide, the electric heat is generated at the outside tube surface. Moreover, the thickness of the tin oxide layer is approximately 1.6×10^{-5} in., which justifies the neglect of temperature drop across such

a layer. The measured outside wall temperature can, therefore, be taken as the temperature at the outer tube radius. Using polar coordinates, the governing energy equation for the tube wall takes the form

$$\frac{\partial^2 T_w}{\partial r^2} + \frac{1}{r}\frac{\partial T_w}{\partial r} + \frac{1}{r^2}\frac{\partial^2 T_w}{\partial \theta^2} = 0 \tag{3.2}$$

where the angle θ is measured clockwise from the vertex of the tube.

On the outer tube surface, the temperature is measured at eight discrete points. A periodic function $F(\theta)$ is used to approximate the outside tube wall temperature. If it is assumed that the electric coating of the glass tube is uniform and the resistance is a weak function of temperature, then the heat generated around the outer circumference of the tube can be considered uniform. Moreover, the heavy insulation insured a very small heat loss. Consequently, the radial temperature gradient at the outer tube surface is constant, and the thermal boundary conditions there can be written as

$$T_w (r_2, \theta) = F (\theta) \tag{3.3}$$

and

$$\left(\frac{\partial T_w}{\partial r}\right)_{r_2,\ \theta} = \frac{q''_o}{k_w} = \text{constant} \tag{3.4}$$

The details of the solution of Eq. (3.2), subject to the boundary conditions given by Eqs. (3.3) and (3.4), are presented in Appendix E. The final results for the nondimensional wall temperature are given below:

$$\tau_w (r,\theta) = \alpha_0 + q_c \ \ell n \ R + \sum_{n=1}^{4} \left[\frac{\alpha_n}{2} \left(R^n + R^{-n} \right) \cos n\theta \right] \qquad (3.5)$$

where

$$\tau_w (R, \theta) = \frac{T_w (r, \theta) - T_{w,o5}}{T_{w,o1} - T_{w,o5}} \qquad (3.6)$$

$$R = \frac{r}{r_2} \qquad (3.7)$$

and

$$q_c = \frac{q_o'' \ r_2}{k_w \left(T_{w,o1} - T_{w,o5} \right)} \qquad (3.8)$$

The outside wall temperatures $T_{w,o}$ are numbered 1 through 5 and are located 45^o apart, starting clockwise from the top of the tube. In Eq. (3.5), α_j's are the coefficients of the nondimensional temperature distribution function $f(\theta)$ on the outside surface of the tube, and are given by

$$\left.\begin{aligned}
\alpha_0 &= \frac{1}{4}\left(\frac{1}{2}\,\tau_{w,o1} + \tau_{w,o2} + \tau_{w,o3} + \tau_{w,o4} + \frac{1}{2}\,\tau_{w,o5}\right) \\
\alpha_n &= \frac{1}{2}\left(\frac{1}{2}\,\tau_{w,o1} + \tau_{w,o2}\cos\frac{n\pi}{4} + \tau_{w,o3}\cos\frac{n\pi}{2}\right. \\
&\quad \left. + \tau_{w,o4}\cos\frac{3n\pi}{4} + \frac{1}{2}\,\tau_{w,o5}\right) \qquad (n \neq 0,4) \\
\alpha_4 &= \frac{1}{4}\left(\frac{1}{2}\,\tau_{w,o1} - \tau_{w,o2} + \tau_{w,o3} - \tau_{w,o4} + \frac{1}{2}\,\tau_{w,o5}\right)
\end{aligned}\right\} \tag{3.9}$$

where $\tau_{w,oj}$ is the nondimensional outside wall temperature measured at 45^{o} intervals.

The heat flux at any point along the tube wall is given by

$$q'' = -k_w \frac{\partial T_w}{\partial r} \tag{3.10}$$

which when combined with Eq. (3.5) can be written as

$$q'' = \frac{k_w}{r_2}\left(T_{w,o1} - T_{w,o5}\right)\left\{\frac{q_c}{R} + \sum_{n=1}^{4}\left[\frac{n\alpha_n}{2}\left(R^{n-1} - R^{-n-1}\right)\cos n\theta\right]\right\} \tag{3.11}$$

The inside tube wall temperature and the heat flux distribution can then be calculated by utilizing Eqs. (3.5) and (3.11) and the measured outside wall temperatures. The results of calculations will be given in a subsequent section, after a similar analysis has been presented for the metal tube.

2. Metal tube

The basic difference between the heat conduction equation formulation for the metal tube and that for the glass tube is in the method of heat supply. The metal tube was direct resistance heated with a dc electric power source, which adds a generation term to the energy equation. As in the case of the glass tube, the heavy insulation limited the heat loss from the outer surface of the metal tube. The temperature gradient is, therefore, approximately equal to zero at the outer radius of the tube. The energy equation for the tube wall in terms of polar coordinates takes the form

$$\frac{\partial^2 T_w}{\partial r^2} + \frac{1}{r}\frac{\partial T_w}{\partial r} + \frac{1}{r^2}\frac{\partial^2 T_w}{\partial \theta^2} = -\frac{q'''}{k_w} \tag{3.12}$$

where

$$q''' = \frac{I\,V}{\pi\left(r_2^{\,2} - r_1^{\,2}\right) L_T} \tag{3.13}$$

together with the following boundary conditions:

$$T_w\left(r_2, \theta\right) = F\ (\theta) \tag{3.14}$$

and

$$\left(\frac{\partial T_w}{\partial r}\right)_{r_2, \theta} = 0 \tag{3.15}$$

Once more, the details of solution are presented in Appendix E, and the final results are given by

$$\tau_w\,(R,\theta) = \alpha_0 + \frac{q^*}{2}\,\ell n\ R + \sum_{n=1}^{4}\left[\frac{\alpha_n}{2}\left(R^n + R^{-n}\right)\cos\ n\theta\right] + q^*\left(\frac{1 - R^2}{4}\right) \tag{3.16}$$

where

$$q^* = \frac{q'''\ r_2^2}{\left(T_{w,o1} - T_{w,o5}\right) k_w} \tag{3.17}$$

Utilizing Eqs. (3.10) and (3.16), one may express the heat flux as

$$q'' = \frac{k_w}{r_2}\left(T_{w,o1} - T_{w,o5}\right)\left\{\frac{q^*}{2R} + \sum_{n=1}^{4}\left[\frac{n\alpha_n}{2}\left(R^{n-1} - R^{-n-1}\right)\cos\ n\theta\right] - \frac{q^*\ R}{2}\right\} \tag{3.18}$$

The circumferential wall temperature and heat flux distributions around the inner tube surface were calculated using Eqs. (3.16) and (3.18); the results will be given in the next section.

3. Calculated wall temperature and heat flux distributions

The results of the tube wall analysis for the glass and the metal tube are presented in this section. The local wall temperature $T_{w,i}$ and heat flux q''_i on the inside tube wall at the measuring section can now

be calculated from the experimental observation. Furthermore, the circumferentially averaged values of these quantities can be determined according to

$$\bar{T}_{w,i} = \frac{1}{\pi} \int_0^{\pi} T_{w,i} \, d\theta \tag{3.19}$$

$$\bar{q}''_i = \frac{1}{\pi} \int_0^{\pi} q''_i \, d\theta \tag{3.20}$$

The local heat transfer coefficient and Nusselt number at any circumferential location may be defined as

$$h\ (\theta) = \frac{q''_i}{T_{w,i} - T_b} \tag{3.21}$$

$$Nu\ (\theta) = \frac{h(\theta)\ d_1}{k} \tag{3.22}$$

The average heat transfer coefficient and Nusselt number over the perimeter at any given cross-section may be found from the relation

$$h = \frac{\bar{q}''_i}{\bar{T}_{w,i} - T_b} \tag{3.23}$$

$$Nu = \frac{hd_1}{k} \tag{3.24}$$

Results of the circumferential variations of the inside wall temperature, heat flux, and Nusselt number for two representative runs

are presented in Figs. 10 through 13 for both glass and metal tubes. The upper grid shows the distributions of $T_{w,i}$, and the lower one displays the corresponding distribution of $q''_i/\bar{q}''_i$ and Nu (θ)/Nu.

Examination of the circumferential wall temperature distribution along the inside surface of the tube indicates that the temperature difference between the top and bottom of the tube increases with increasing average heat flux for both glass and metal tubes. The solid lines represent the results obtained from the solution of the two-dimensional conduction equation for the tube wall. The data points shown were obtained from the measured outside wall temperatures by subtracting a circumferentially constant temperature drop across the tube wall. Such a drop was, in turn, obtained by solving the one-dimensional heat conduction equation for the tube wall and using the average heat flux. It is quite clear that these data points fall very close to the solid line. A quantitative comparison between the two procedures is shown in Table 1, where the inside wall temperatures for Run 25 for ethylene glycol in a metal tube are listed.

Table 1. Inside tube wall temperatures as obtained by one-dimensional and two-dimensional procedures

θ	0	45	90	135	180
1-D	241.08°F	224.20	200.78	190.21	188.04
2-D	241.88°F	224.99	201.57	191.00	188.84

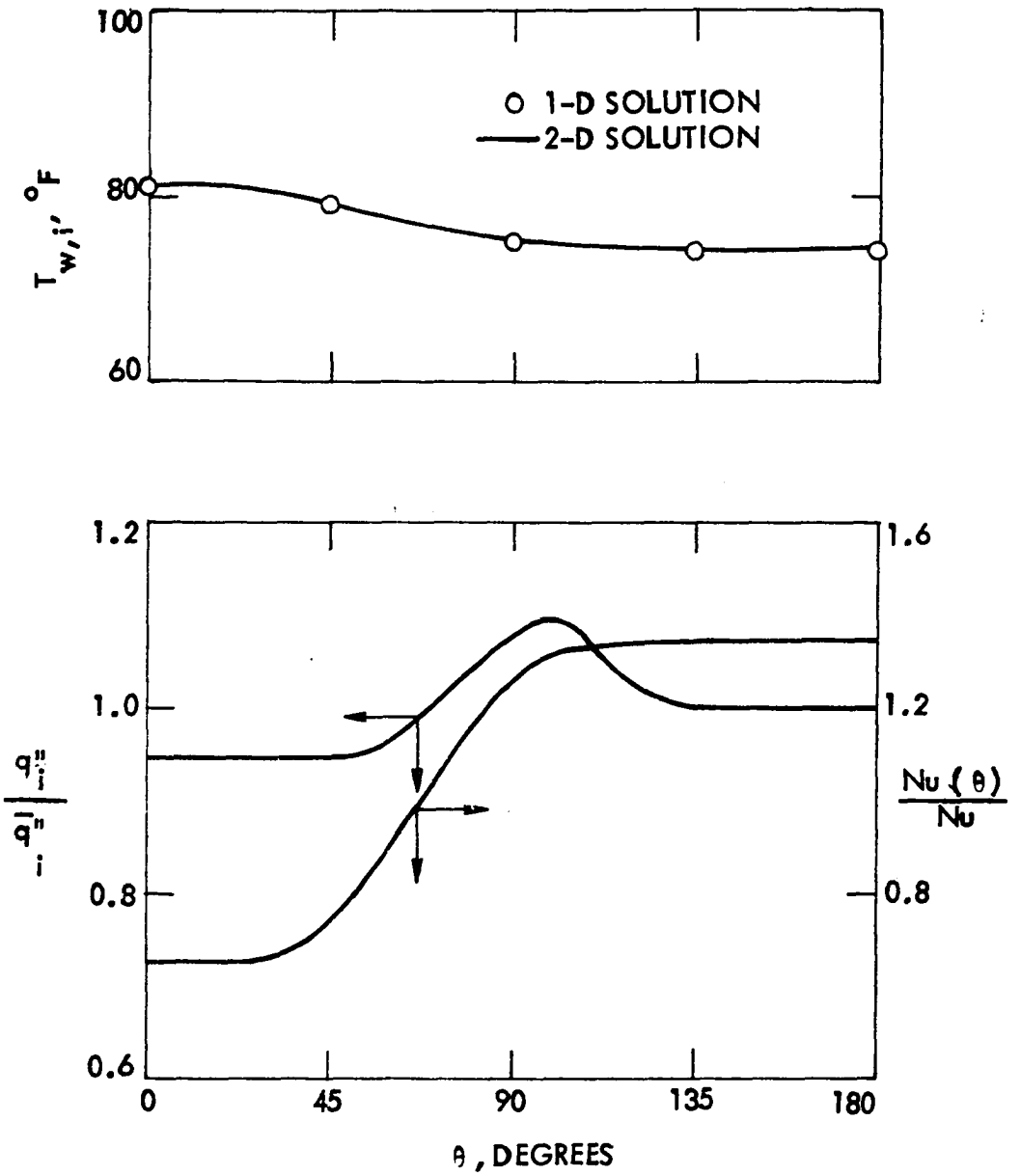

Fig. 10. Circumferential variation of inside wall temperature, heat flux, and Nusselt number for water with glass tube - Run:4

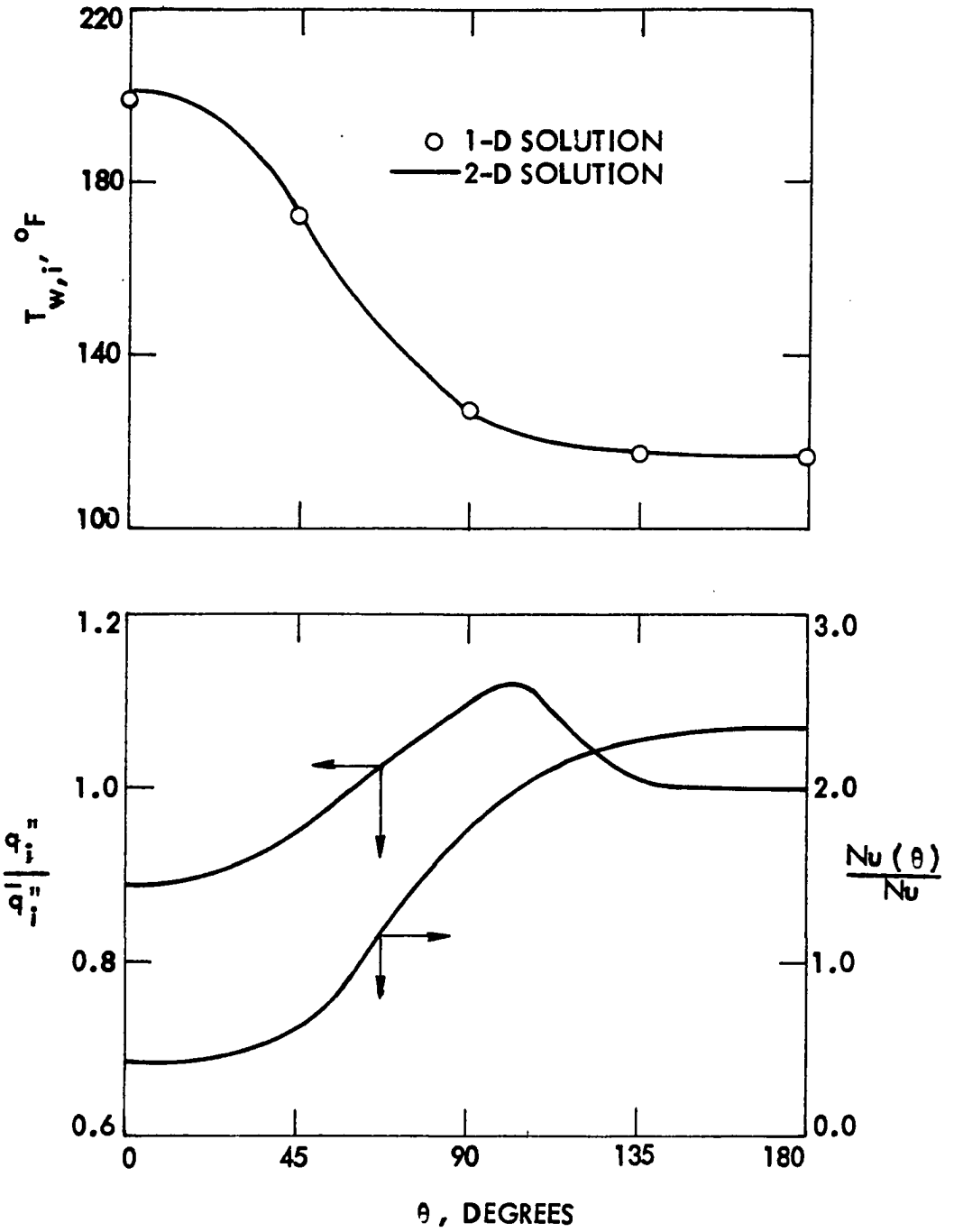

Fig. 11. Circumferential variation of inside wall temperature, heat flux, and Nusselt number for water with glass tube - Run:31

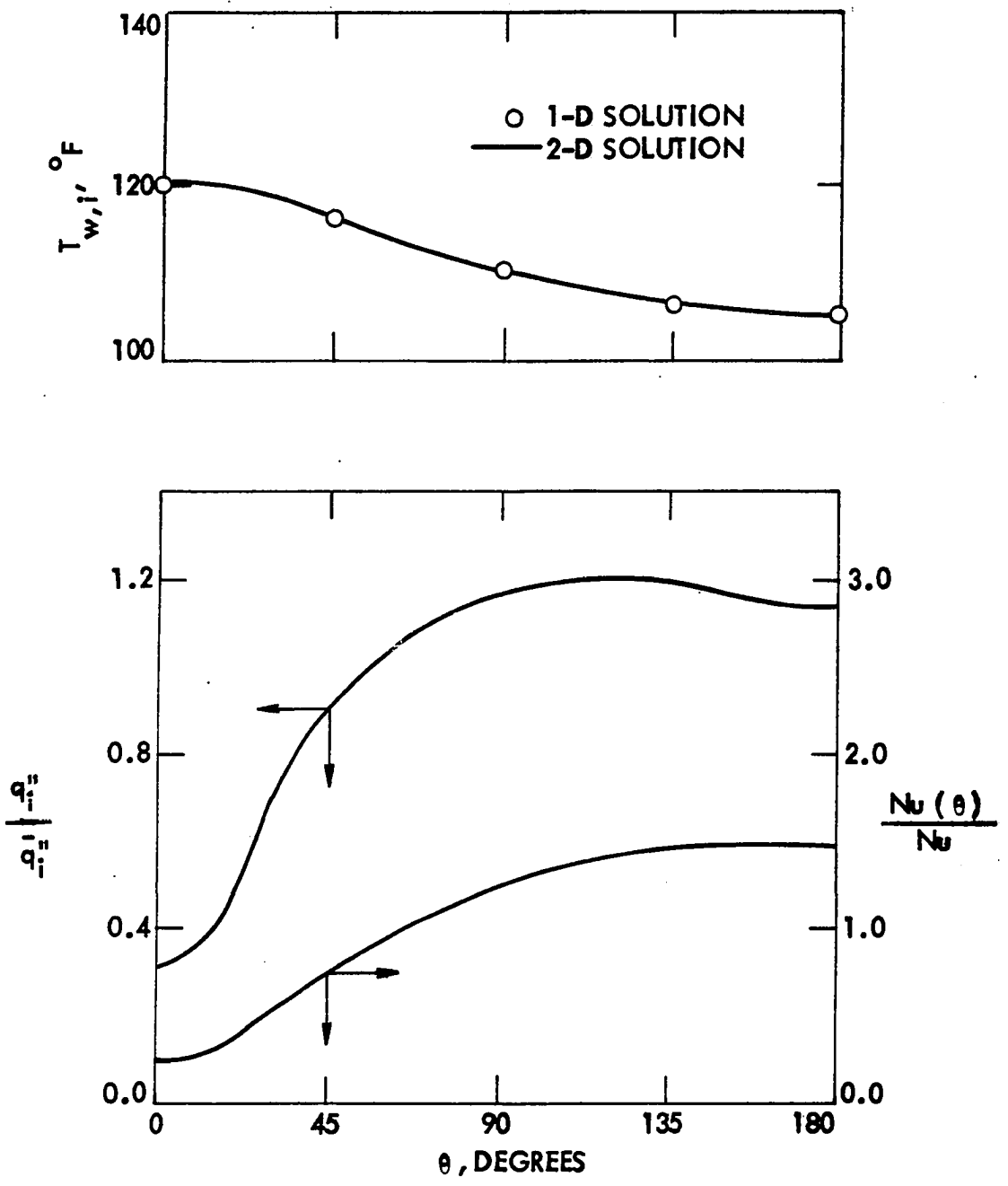

Fig. 12. Circumferential variation of inside wall temperature, heat flux, and Nusselt number for ethylene glycol with metal tube - Run:4

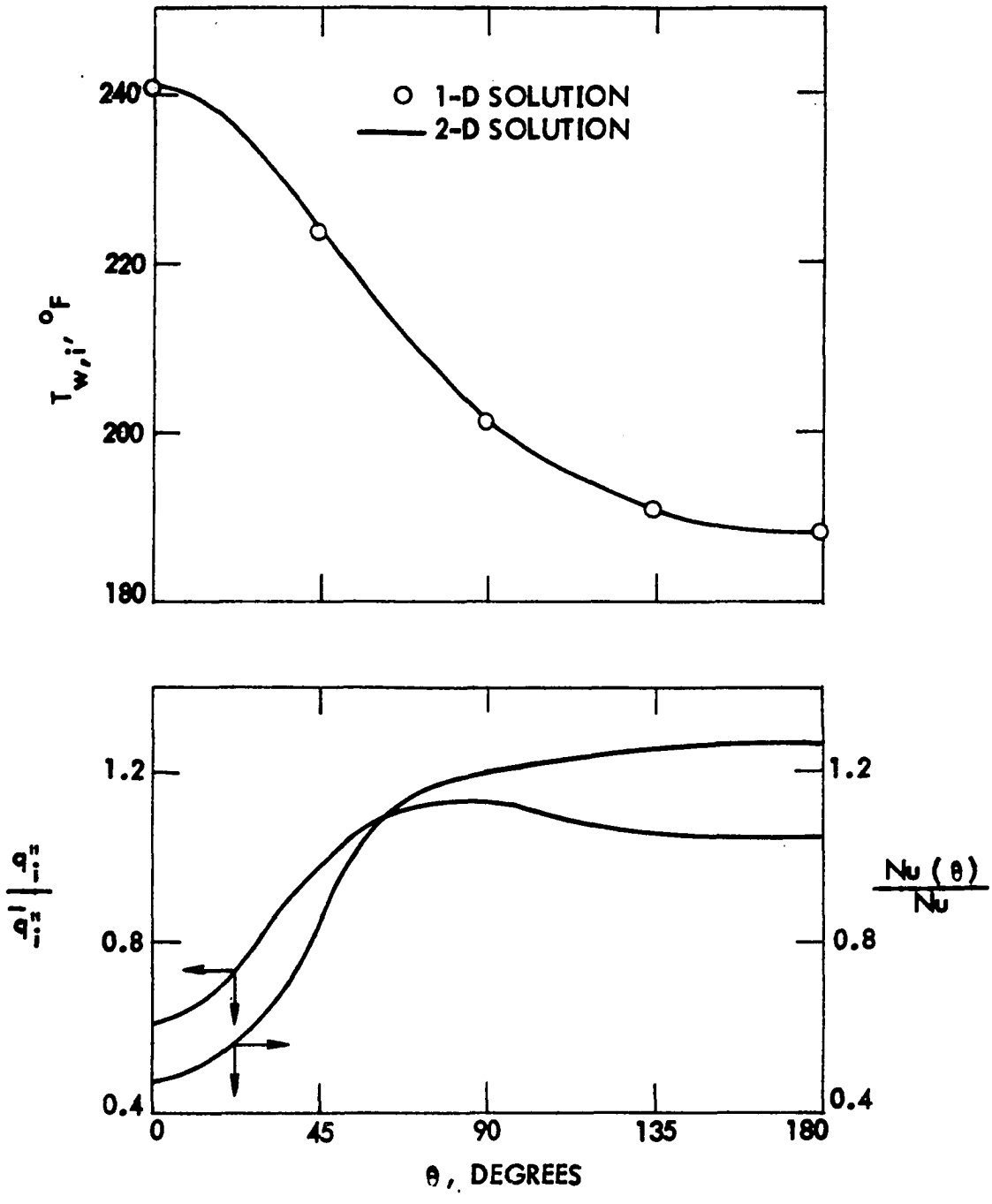

Fig. 13. Circumferential variation of inside wall temperature, heat flux, and Nusselt number for ethylene glycol with metal tube - Run:25

This comparison suggests that the average inside wall temperature is practically the same for both procedures. Because of the simplicity of the one-dimensional, circumferentially-uniform temperature drop across the tube wall, this procedure was used to obtain the inside mean wall temperature for all runs of glass and metal tubes, as was pointed out earlier in the data reduction section.

Next, attention may be given to the lower grid of Figs. 10 through 13. Since the circumferential conductance of the metal tube is about ten times that of the glass tube, the variation of $q_i''/\bar{q}_i''$ over the tube periphery of the glass tube is much smaller than that for the metal tube. However, the level of the average heat flux does not seem to have as much effect on such variations as on the circumferential wall temperature distribution. On the other hand, it is apparent from the foregoing figures, that the local Nusselt number varies considerably around the tube perimeter. The Nusselt number rises from a minimum at the top of the tube to a maximum at bottom. The local values of the Nusselt number in a given cross-section at the upper and lower points may differ by a factor of six or more. Moreover, the Nusselt number near the top of the tube for some metal tube runs is even lower than in a pure forced flow. This is probably due to a relatively hot fluid concentrated near the top so that no free convection takes place. The aforementioned results seem to be in general agreement with the trends presented by Petukhov and Polyakov [20].

Further examination of $Nu(\theta)/Nu$ distribution reveals that the circumferentially averaged Nusselt number obtained from the area under the curve is different from that defined by Eq. (3.24), in other words,

$$Nu \neq \frac{1}{\pi}\int_0^{\pi} Nu\ (\theta)\ d\theta$$

This is due to the fact that $T_{w,i} - T_b$ is a function of the angle θ. However, as far as the designer is concerned, the circumferentially averaged Nusselt number, based on the average wall temperature, is of a greater importance than the local value. Therefore, the average Nusselt number was used in presenting all the heat transfer results for both the glass and metal tubes.

IV. RESULTS AND DISCUSSION

A. Heat Transfer

1. Experimental results

Typical sets of wall temperature profiles are given for the glass tube in Figs. 10 and 11, and for the metal tube in Figs. 12 and 13. It is apparent that both tubes supported rather large circumferential temperature gradients. The temperature difference between the top and bottom of the tube increases as the heat flux is increased due to the increasing intensity of the secondary flow. This temperature difference ranged from 3 to 100 ^{o}F for the glass tube and from from 3 to 90 ^{o}F for the metal tube. The latter results suggest that even though the metal tube circumferential conductance is about ten times that of the glass tube, the metal tube is not quite faithful to the "IC" boundary condition.

To obtain the water data, Reynolds numbers from 675 to 1750 and Prandtl numbers from 4 to 8 were used; for ethylene glycol data collection, Reynolds numbers from 50 to 300 and Prandtl numbers from 35 to 175 were used. The static pressure at the test section inlet was kept at about 5 psig.

Since the present work is concerned with the combined forced and free convection in fully-developed laminar flows, it was necessary to verify that virtually all the data were taken in the fully-developed region. This was particularly important when ethylene glycol was used as a working fluid, due to its high Prandtl number values. The variation of the Nusselt number as a function of the reduced length X, for

various values of the Rayleigh number, is shown in Fig. 14 for water flow in the glass tube and in Fig. 15 for ethylene glycol flow in the metal tube. Also shown, as a limiting cases, are the analytical prediction for pure forced convection with parabolic velocity distribution [5] and with Pr = 5 [27]. The pronounced effect of free convection is quite clear from the present data which are two to six times higher than the constant property predictions. The vertical spread in the data represents a range of heat fluxes, with the highest Nusselt number corresponding to the highest heat flux. Since the Rayleigh number was a dependent variable, lines of constant Rayleigh number values could only be obtained by interpolating the data. Estimated lines of constant Rayleigh number values are shown in these figures; these lines are essentially horizontal for the range of the reduced length considered. Since a constant Nusselt number represents the classical interpretation of the fully-developed condition, it is apparent that fully-developed conditions were obtained prior to the measuring sections.

Since the data were taken under fully-developed conditions, a more detailed comparison can be obtained by using the Nusselt and Rayleigh numbers as correlation parameters in accordance with the example given in [8,27]. Such plots are shown in Fig. 16 for water and in Fig. 17 for ethylene glycol; data from both tubes tested are included. The straight-line character of the four sets of data is quite clear from the above figures. Moreover, the scatter of the experimental data around the mean line seems to be very reasonable when compared with the results of other investigations for both gases and liquids.

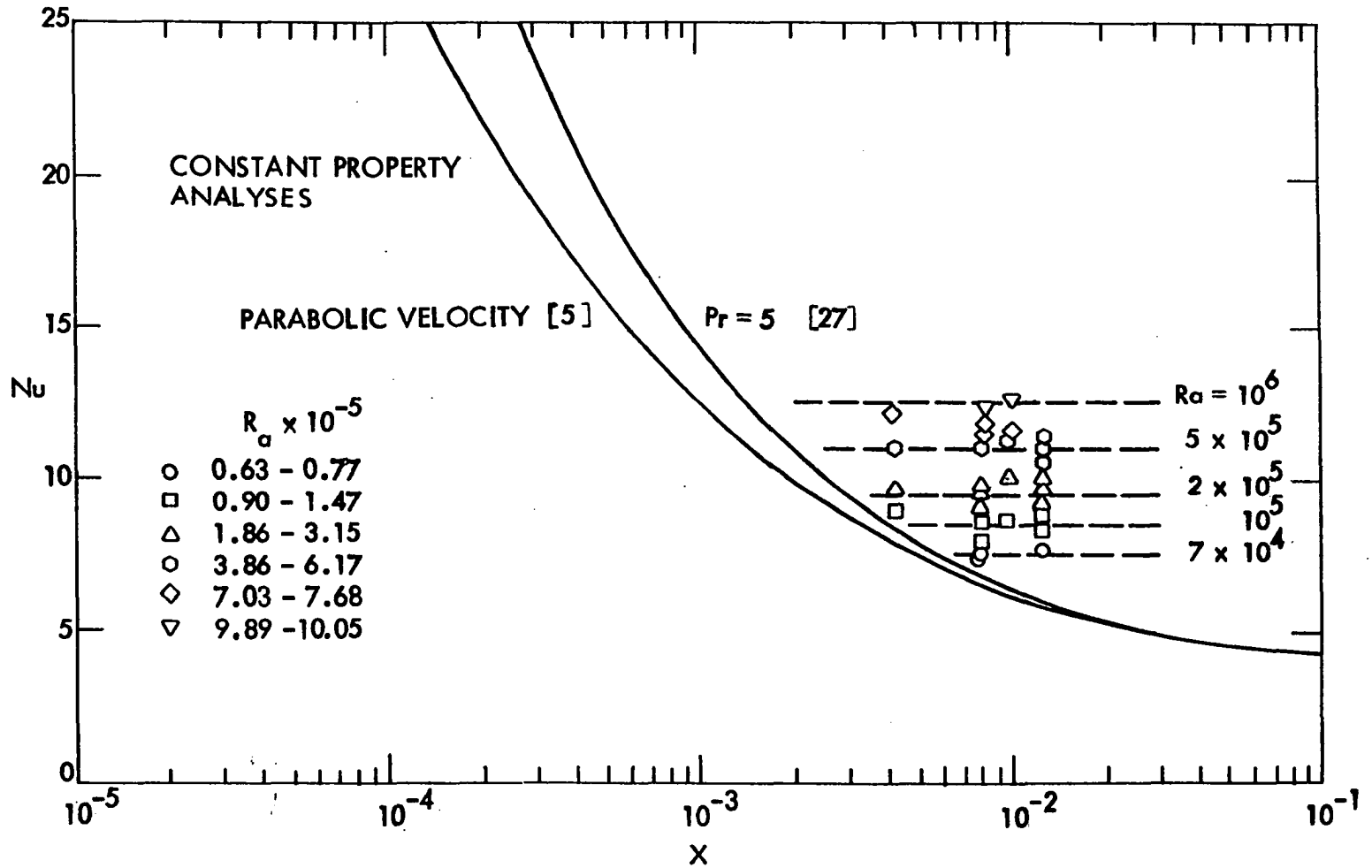

Fig. 14. Nusselt number as a function of reduced length for water with glass tube

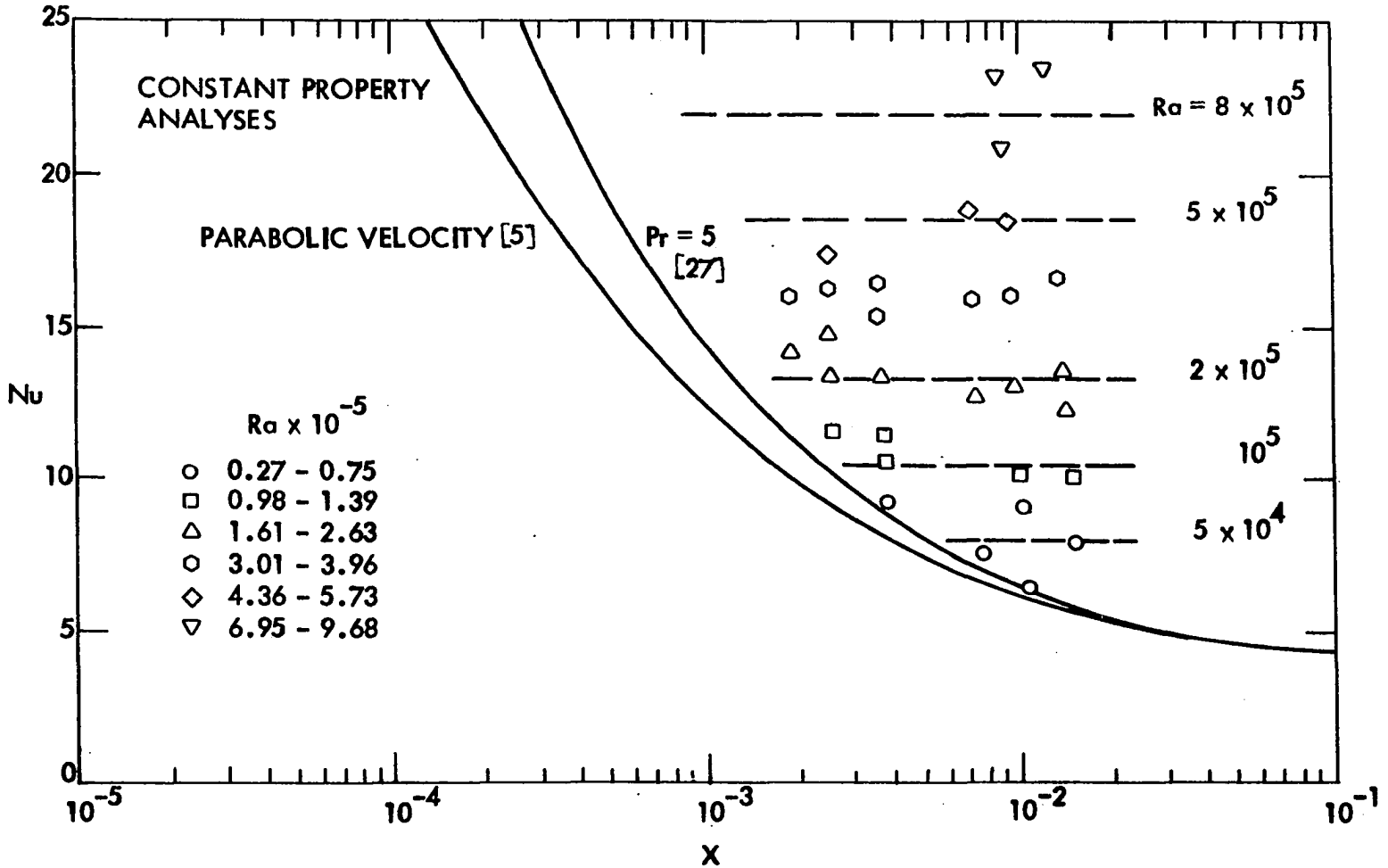

Fig. 15. Nusselt number as a function of reduced length for ethylene glycol with metal tube

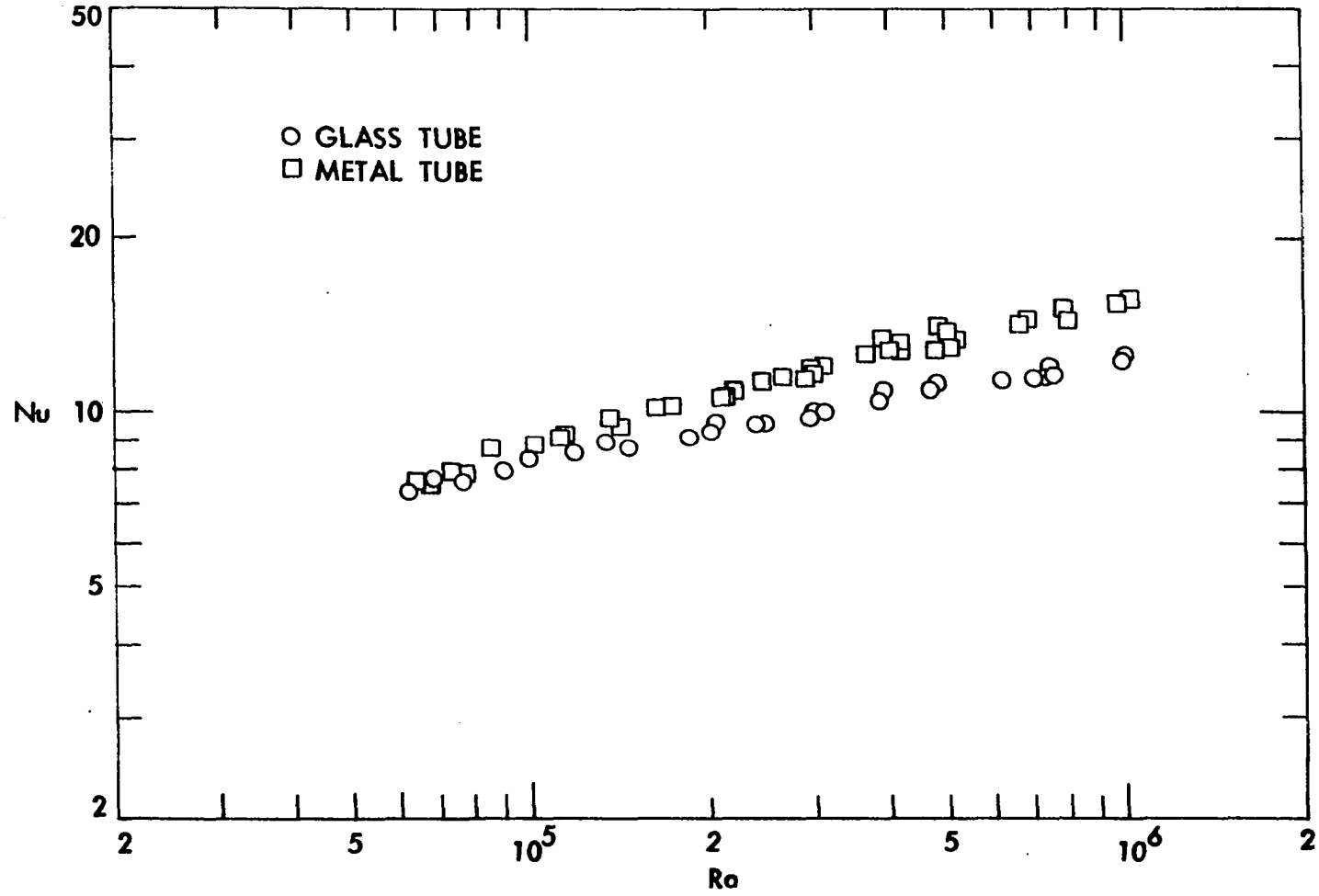

Fig. 16. Fully-developed heat transfer data for water with different tubes

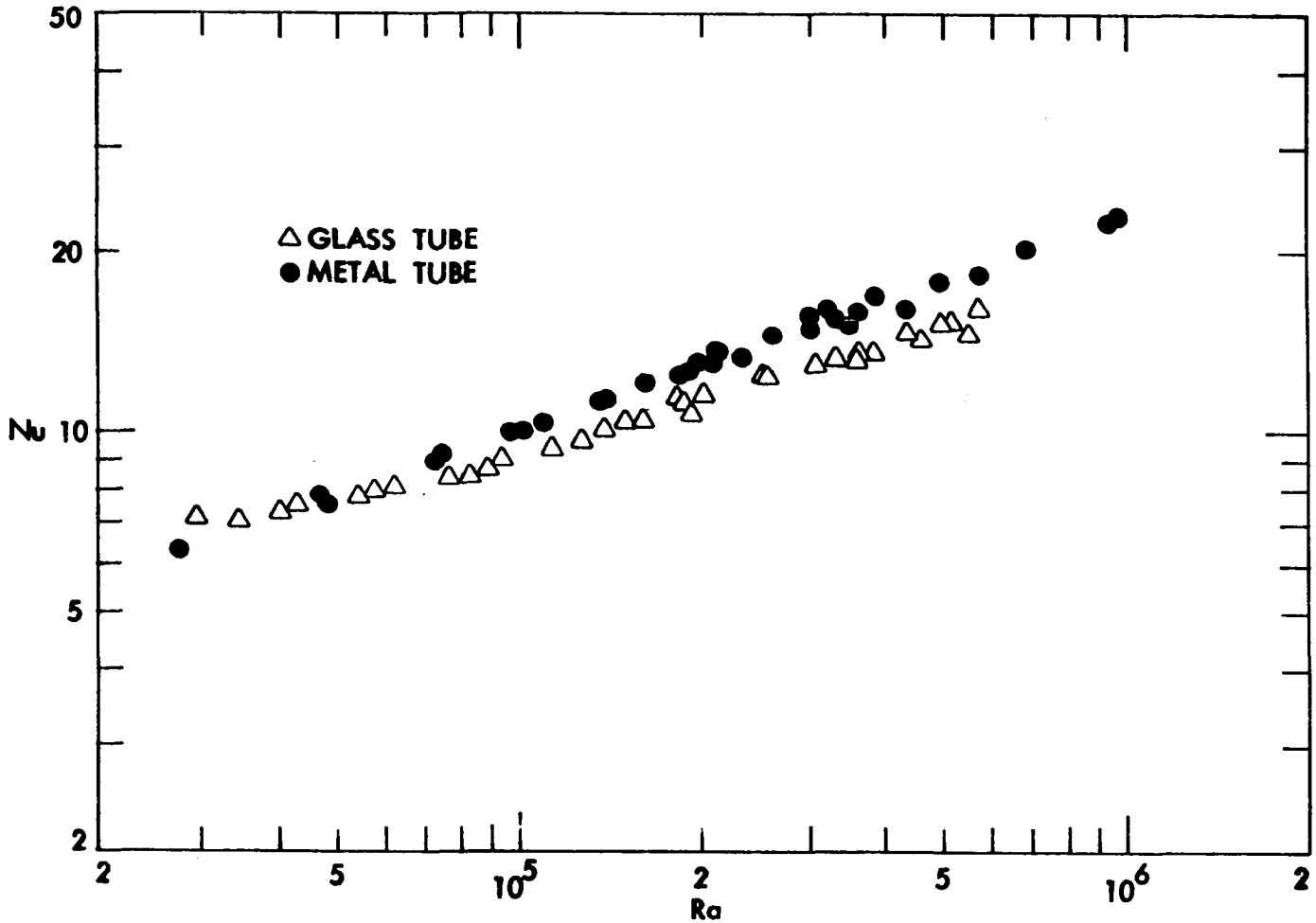

Fig. 17. Fully-developed heat transfer data for ethylene glycol with different tubes

The metal tube data for both fluids are well above the glass tube data at higher Rayleigh numbers, where circumferential heat flow would be important. The analysis of the heat flux distribution around the tube periphery presented in the previous chapter reveals that the heat flux near the bottom of the tube increases as the circumferential tube wall conductance increases. This intensifies the secondary flow which, in turn, elevates the heat transfer coefficient. Moreover, the ethylene glycol data lie above the water data for the respective tubes. This suggests that the Nusselt number is affected not only by the Rayleigh number and other variations in the physical properties of the working fluid, but also by the circumferential conductance of the tube wall.

In view of the variable fluid properties and the pronounced effect of the tube wall circumferential conductance, it is not appropriate to make a direct comparison with other work reported in the literature except that for the glass tube water data given in [27] and the limiting "IC" and "ZC" boundary condition analyses presented in [15]. Such a comparison is shown in Fig. 18 with the data points of the water runs omitted, since Fig. 16 indicates that the data can be adequately represented by a straight line. Figure 18 shows that the metal tube water data are below the "IC" prediction. This is quite understandable since the metal tube, with a sizable circumferential resistance, is not a perfect model for the "IC" boundary condition. On the other hand, the glass tube water data lie, in general, below the "ZC" prediction for $Ra < 2.5 \times 10^5$, and above the prediction for higher Rayleigh numbers. When compared with the glass tube water data of Bergles and Simonds [27], the present data have

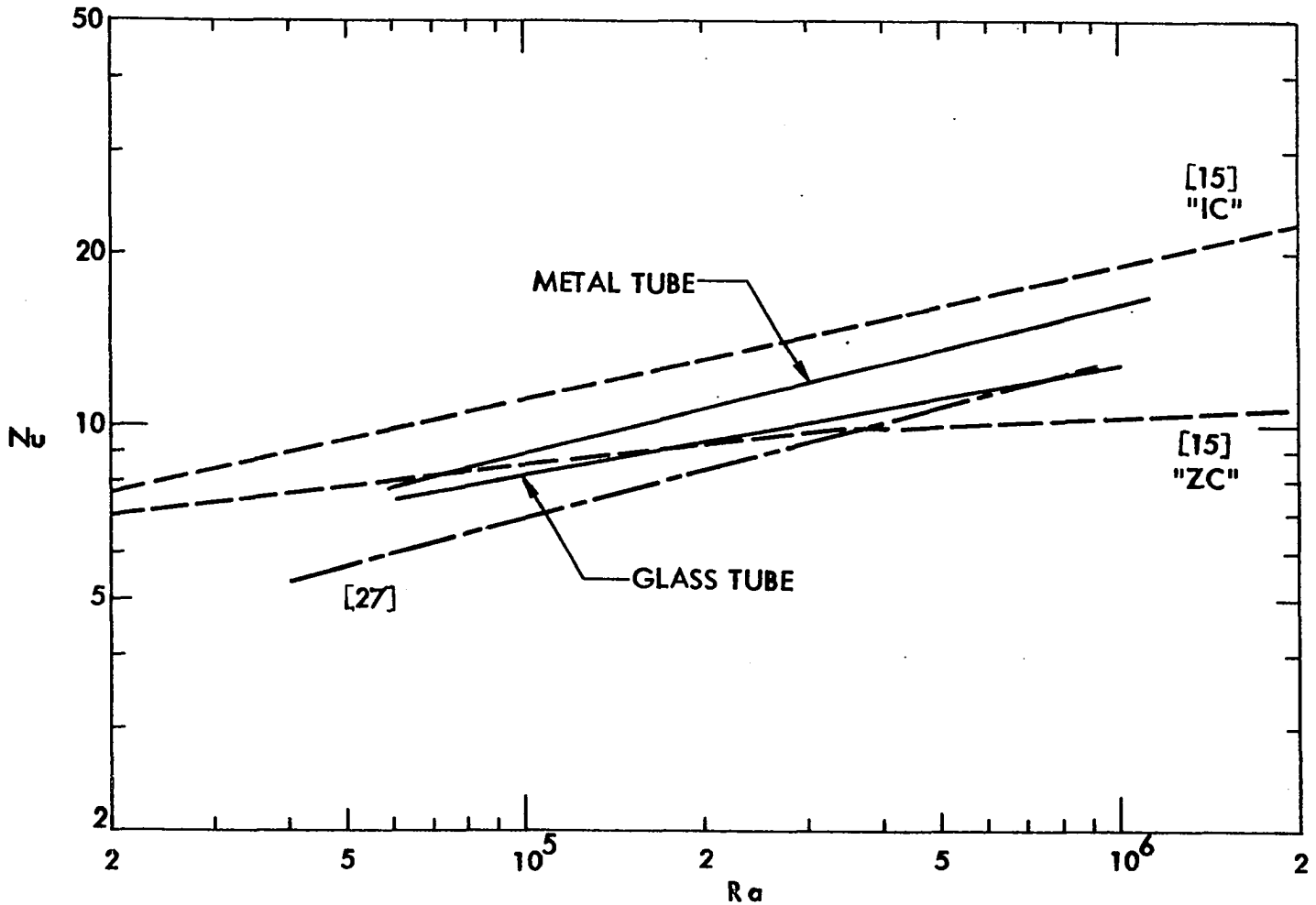

Fig. 18. Comparison of present heat transfer data for water with results from previous investigations

less scatter and are in better agreement with the "ZC" boundary condition prediction. The fact that the present data are higher than the "ZC" prediction at large Rayleigh numbers might be due to the glass tube not being quite faithful to the boundary condition of the analysis. A partial explanation for the behavior of the data at low Rayleigh numbers is that the experimental uncertainty in Nusselt numbers is relatively large at low Rayleigh numbers due to the lower heat flux levels and temperature differences. However, since much experimental data for both glass and metal tubes are reported below the "ZC" prediction, the accuracy of the analysis of [15] in the range of low Rayleigh numbers may be open to question.

2. Correlation of data

Different procedures were used to best correlate the four sets of heat transfer data and to account for the variable transport properties and the tube wall parameters. For the variable fluid properties, the viscosity correction factor proposed by Colburn [36] was first employed. All properties were evaluated at the fluid bulk temperature with the variable property effects lumped into a wall-to-bulk fluid viscosity ratio $(\mu_w/\mu_b)^n$. The viscosity correction factor is a purely empirical quantity, and is not derivable from either the usual dimensional analysis or the governing differential equations. Sieder and Tate [37] suggested $n = -0.14$ based on their experimental results for a fully developed laminar flow of three oils with widely different temperature coefficients of viscosity. The above value of n was confirmed by results of the analysis given by Deissler [38] for liquid metals and by those presented by Shannon and Depew [24] for an exponential variation of viscosity with temperature.

As an example of such a heat transfer data correlation procedure, Fig. 19 shows the viscosity correction factor as it was applied to the metal tube data for both water and ethylene glycol. The wall-to-bulk viscosity ratio ranged from 0.55 to 0.88 for the water data, and from 0.20 to 0.75 for ethylene glycol runs. It is quite clear from the figure that the viscosity correction factor, with $n = -0.14$, can not, by itself, account for the variable property effects. Even when the exponent was varied, the data for both fluids could not be reconciled.

The inadequacy of the viscosity correction factor to account for the variable fluid properties is due to the fact that no property ratio other than viscosity is considered, with the understanding that such properties usually vary much less than viscosity does. This is not quite true for the fluids under consideration, for which the thermal conductivity at 50 ^{o}F differs by about 85 percent from its value at 200 ^{o}F, while the isobaric thermal expansion coefficient of water at 50 ^{o}F is 17 percent of its value at 200 ^{o}F. There is, therefore, enough justification for including an empirical correction factor for properties other than viscosity. The recent proposal by Fand and Keswani [39] to extend the viscosity correction ratio method to include a multiplying correction factor for each dimensionless parameter is somewhat impractical due to the difficulty of obtaining the different exponents.

Fluid velocity and temperature measurements [19, 11] reveal the existence of a thin layer near the wall where velocity and temperature change abruptly. Since the heat transfer occurs at this boundary, it seems that the mean film temperature is a reasonable choice for evaluation of all fluid properties. This choice, in a sense, resembles both

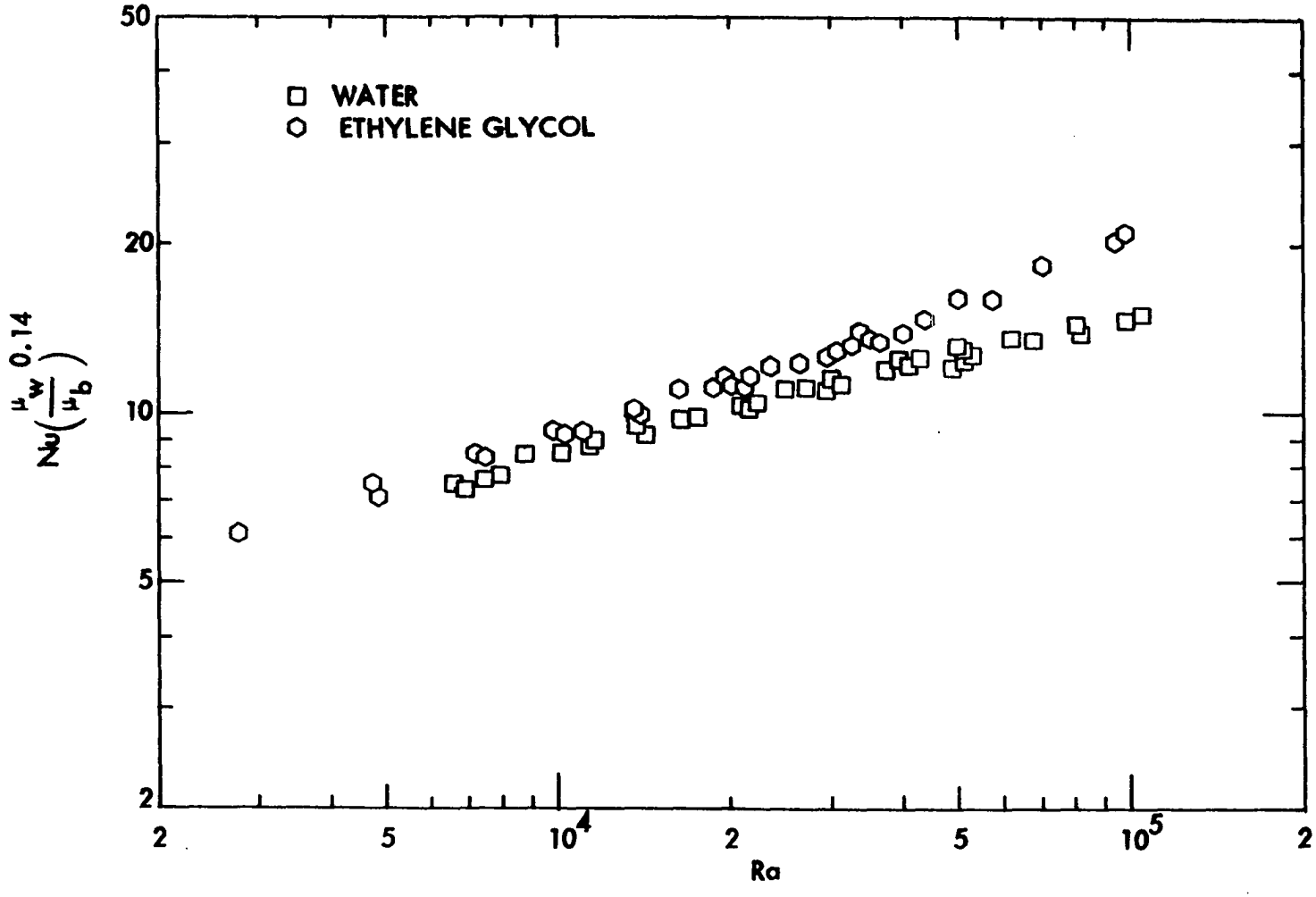

Fig. 19. Viscosity correction factor applied to metal tube with different fluids

the boundary and bulk temperature effects on the fluid properties. Composite plots of the Nusselt versus the Rayleigh numbers for water and ethylene glycol data when film temperature was used are shown in Fig. 20 for the glass tube and in Fig. 21 for the metal tube. It is clear that the ethylene glycol data are higher than those for water for the corresponding tube and that the straight-line character of the data is still preserved. In order to account for the different physical properties of various fluids and reconcile the water and ethylene glycol data for the same tube, the Prandtl number was used as an additional correlating parameter. The dimensionless group $Nu/Pr^{0.34}$ seems to yield acceptable results when plotted versus Gr as shown in Fig. 22 for both glass and metal tubes.

The Grashof number is used in order to avoid having the Prandtl number appear in both the ordinate and abscissa. The water and ethylene glycol data have now been brought together for both the individual tubes; however, the metal tube data are still higher than the data for the glass tube. The discrepancy can be reconciled by considering the tube wall effect.

A steady state energy balance of the tube element ds , shown in Fig. 23, yields

$$q_o'' + q'''t - h(\theta)\ (T_{w,i} - T_b) + k_w \frac{\partial^2}{\partial s^2} \int_{r_1}^{r_2} T_w dr = 0 \qquad (4.1)$$

where q_o'' is the outside peripheral wall heat flux, and q''' is the rate of heat generation per unit volume. For the glass tube, $q''' = 0$, while for the metal tube $q_o'' = 0$. If the radial wall temperature variation

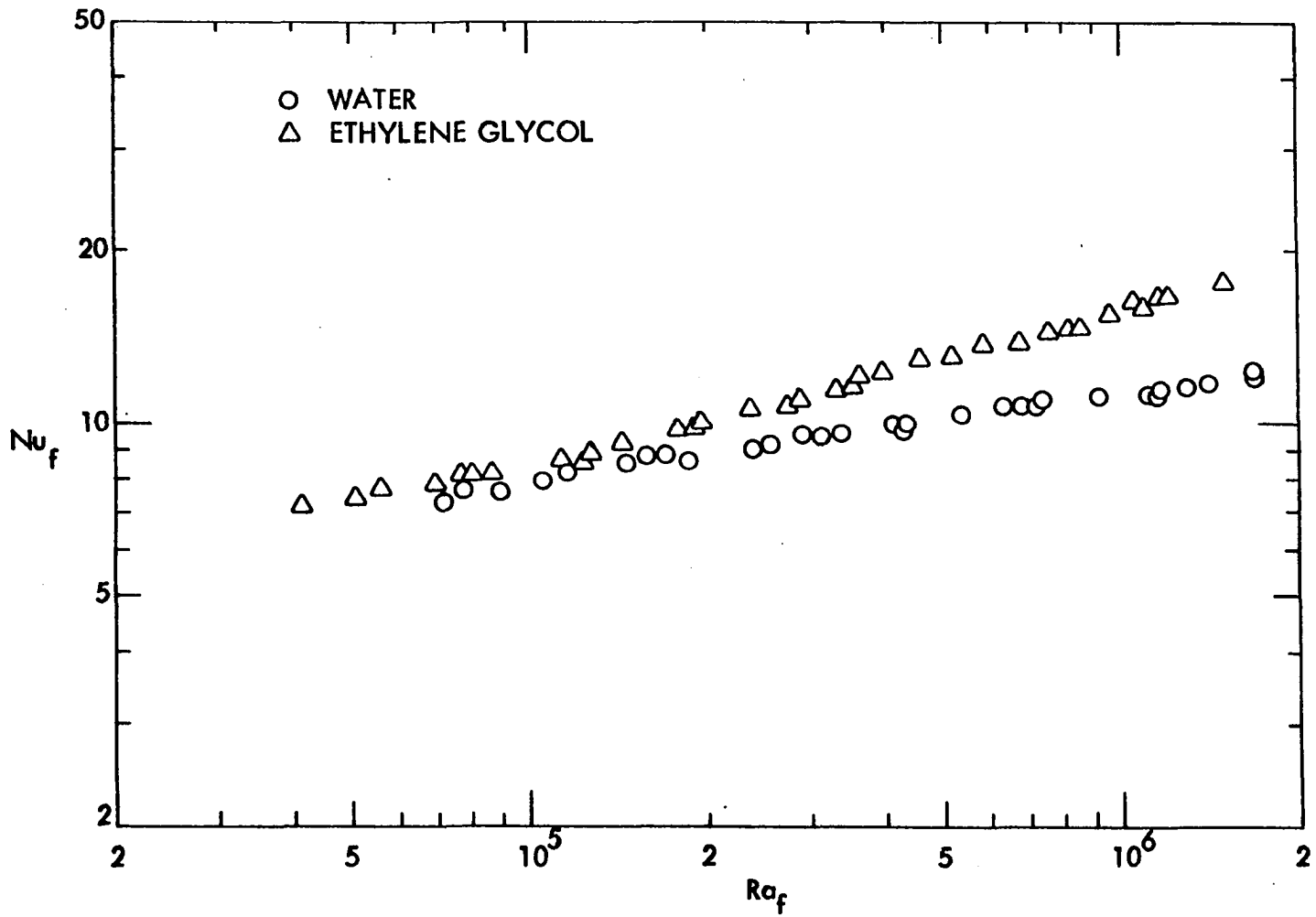

Fig. 20. Heat transfer data evaluated at film temperature for glass tube with different fluids

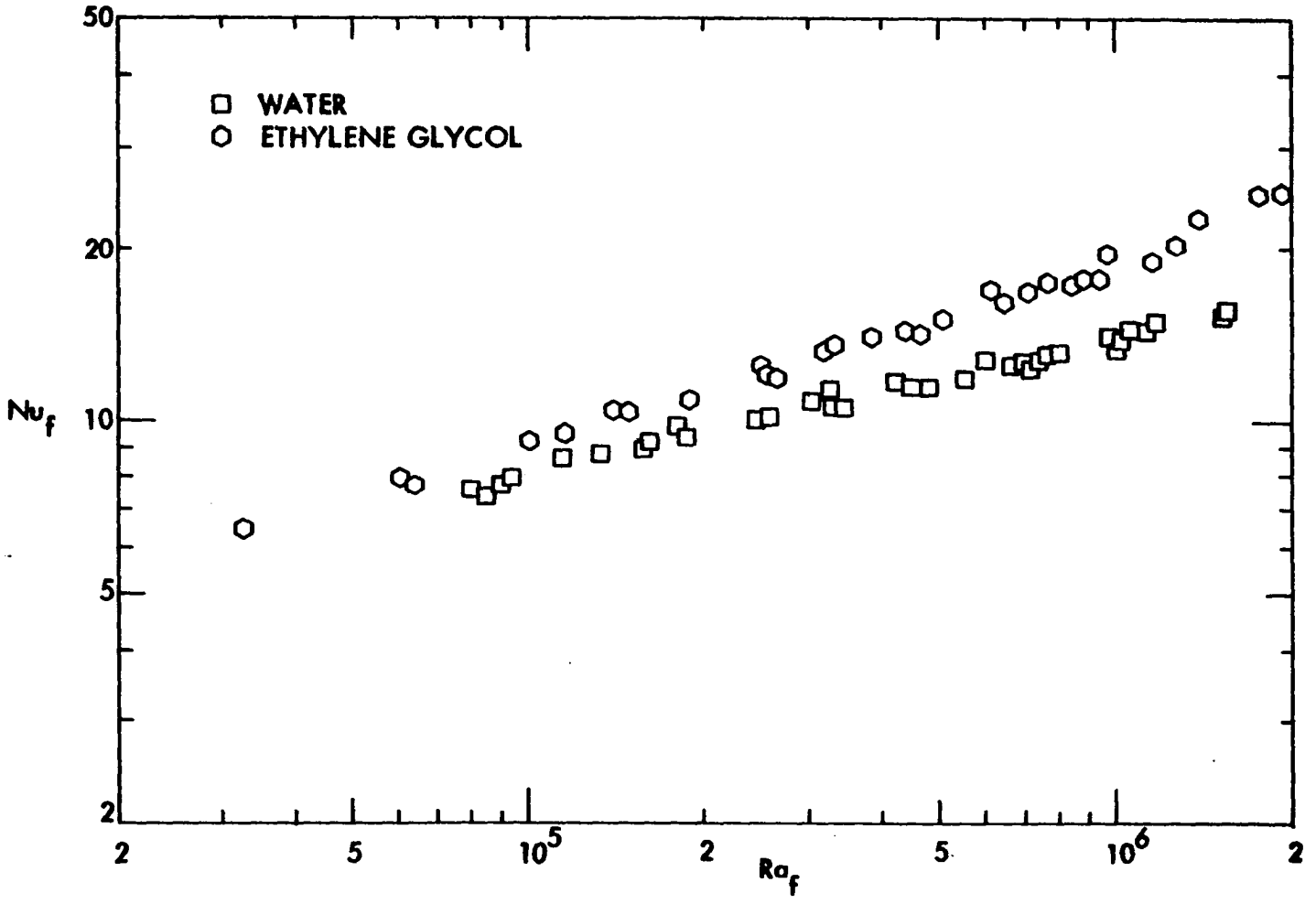

Fig. 21. Heat transfer data evaluated at film temperature for metal tube with different fluids

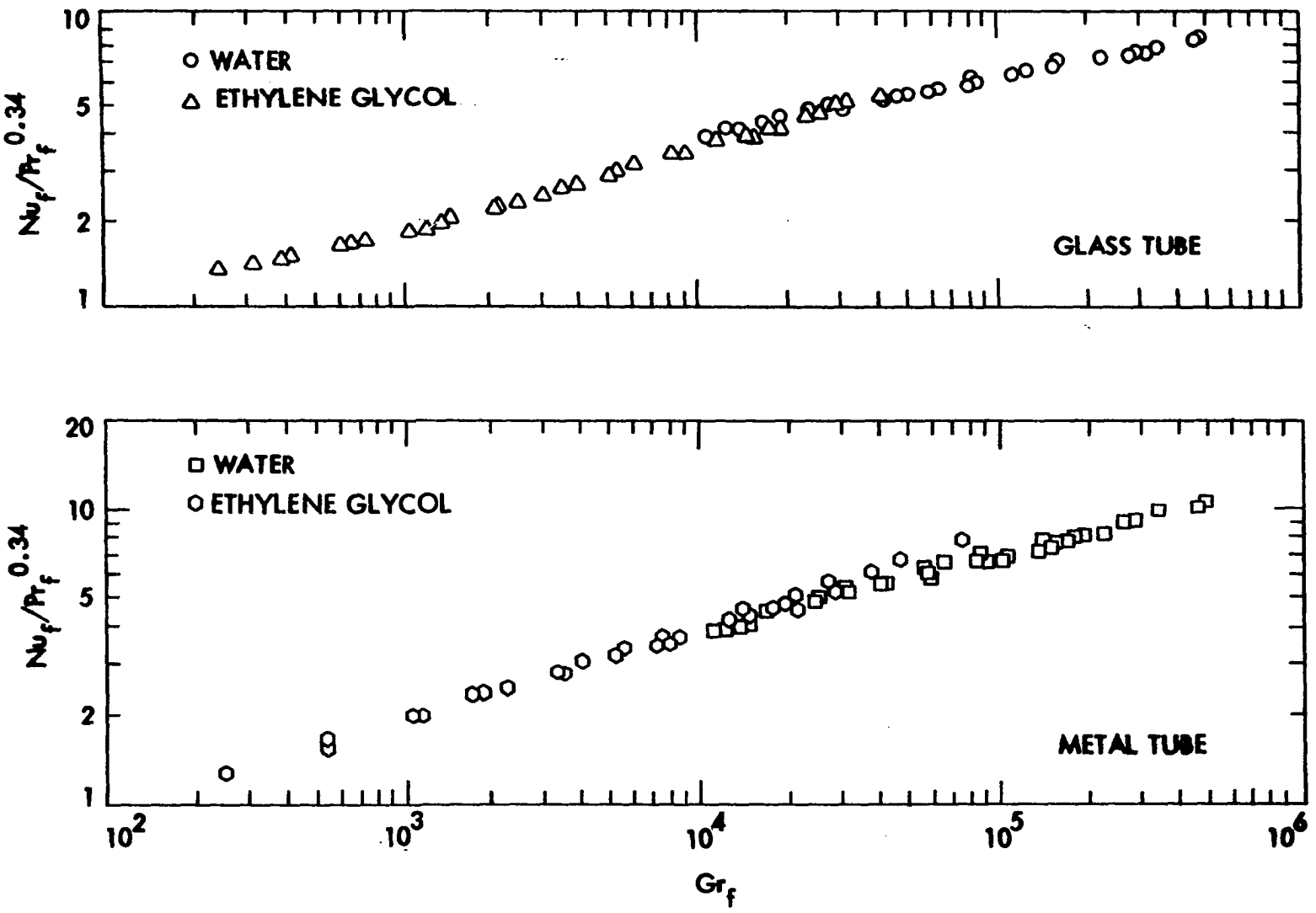

Fig. 22. Correlation of water and ethylene glycol data including Prandtl number effect for different tubes

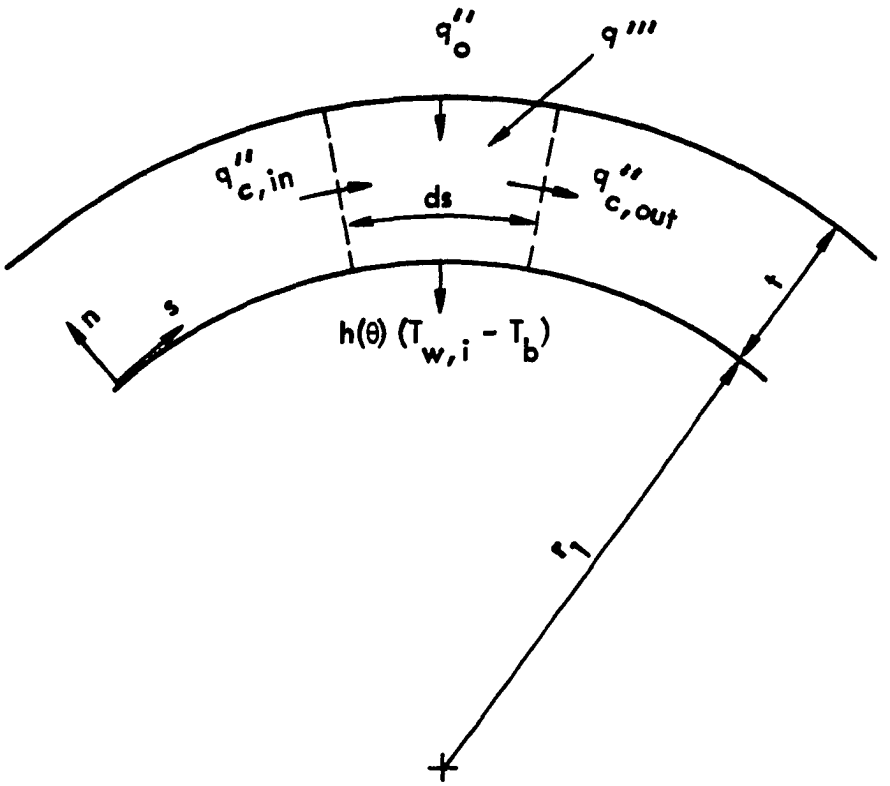

Fig. 23. Steady-state energy balance for a tube wall element

across the thin tube wall is neglected compared to the circumferential variation, then

$$\int_{r_1}^{r_2} T_w dr \cong t\ T_{w,i}$$

where $T_{w,i}$ is the inside tube wall temperature. After the circumferential coordinate s is nondimensionalized by the characteristic dimension d_1, and the local heat transfer coefficient $h(\theta)$ is replaced by an average value h, Eq. (4.1) can be written as

$$\frac{q''_o}{h} + \frac{q'''t}{h} - (T_{w,i} - T_b) + \frac{1}{Pw}\frac{\partial T_{w,i}}{\partial s^{*2}} = 0 \qquad (4.2)$$

where $Pw = (hd_1/k_w)(d_1/t)$ is the tube wall parameter and $s^* = s/d_1$ is a dimensionless circumferential coordinate. The tube wall parameter represents the ratio between the peripheral and radial thermal resistances and can be regarded as an extension of the nondimensional group proposed by both Iqbal et al. [40] and Shah and London [41]. It can also be interpreted as the product of a Biot number and a two-dimensional geometrical ratio. The two extreme theoretical values of Pw, zero and infinity, correspond to the "IC" and "ZC" tube boundary conditions, respectively.

The tube wall parameter Pw was used to account for the tube wall effect. The criteria for determining the exponent of this parameter was to bring together the glass and metal tube data shown in Fig. 22. The final correlation of fluid property and tube wall effects is presented in Fig. 24. With least squares technique, it was found that the following

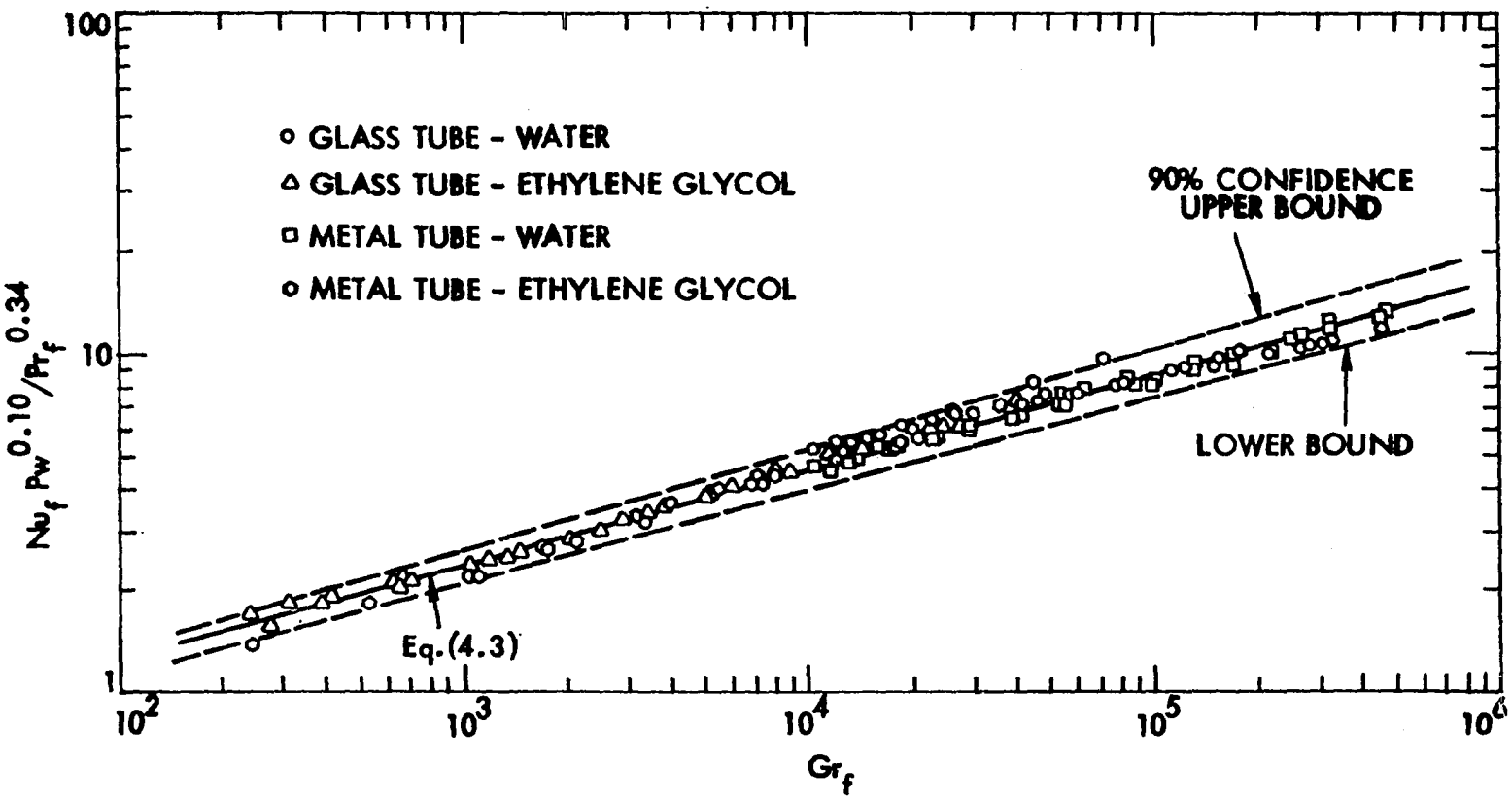

Fig. 24. Final correlation of heat transfer data

equation suitably represented the experimental data:

$$Nu_f = 0.34\ Gr_f^{0.28}\ Pr^{0.34} / Pw^{0.10} \tag{4.3}$$

An error analysis, for which the subroutine ME0226 developed by Mischke and Hall [42] was used, revealed the 90 percent confidence limits on the constant in Eq. (4.3) to be 0.324 as a lower bound and 0.362 as an upper bound. The corresponding confidence limits on the exponent of Gr_f were 0.276 and 0.287, respectively.

The tube wall parameter can be rearranged to read

$$Pw = Nu \left(\frac{k}{k_w}\right)\left(\frac{d_1}{t}\right) \tag{4.4}$$

Combining Eqs. (4.3) and (4.4), one obtains a more convenient, yet accurate, representation of Eq. (4.3) which gives the heat transfer coefficient explicitly as

$$Nu_f = 0.377\ Gr_f^{0.256}\ Pr_f^{0.31} / Pw_f^{*\,0.09} \tag{4.5}$$

where $Pw^{*} = (k/k_w)(d_1/t)$ is the modified tube wall parameter.

A comparison of the present heat transfer correlation with data of previous investigators for various fluids and tube materials is presented in Fig. 25. Since the film temperature is used in the present correlation, it was necessary to recalculate some of the previous data using an estimate of the tube wall temperature level. The lines shown in Fig. 25 represent the mean value for the range of wall temperatures expected. All data of previous investigations fall within the 90 percent confidence

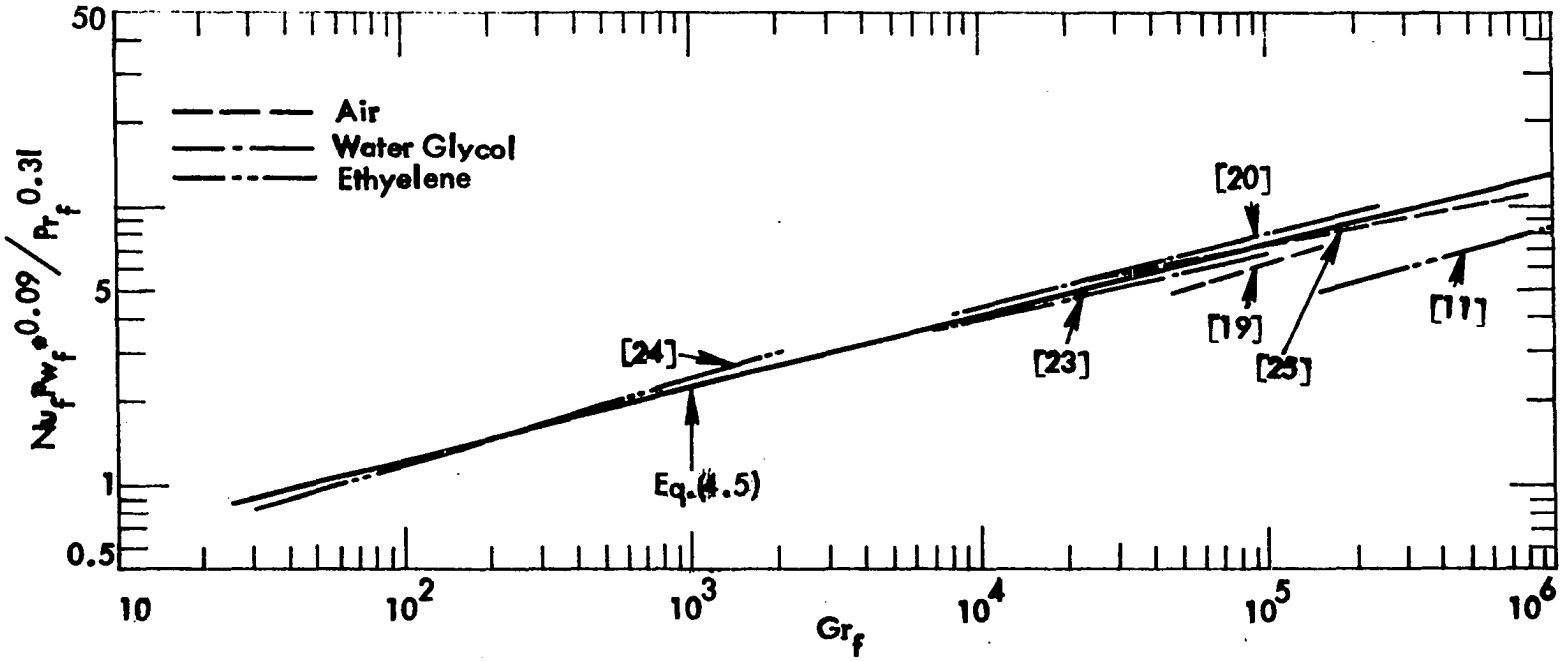

Fig. 25. Comparison of present heat transfer correlation with data from previous investigations

limits of the present correlation, with the exception of the ethylene glycol data presented by Siegwarth et al. [11].

Siegwarth et al. used a 2.5-in i.d aluminum pipe with a 1-in. thick wall. When the tube wall effect was considered, the present tube wall parameter was developed under the assumption that the radial temperature variation across the tube wall could be neglected as compared to the circumferential variation. Since this assumption is not quite valid for the extremely thick aluminum tube, some deviation of the data is to be expected. However, with a value of P_w^* of approximately 0.004, the change is expected to be very small, but is expected to cause a slightly larger deviation of the data.

A more likely explanation for the discrepancy is that axial conduction along the tube wall is responsible for an increase in the actual bulk fluid temperature over the calculated value with the assumption of a constant axial heat flux. This results in a calculated Nusselt number which is too low and a calculated Grashof number which is too high.

B. Pressure Drop

Isothermal friction factor data for water flow in the glass tube are presented in Fig. 26. Meriam blue fluid (1.75 specific gravity) was used as the indicating fluid in the inclined manometer. The experimental data are in good agreement with the Darcy friction factor prediction of 64/Re for laminar flow in tubes.

As for the data for pressure drop during heating, no consistent trend in the experimental results was observed. The isothermal pressure

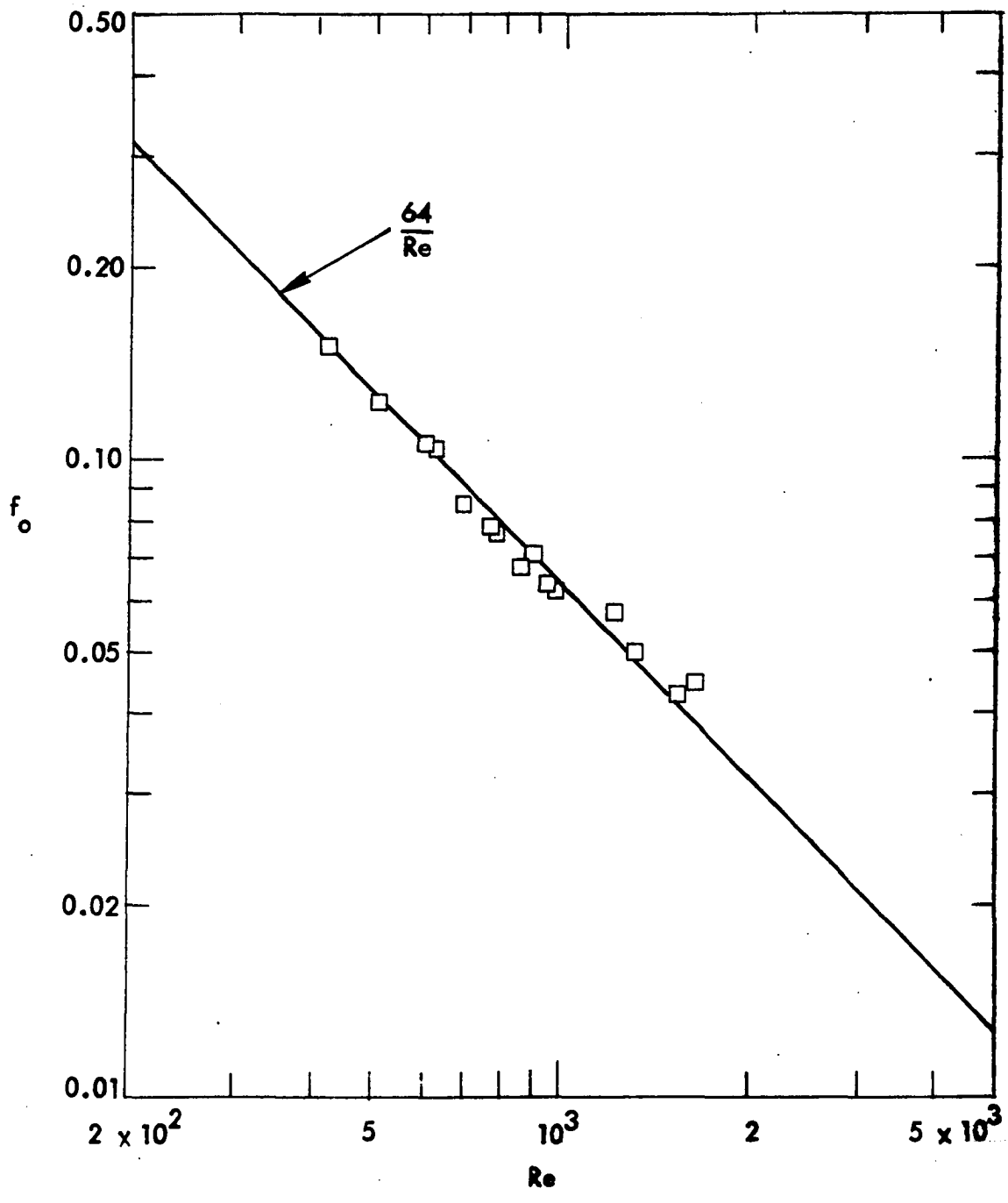

Fig. 26. Isothermal friction factor for water with glass tube

drop across the test section varied between 0.003 psi and 0.007 psi. It was very difficult to obtain any accurate measurements of the secondary flow effects on such extremely low pressure drops. Different measuring techniques were considered; these included the use of either a micromanometer or a differential pressure transducer. The fact that the indicating fluid for the micromanometer is water eliminated the possibility of its use with water as a working fluid. On the other hand, no differential pressure transducer was found to cover such low pressure ranges while at the same time allowing corrosive media on both sides. Therefore, it was decided that pressure drop measurements would be taken only for ethylene glycol runs, since the pressure drop level was more than ten times that for water.

The friction factor data for ethylene glycol, with and without heating, are presented in Fig. 27 for the glass tube and in Fig. 28 for the metal tube. Mercury was the indicating fluid used in the inclined manometer. All fluid properties for the heating runs were evaluated at the mean film temperature at an axial location halfway along the heated section. The isothermal pressure drop data were obtained over a range of Reynolds numbers from 20 to 300. The nonisothermal pressure drop runs were obtained in an interval of Re = 70 to 400 and Pr = 40 to 120.

The agreement between the isothermal friction factor for ethylene glycol with both glass and metal tubes and Darcy's formula is satisfactory. The nonisothermal friction factor iata, on the other hand, are as much as 50 percent higher than the corresponding isothermal values at large Reynolds numbers.

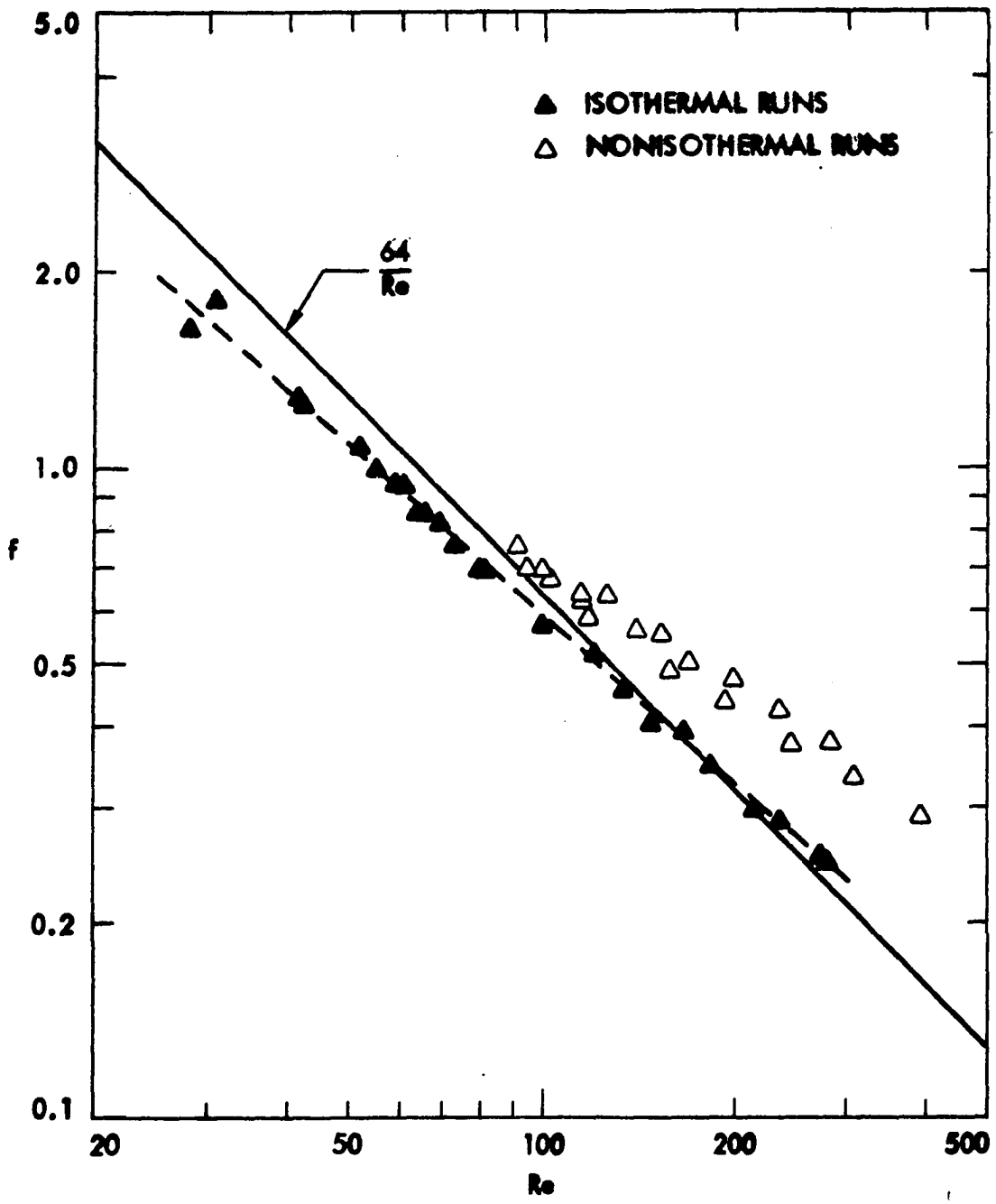

Fig. 27. Friction factor data for ethylene glycol with glass tube

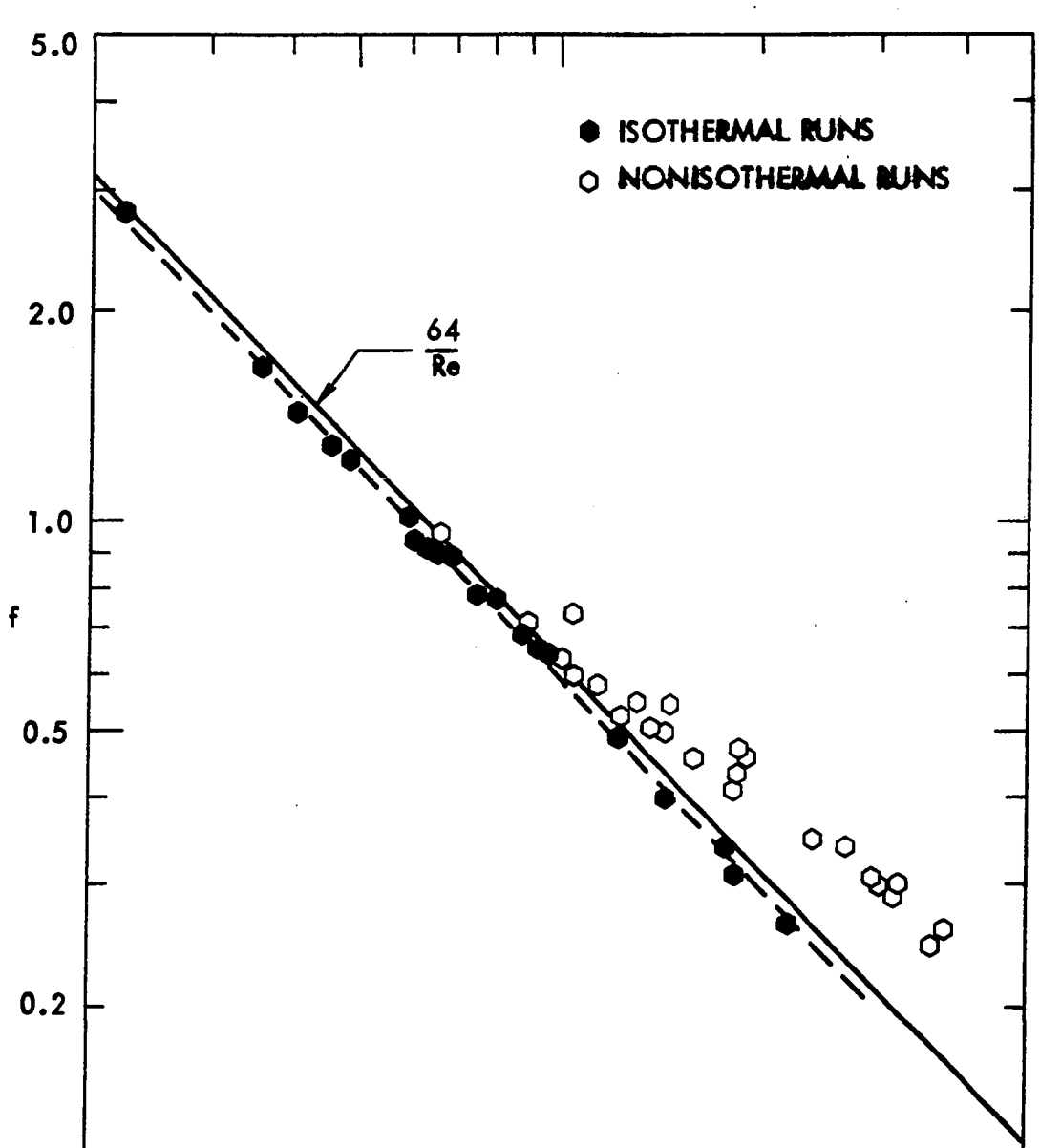

Fig. 28. Friction factor data for ethylene glycol with metal tube

The nonisothermal friction factor data for glass and metal tubes were combined in Fig. 29 as a ratio of f_f/f_o versus Ra_f. The value of f_o was obtained from the curve representing the isothermal data for each tube. The ratio f_f/f_o increases with increasing Rayleigh number as a result of the secondary flow intensity. On the other hand, it seems that f_f/f_o approaches unity at low Rayleigh numbers, as expected. The scatter of the data is largely due to the extremely low pressure drop level and is somewhat magnified by an expanded ordinate. In any event, the tube wall effects do not seem to have a pronounced effect on the friction factor data. A single straight line was, therefore, fitted through the data for the range of Ra_f from 5×10^4 to 2×10^6. A more complex expression which would satisfy the lower limit value of the ratio f_f/f_o was not felt to be warranted. A least squares technique yields the following equation for the line:

$$\frac{f_f}{f_o} = 0.24\ Ra_f^{0.134} \tag{4.6}$$

Using the subroutine ME0226 [42] gave the 90 percent confidence limits on the constant in Eq. (4.6) as 0.266 and 0.218; the corresponding limits on the exponent of Ra_f were 0.141 and 0.126.

Analytical predictions applicable to the range of Rayleigh and Prandtl numbers used for the experimental data are not available. Nevertheless, Fig. 29 shows that the present friction factor data are contained within the "IC" and "ZC" predictions of Newell and Bergles [15] for Pr = 4.5. The present data, however, do not reflect the large difference in

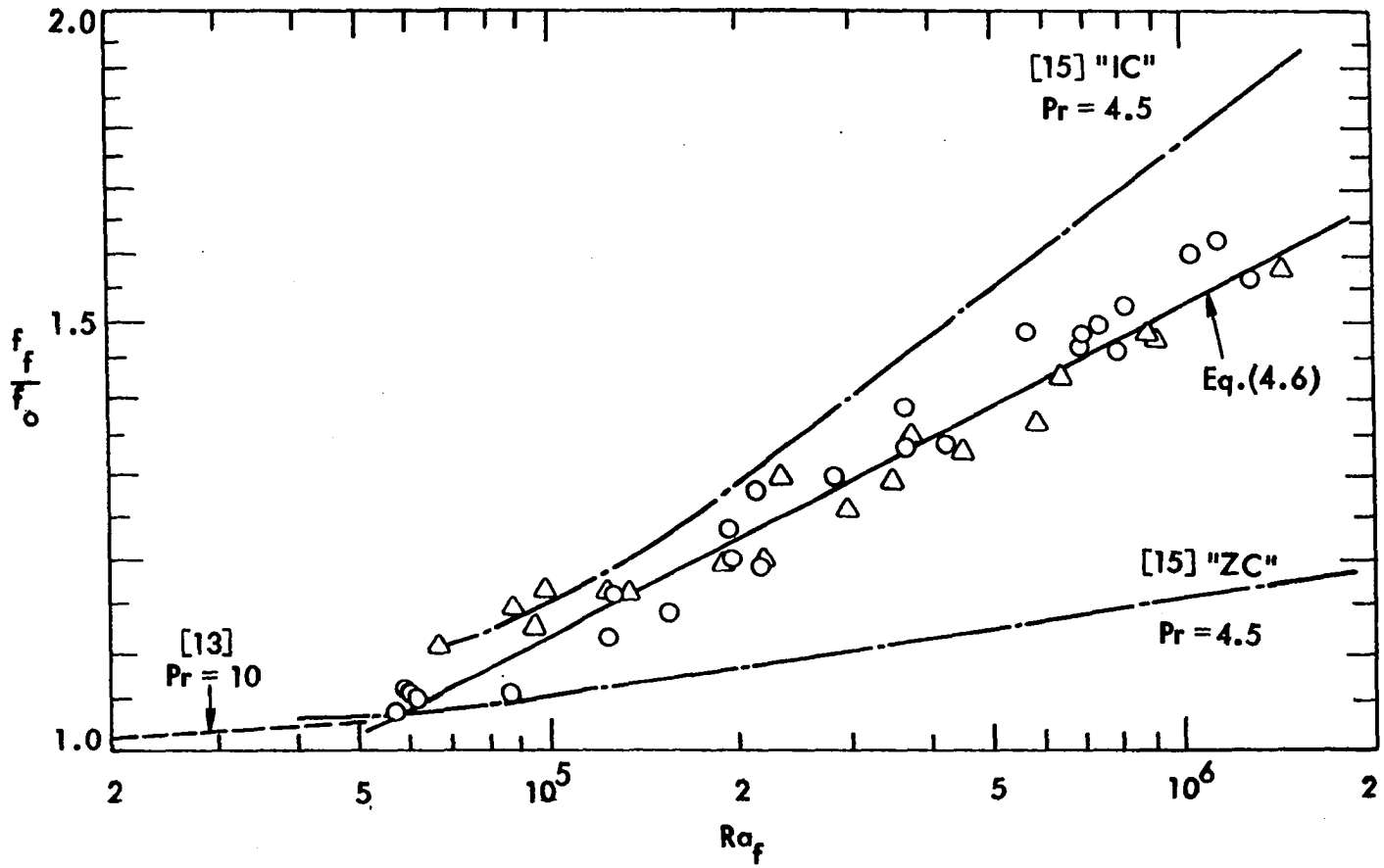

Fig. 29. Comparison of friction factor data for ethylene glycol with results from previous investigations

friction factor between the two boundary conditions of [15]. At low Rayleigh numbers the present experimental results seem to approach the boundary vorticity prediction [13] for Pr = 10. This is in agreement with the fact that the boundary vorticity is applicable only for values of Rayleigh numbers between 10^3 and 10^5.

V. CONCLUSIONS AND RECOMMENDATIONS

An experimental study has been conducted to investigate the effects of fluid property variations, particularly density and viscosity, on a fully-developed laminar flow heat transfer and pressure drop in horizontal tubes with uniform wall heat flux. The test apparatus constructed specifically for this program has proven to be quite suitable in that it allowed maximum flexibility in testing various fluids and test sections. The following conclusions may be drawn from this study:

1. The heat transfer coefficient deviates substantially, by up to a factor of six, from the traditional analytical predictions, mainly due to the inadequacy of the constant property assumptions. The experimental results reveal that the Nusselt number is affected not only by the Rayleigh number and other variations in the physical properties of the working fluid, but also by the circumferential conductance of the tube wall.

2. If the variable property effects are expressed simply as a wall-to-bulk viscosity ratio, a satisfactory correlation cannot be obtained.

3. Evaluating all fluid properties at the film temperature and using Prandtl number as an additional correlation parameter seems to yield acceptable results in bringing the water and ethylene glycol heat transfer data for a given tube together.

4. The tube wall parameter $Pw = \frac{hd_1}{k_w} \frac{d_1}{t}$ was developed to account for the tube wall effects. It represents the ratio between the radial and peripheral tube conductance and can also be regarded as the product of a Biot number and a two-dimensional geometrical factor. The tube wall

parameter was used successfully to reconcile the glass and metal tube data.

5. The final heat transfer correlation, which includes both Prandtl number and the tube wall correlating parameters, is in good agreement with most of the available data from previous investigations for various fluids and tube wall materials. A plausible explanation for the only set of data that deviate substantially from the correlation is given in terms of axial conduction along the very thick wall aluminum tube.

6. The pressure drop data indicate that the friction factor increases with increasing Rayleigh numbers. However, the type of tube wall has a much less pronounced effect on the friction factor than on the heat transfer coefficient.

7. Within the range of Rayleigh and Prandtl numbers considered in the friction factor tests, no applicable data are available for comparison. However, the present data are within the lower and supper bounds of the available analytical predictions.

Although this study has resolved many practical questions pertaining to accurate predictions of laminar flow heat transfer and pressure drop, the following areas need further investigation:

1. The present heat transfer correlation development is based on the four sets of data for two working fluids and two test section materials. Even though the final correlation seems to be in good agreement with the available data from previous investigations using different fluids and tubes, a testing of higher viscosity fluids and test

sections with higher circumferential conductance would provide a more extensive check of the present correlation.

2. The nonisothermal pressure drop tests were limited to ethylene glycol due to the difficulty of measuring the extremely low pressure drops for distilled water. It would be desirable to develop a means for obtaining pressure drop data for liquids with low Prandtl numbers, such as water, and to extend the range to high Prandtl number fluids. These tests would be useful in assessing the range of validity of the proposed correlation.

3. The present study was focused on the fully-developed case since the developing length for the combined forced and free convection flow is much shorter than that required in the absence of free convection effects. However, a study of the variable fluid properties and the tube wall effects in the entrance region might prove to be helpful for designing relatively short heat exchangers.

4. The present experimental results suggest that future analytical studies should consider the conjugated problem with variable fluid properties, where the energy equations for the wall-fluid system are coupled with the mementun equations for the fluid.

5. The present investigation should be extended to the other classical boundary condition of uniform wall temperature, which is approximated in many practical applications. Even though considerable experimental work has been done in this area, a consideration of the tube wall effect, particularly in case of finite wall thermal resistance, is still lacking.

VI. APPENDIX A:

WORKING FLUID PROPERTIES

This appendix contains the physical and transport properties of both water and ethylene glycol. Six properties were utilized for each fluid: density, isobaric thermal expansion coefficient, enthalpy, viscosity, thermal conductivity, and Prandtl number. The working fluid properties depend strictly on two state variables, pressure and temperature. Since the pressure variations in the system were too small to affect the fluid properties, they were adequately represented by functions of temperature.

All properties were put in analytical form by fitting a power polynomial through the data points. The polynomial expression for each property has been compared with the reference data and, within the listed temperature range, has be found to deviate by no more than the percentage error indicated.

A. Distilled Water

The data points listed below were taken from the ASME Steam Tables [43] corresponding to 20 psia.

1. Density

Data points:

T (^{o}F)	ρ (lbm/ft^3)
50	62.4220
100	61.9963
150	61.1995
200	60.0962

Equation:

$$\rho = 62.422 - 0.21862\ \theta - 0.21785\ \theta^2 + 0.01077\ \theta^3 \quad \text{lbm/ft}^3 \qquad \text{(A.1)}$$

where

$$\theta = \frac{T - 50^{\circ}F}{50^{\circ}F} \qquad \text{(A.2)}$$

Temperature range: 50-200 $^{\circ}F$

Maximum error: 0.02%

2. Isobaric thermal expansion coefficient

The isobaric thermal expansion coefficient is defined by the equation

$$\beta = -\frac{1}{\rho}\left(\frac{\partial \rho}{\partial T}\right)_p \qquad \text{(A.3)}$$

By using Eq. (A.1), one can write β as

$$\beta = -\frac{-0.21862 - 0.43570\ \theta + 0.03231\ \theta^2}{50(62.422 - 0.21862\ \theta - 0.21785\ \theta^2 + 0.01077\ \theta^3)}\ \frac{1}{^{\circ}F} \qquad \text{(A.4)}$$

where

$$\theta = \frac{T - 50^{\circ}F}{50^{\circ}F} \qquad \text{(A.5)}$$

3. Enthalpy

Data points:

T ($^{\circ}F$)	μ (lb-sec/ft^2)
50	18.11
200	168.11

Equation:

$$i = T - 31.89 \text{ Btu/lbm} \tag{A.6}$$

Temperature range: 50-200 ^{o}F

Maximum error: 0.03%

In the data reduction, an expression for fluid temperature as a function of enthalpy was needed. Eq. (A.6) was rearranged to yield

$$T = i + 31.80\ ^{o}F \tag{A.7}$$

4. Viscosity

Data points:

T (^{o}F)	μ (lb-sec/ft^2)
50	271.4×10^{-7}
100	142.0
150	89.1
200	62.6

Equation:

$$\mu = \exp(5.6036 - 0.76097\ \theta + 0.1245\ \theta^2 - 0.01133\ \theta^3)$$

$$\times\ 0.0115826 \quad \text{lbm/ft-hr} \tag{A.8}$$

where

$$\theta = \frac{T - 50^{o}F}{50^{o}F} \tag{A.9}$$

Temperature range: 50-200 ^{o}F

Maximum error: 0.74%

5. Thermal conductivity

Data points:

T (^{o}F)	k (Btu/hr-ft-^{o}F)
50	0.3392
100	0.3633
150	0.3806

Equation:

$$k = 0.3392 + 0.0275\ \theta - 0.0034\ \theta^2 \quad \text{Btu/hr-ft-}^{o}\text{F} \tag{A.10}$$

where

$$\theta = \frac{T - 50^{o}F}{50^{o}F} \tag{A.11}$$

Temperature range: 50-200^{o}F

Maximum error: 0.13%

6. Prandtl number

Data points:

T (^{o}F)	Pr
50	9.28
100	4.52
150	2.71
200	1.86

Equation:

$$Pr = \exp(2.2279 - 0.84747\ \theta + 0.14015\ \theta^2 - 0.012083\ \theta^3) \tag{A.12}$$

where

$$\theta = \frac{T - 50^{\circ}F}{50^{\circ}F} \tag{A.13}$$

Temperature range: 50-200°F

Maximum error: 0.28%

B. Ethylene Glycol

The physical properties of ethylene glycol were taken from references [44, 45].

1. Density

Equation: The following expression for the specific volume v, cm^3/gm, as a function of temperature T, °C, was reported in reference [44].

$$v = 0.924848 + 6.2796 \times 10^{-4}\ \theta + 9.2444 \times 10^{-7}\ \theta^2 + 3.057 \times 10^{-9}\ \theta^3 \quad cm^3/gm \tag{A.14}$$

where

$$\theta = T - 65^{\circ}C \tag{A.15}$$

The density can be obtained from Eq. (A.14), according to the relation

$$\rho = \frac{62.43}{v} \quad lbm/ft^3 \tag{A.16}$$

Temperature range: 40-340 °F

Maximum error: 0.18%

2. Isobaric thermal expansion coefficient

The definition of β, as give by Eq. (A.3), can also be rearranged to read

$$\beta = \frac{1}{v}\left(\frac{\partial v}{\partial T}\right)_p \qquad (A.17)$$

Using Eq. (A.14), one can express β as

$$\beta = \frac{6.2796 \times 10^{-4} + 1.84888 \times 10^{-6}\ \theta + 9.171 \times 10^{-9}\ \theta^2}{1.8(0.924848 + 6.2796 \times 10^{-4}\ \theta + 9.2444 \times 10^{-7}\ \theta^2 + 3.057 \times 10^{-9}\ \theta^3)} \quad 1/^{\circ}F \qquad (A.18)$$

3. Enthalpy

Data points:

T ($^{\circ}$F)	c_p (Btu/lbm-$^{\circ}$F)
60	0.553
140	0.598
220	0.650

Equation:

$$c_p = 0.553 + 0.04150\ \theta + 0.0035\ \theta^2 \quad \text{Btu/lbm-}^{\circ}F \qquad (A.19)$$

where

$$\theta = \frac{T - 60^{\circ}F}{80^{\circ}F} \qquad (A.20)$$

Eq. (A.19) was integrated along the isobar p = 0 psig and the enthalpy was arbitrarily chosen to be zero at the freezing point T = 9.14 $^{\circ}$F. The final result is given by

$$i = 27.4786 + 44.24\ \theta + 1.66\ \theta^2 + 0.09333\ \theta^3 \quad \text{Btu/lbm} \quad \text{(A.21)}$$

Temperature range: 40-300 ^{o}F

Maximum error: For specific heat at constant pressure, the maximum error was 0.12%. The expression for enthalpy was numerically differentiated and compared with the computed values of specific heat. The comparison showed no difference within the accuracy of computation.

Eq. (A.21) was also rearranged to yield an expression for temperature as a function of enthalpy.

4. Viscosity

Data points:

T (^{o}F)	μ (centipoise)
40	45.0
100	10.38
160	3.86
220	1.89
280	1.10

Equation:

$$\mu = \exp(3.80666 - 1.79809\ \theta + 0.38590\ \theta^2 - 0.05878\ \theta^3 + 0.004173\ \theta^4) \times 2.42 \quad \text{lbm/hr-ft} \quad \text{(A.22)}$$

where

$$\theta = \frac{T - 40^{o}F}{60^{o}F} \quad \text{(A.23)}$$

Temperature range: 40-300 ^{o}F

Maximum error: 0.56%

5. Thermal conductivity

Data points:

T (^{o}F)	k (Btu/hr-ft-^{o}F)
50	0.1710
150	0.1480

Equation:

$$k = 0.1825 - 2.3 \times 10^{-4} T \quad \text{Btu/hr-ft-}^{o}\text{F} \tag{A.24}$$

Temperature range: 40-350 ^{o}F

Maximum error: There is no difference between the computed value and the input data within the accuracy of computation.

6. Prandtl number

Data points:

T (^{o}F)	Pr
40	340.587
120	65.754
200	26.468
280	15.620

Equation:

$$Pr = \exp(5.83067 - 2.12950\ \theta + 0.54344\ \theta^2 - 0.058687\ \theta^3) \tag{A.25}$$

where

$$\theta = \frac{T - 40^{o}\text{F}}{80^{o}\text{F}} \tag{A.26}$$

Temperature range: 40-300^{o}F

Maximum error: 0.69%

VII. APPENDIX B:

CALIBRATION OF FLOWMETER

The flowmeter used was a Brooks rotameter, Model 1307, Size 7, Serial No. 7210-36292. Two spherical floats of Pyrex (specific gravity 2.20) and Monel (specific gravity 8.84) were used to provide accurate measurements of the flow rate within the range of interest. The flowmeter was calibrated by weighing the fluid collected for a measured time interval at different flow settings. A constant-head tank was used to supply the desired flow rate. Since the viscosity immunity ceiling of both floats is 5 centistokes, it was necessary to calibrate the flowmeter when using water and ethylene glycol. The calibration data for both fluids are given below.

A. Distilled Water

The Pyrex and Monel floats were both calibrated with distilled water. The duration of each calibration run ranged from 5 to 15 minutes for the Pyrex float, and from 3 to 10 minutes for the Monel float. The calibration data, taken at an average temperature of $68^{\circ}F$, are given in Table 2, and the calibration curve is shown in Fig. 30.

Table 2. Flowmeter calibration data for distilled water

Flowmeter reading (percent)	Actual flow rate (lbm/min)	
	Pyrex float	Monel float
10.0	0.075	0.320
20.0	0.244	0.703
30.0	0.395	1.067
40.0	0.536	1.405
50.0	0.670	1.730
60.0	0.794	2.039
70.0	0.919	2.336
80.0	1.035	2.576
90.0	1.142	2.841
100.0	1.248	3.100

A polynomial expression of the mass flow rate as a function of the float position was obtained by fitting a power polynomial through the experimental data points. The final expression for the Pyrex float is given by

$$\dot{m} = 0.0750 + 0.507333\ FP - 0.0504\ FP^2 + 0.003867\ FP^3 \text{ lbm/min} \quad \text{(B.1)}$$

where

$$FP = \frac{\text{Pyrex float reading} - 10}{30} \quad \text{(B.2)}$$

The expression for the Monel float is given by

$$\dot{m} = 0.703 + 1.473\ FM - 0.137\ FM^2 \text{ lbm/min} \quad \text{(B.3)}$$

where

$$FM = \frac{\text{Monel float reading} - 20}{40} \quad \text{(B.4)}$$

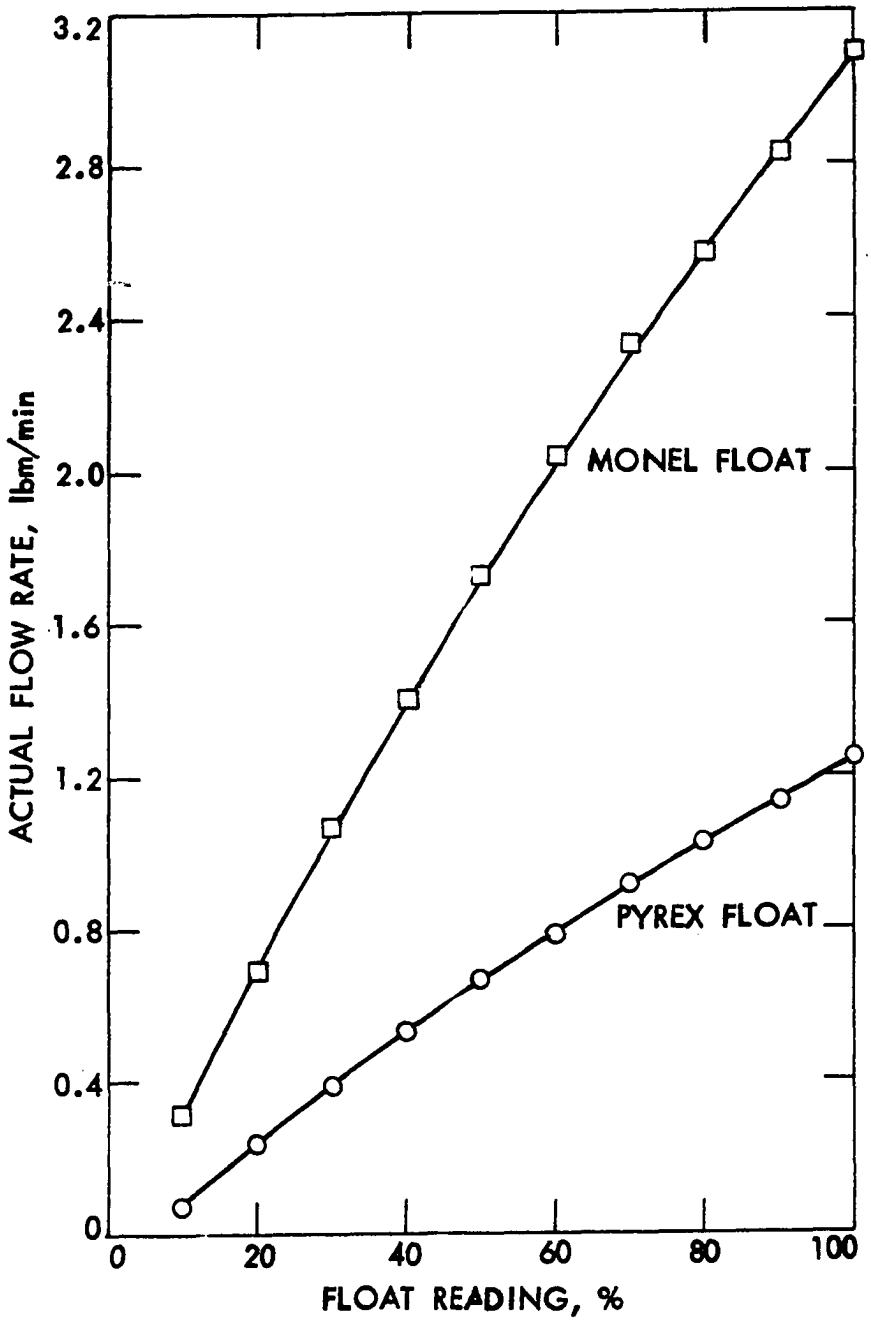

Fig. 30. Calibration curve for flowmeter with water

B. Ethylene Glycol

In order to obtain the desired range of flow rate for ethylene glycol, it was only necessary to calibrate the Monel float. Since the flow rates were generally lower than those of water, the duration of each run was increased to range from 5 to 18 minutes. The calibration data for an average fluid temperature of 78°F are given below; the calibration curve is shown in Fig. 31.

Table 3. Flowmeter calibration data for ethylene glycol

Flowmeter reading (percent)	Actual flow rate (lbm/min)
10.0	0.0287
20.0	0.1109
30.0	0.2405
40.0	0.4159
50.0	0.6869
60.0	0.9417
70.0	1.1726
80.0	1.3728
90.0	1.5860
100.0	1.8406

During the heat transfer and pressure drop runs, provisions were made to keep the inlet fluid temperature to the flow meter as close as possible to 78°F to avoid any errors in the calibration data. Due to the nature of the calibration curve, it was not possible to fit accurate power polynomial through the data points. However, numerical interpolation of the data points was performed whenever needed.

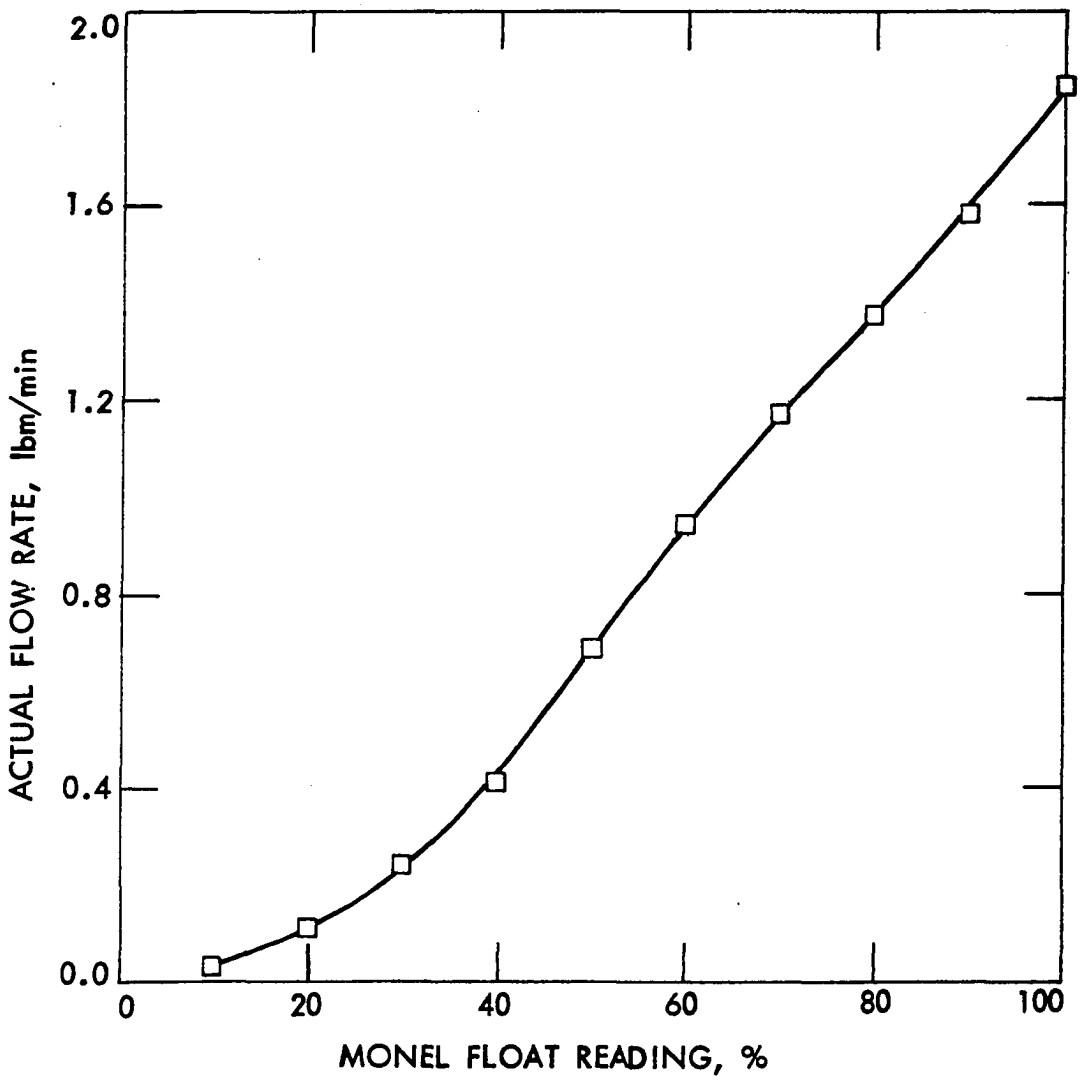

Fig. 31. Calibration curve for flowmeter with ethylene glycol

VIII. APPENDIX C:

DUMMY LOAD CHARACTERISTICS

The total load resistance consists of three elements: test section, power cables, and dummy load. Resistance calculations for each element are given below:

Test section Various measurements of the voltage drop across the stainless steel tube and the current through it showed the average value of the test section resistance at room temperature to be

$$R_t = 0.0525 \text{ ohm}$$

Power cables Power connections to the test section were made with about 40 feet of No. 3/0 TWH copper cables

$$\rho_e = 1.673 \times 10^{-6} \text{ ohm-cm}$$

$$A = 0.132 \text{ in.}^2$$

$$R_c = \frac{\rho_e L}{A}$$

$$= \frac{1.673 \times 10^{-6} \times 40 \times 30.48}{0.132 \times (254)^2}$$

$$= 0.0024 \text{ ohm}$$

Dummy load The dummy load consists of 18 power resistors, each with an electric resistance of 7.1 ohm and a maximum current capacity of 12 amp.

The power resistors were arranged in three rows, each having six elements connected in parallel. It was possible to connect one, two, or three

parallel rows in series with the test section, depending on the power level required. The calculations for these three possibilities are listed below.

Six elements in parallel

Maximum allowable current, $I_m = 6 \times 12 = 72$ amp

Total dummy load resistance, $R_d = \frac{7.1}{6}$

$= 1.1833$ ohm

The total load resistance, $R_\ell = R_t + R_c + R_d$

$= 0.0525 + 0.0024 + 1.1833$

$= 1.2382$ ohm

Twelve elements in parallel

$I_m = 12 \times 12 = 144$ amp

$R_d = \frac{7.1}{12} = 0.5197$ ohm

$R_\ell = 0.0525 + 0.0024 + 0.5197$

$= 0.6466$ ohm

Eighteen elements in parallel

$I_m = 18 \times 12 = 216$ amp

$R_d = \frac{7.1}{18} = 0.3944$ ohm

$$R_{\ell} = 0.0525 + 0.0024 + 0.3944$$

$$= 0.4493 \text{ ohm}$$

With these three arrangements, it was possible to match the dummy load characteristics with the dc generator characteristics while allowing for the selection of different power levels within the allowable range of current capacity. The combined characteristics of the dummy load and the dc generator are shown in Fig. 9.

IX. APPENDIX D:

HEAT LOSS

The heat loss from the outside surface of the tube was calculated from the measured outer tube wall temperature and the room temperature using the thickness and thermal conductivity of different insulating layers. As mentioned earlier in the text, a thin insulating paper was used to electrically insulate the thermocouple beads from the tube wall. A Scotch Glass Cloth Electric Tape No. 27 was then used to cover the thermocouple beads. Finally, the tube was heavily insulated with glass fiber insulation, with small air gap being left between the tube and the inner surface of the insulation. The dimensions of various material layers for the metal tube and their thermal conductivities are given in the table below.

Table 4. Dimensional and property information for calculations of metal tube heat loss

	d_i (in.)	d_o (in.)	k (Btu/hr-ft-^oF)
Metal tube (1-2)	0.401	0.441	9.4
Insulating paper (2-3)	0.441	0.447	0.0642
Tape No. 27 (3-4)	0.447	0.459	0.10
Air gap (4-5)	0.459	0.563	0.015
Glass fiber (5-6)	0.563	2.438	0.022

The following equation for heat conduction through a composite wall was used to obtain the heat loss per unit length of the tube:

$$q'_{\ell} = \frac{2\pi \left(T_3 - T_6\right)}{\sum_{n=3}^{5} \frac{\ell n \left(d_o/d_i\right)_n}{k_n}} \tag{D.1}$$

where the numbers correspond to the various layers designated in Table 4. On the outer surface of the insulating tube, the heat loss due to free convection is given by

$$q'_{\ell} = h_{nc} \pi d_6 \left(T_6 - T_{\infty}\right) \tag{D.2}$$

where h_{nc} is the natural convection heat transfer coefficient and T_{∞} is the ambient temperature. Combining Eqs. (D.1) and (D.2), the heat loss per unit length of the tube can be easily calculated from the following expression:

$$q'_{\ell} = \frac{\pi \left(T_3 - T_{\infty}\right)}{\frac{1}{2} \sum_{n=3}^{5} \frac{\ell n \left(d_o/d_i\right)_n}{k_n} + \frac{1}{h_{nc}\, d_6}} \tag{D.3}$$

Run 25 for ethylene glycol in the metal tube was used to obtain the magnitude of the heat loss as a percentage of the total heat added. The variables pertinent to the heat loss calculations, taken from Appendix F, are given below

q = 3904.8 Btu/hr

q' = 976.2 Btu/hr-ft

T_3 = 207.6 ^{o}F

T_{∞} = 76.0 ^{o}F

The outer temperature of the glass fiber tube T_6 and the natural convection heat transfer coefficient h_{nc} were obtained through an iterative procedure, using the equation given in reference [46] :

$$Nu_f = 0.53\ (Gr_f\ Pr_f)^{0.25} \qquad (D.4)$$

The final results are given by

$$T_6 = 93.2\ ^{o}F$$

$$h_{nc} = 0.819\ Btu/hr\text{-}ft^2\text{-}^{o}F$$

Using Eq. (D.3), the heat loss per unit length of the tube can then be calculated as

$$q'_\ell = \frac{\pi\ (207.62 - 76.0)}{\frac{1}{2}\left[\frac{\ell n\left(\frac{0.459}{0.447}\right)}{0.10} + \frac{\ell n\left(\frac{0.563}{0.459}\right)}{0.015} + \frac{\ell n\left(\frac{2.438}{0.563}\right)}{0.022}\right] + \frac{12}{0.812 \times 2.438}}$$

$$= 8.94\ Btu/hr\text{-}ft$$

The heat loss, as a percentage of the total heat added, is given by

$$\frac{q'_\ell}{q'} = \frac{8.94}{976.2} = 0.92\%$$

Similar calculations for various runs indicated that an average value for the heat loss could be set at 1.5 percent of the total heat added.

X. APPENDIX E:

CIRCUMFERENTIAL HEAT FLUX DISTRIBUTION

This appendix contains the details of the solution of the two-dimensional energy equation for the tube wall which was presented in Chapter III. Since the glass and metal tubes have different boundary conditions on the outside surface, their respective solutions will be dealt with separately.

A. Glass Tube

When polar coordinates are used the heat conduction equation for the tube wall takes the form

$$\frac{\partial T_w}{\partial r^2} + \frac{1}{r}\frac{\partial T_w}{\partial r} + \frac{1}{r^2}\frac{\partial^2 T_w}{\partial \theta^2} = 0 \qquad \text{(E.1)}$$

When the nondimensional variables

$$\tau_w\left(R,\theta\right) = \frac{T_w\ (r,\theta) - T_{w,o5}}{T_{w,o1} - T_{w,o5}} \qquad \text{(E.2)}$$

and

$$R = \frac{r}{r_2} \qquad \text{(E.3)}$$

are used, Eq. (E.1) can be written as

$$\frac{\partial^2 \tau_w}{\partial R^2} + \frac{1}{R}\frac{\partial \tau_w}{\partial R} + \frac{1}{R^2}\frac{\partial^2 \tau_w}{\partial \theta^2} = 0 \qquad \text{(E.4)}$$

The angle θ is measured clockwise from the vertex of the tube, and the outside wall temperatures $T_{w,o}$ are numbered 1 through 5 to signify 45^{o} intervals.

On the outer tube surface, the temperature is measured at eight discrete points. A periodic function $f(\theta)$ is used to approximate the nondimensional outside tube wall temperature, as will be explained later. Since the heat is generated uniformly around the outer circumference of the tube and the heavy insulation resulted in a very small heat loss, the radial temperature gradient is assumed constant. The thermal boundary conditions at the outer surface of the tube can, therefore, be written as

$$\tau_w (1,\theta) = f(\theta) \tag{E.5}$$

and

$$\left(\frac{\partial \tau_w}{\partial R}\right)_{1,\theta} = \frac{q_o'' r_2}{k_w \left(T_{w,o1} - T_{w,o5}\right)} = q_c = \text{constant} \tag{E.6}$$

Assuming a particular product solution of the form

$$\tau_w (R,\theta) = \phi(R)\ \psi(\theta) \tag{E.7}$$

Eq. (E.4) becomes

$$\phi''\psi + \frac{1}{R}\phi'\psi + \frac{1}{R^2}\phi\psi'' = 0$$

where a prime denotes differentiation with respect to the argument. When the variables are separated, there follows

$$R^2 \frac{\phi''}{\phi} + R \frac{\phi'}{\phi} = - \frac{\psi''}{\psi} = \nu^2 \tag{E.8}$$

where ν is the separation constant. Eq. (E.8) then divides into the two ordinary equations

$$R^2 \phi'' + R \phi' - \nu^2 \phi = 0 \tag{E.9}$$

$$\psi'' + \nu^2 \psi = 0 \tag{E.10}$$

The sign of the separation constant was chosen so that periodic functions, rather than exponential functions, were introduced in the θ-direction.

Eq. (E.9) is an equidimensional equation, with the general solution [47]

$$\phi = A_\nu R^\nu + B_\nu R^{-\nu} \qquad (\nu \neq 0)$$

$$\phi = A_0 + B_0 \ln R \qquad (\nu = 0) \tag{E.11}$$

Eq. (E.10) has the solution

$$\psi = C_\nu \cos \nu\theta + D_\nu \sin \nu\theta \qquad (\nu \neq 0)$$

$$\psi = C_0 + D_0 \theta \qquad (\nu = 0) \tag{E.12}$$

Thus any expression of the form

$$\tau_w (R,\theta) = a_0 + b_0 \ln R + (c_0 + d_0 \ln R)\, \theta \tag{E.13}$$

$$+ \sum_\nu \left[\left(a_\nu R^\nu + b_\nu R^{-\nu} \right) \cos \theta + \left(c_\nu R^\nu + d_\nu R^{-\nu} \right) \sin \nu\theta \right]$$

where ν takes on arbitrary nonzero values, is a solution of Eq. (E.4).

Since τ_w is an even function of θ, it follows that

$$c_0 = d_0 = 0$$

and

$$c_\nu = d_\nu = 0$$

In order for τ_w to be a single-valued function of θ, the trigonometric functions must possess a common period 2π. This requirement serves to determine the permissible values of the separation constant

$$\nu = n \quad (n = 1, 2, 3, \ldots)$$

Hence, the solution of the present problem takes the form

$$\tau_w (R,\theta) = a_0 + b_0 \ell n\ R + \sum_{n=1}^{\infty} \left[\left(a_n R^n + b_n R^{-n} \right) \cos n\theta \right] \tag{E.14}$$

In order to satisfy the boundary conditions given by Eqs. (E.5) and (E.6) at the outer radius of the tube, it follows that

$$f(\theta) = a_0 + \sum_{n=1}^{\infty} \left[\left(a_n + b_n \right) \cos n\theta \right] \tag{E.15}$$

and

$$q_c = b_0 + \sum_{n=1}^{\infty} \left[n \left(a_n - b_n \right) \cos n\theta \right] \tag{E.16}$$

which, when the theory of Fourier series is used, yields

$$a_0 = \frac{1}{\pi}\int_0^{\pi} f(\theta)\, d\theta \tag{E.17}$$

$$b_0 = \frac{1}{\pi}\int_0^{\pi} q_c\, d\theta = q_c \tag{E.18}$$

$$a_n + b_n = \frac{2}{\pi}\int_0^{\pi} f(\theta) \cos n\theta\, d\theta \tag{E.19}$$

$$a_n - b_n = \frac{2}{\pi}\int_0^{\pi} q_c \cos n\theta\, d\theta = 0 \tag{E.20}$$

From Eq. (E.20), it follows that

$$a_n = b_n \tag{E.21}$$

which when combined with Eq. (E.19) gives

$$a_n = \frac{1}{\pi}\int_0^{\pi} f(\theta) \cos n\theta\, d\theta \tag{E.22}$$

Eqs. (E.17), (E.18), and (E.22) serve to determine the constants in the required solution of Eq. (E.14), provided that an expression for $f(\theta)$ is available.

In order to obtain such expression, a Fourier approximation is constructed using the eight discrete measurements of the outside wall temperature, as outlined in references [48, 49]. Since τ_w is an even function of θ, only the cosine terms contribute to the series representation which takes the form

$$f(\theta) \simeq \alpha_0 + \sum_{m=1}^{4} \alpha_m \cos n\,\theta \tag{E.23}$$

The coefficients are determined in such a way that the integrated square error is least, and are given by

$$\left.\begin{aligned}
\alpha_0 &= \frac{1}{4}\left(\frac{1}{2}\,\tau_{w,o1} + \tau_{w,o2} + \tau_{w,o3} + \tau_{w,o4} + \frac{1}{2}\,\tau_{w,o5}\right) \\
\alpha_m &= \frac{1}{2}\left(\frac{1}{2}\,\tau_{w,o1} + \tau_{w,o2}\cos\frac{n\pi}{4} + \tau_{w,o3}\cos\frac{n\pi}{2}\right. \\
&\qquad \left. + \tau_{w,o4}\cos\frac{3n\pi}{4} + \frac{1}{2}\,\tau_{w,o5}\right) \qquad (m \neq 0,4) \\
\alpha_4 &= \frac{1}{4}\left(\frac{1}{2}\,\tau_{w,o1} - \tau_{w,o2} + \tau_{w,o3} - \tau_{w,o4} + \frac{1}{2}\,\tau_{w,o5}\right)
\end{aligned}\right\} \qquad (E.24)$$

where $\tau_{w,oj's}$ are the nondimensional outside wall temperatures measured at 45^{o} intervals.

Hence, when Eq. (E.23) and the orthogonality relations for trigonometric functions are used, Eqs. (E.17) and (E.21) become

$$a_0 = \alpha_0 \qquad (E.25)$$

and

$$\left.\begin{aligned}
a_n &= \frac{\alpha_m}{2} \qquad (n = m) \\
a_n &= 0 \qquad (n \neq m)
\end{aligned}\right\} \qquad (E.26)$$

Upon substitution of Eqs. (E.18), (E.21), (E.25), and (E.26) into Eq. (E.14), the final form of the solution to the conduction equation

for the glass tube becomes

$$\tau_w (R,\theta) = \alpha_0 + q_c \ln R + \sum_{n=1}^{4}\left[\frac{\alpha_n}{2}\left(R^n + R^{-n}\right)\cos n\theta\right] \qquad (E.27)$$

where α's are given by Eq. (E.22).

B. Metal Tube

As the metal tube was direct-resistance-heated with dc power, a generation term is added to the energy equation. The temperature gradient at the outer radius of the metal tube is again approximately equal to zero as a result of the negligible heat losses. The nondimensional energy equation for the tube wall can then be written as

$$\frac{\partial^2 \tau_w}{\partial R^2} + \frac{1}{R}\frac{\partial \tau_w}{\partial R} + \frac{1}{R^2}\frac{\partial^2 \tau_w}{\partial \theta^2} = -q^* \qquad (E.28)$$

where

$$q^* = \frac{q''' r_2^2}{k_w\left(T_{w,o1} - T_{w,o5}\right)} \qquad (E.29)$$

and

$$q''' = \frac{I V}{\pi\left(r_2^2 - r_1^2\right) L} \qquad (E.30)$$

The boundary conditions are

$$\tau_w (1,\theta) = f(\theta) \tag{E.31}$$

and

$$\left(\frac{\partial \tau_w}{\partial R}\right)_{1,\theta} = 0 \tag{E.32}$$

When the transformation

$$\tau_w = \tau_w^* + q^*\left(\frac{1 - R^2}{4}\right) \tag{E.33}$$

is used, as suggested by Black and Sparrow [49], Eq. (E.28) reduces to

$$\frac{\partial^2 \tau_w^*}{\partial R^2} + \frac{1}{R}\frac{\partial \tau_w^*}{\partial R} + \frac{1}{R^2}\frac{\partial^2 \tau_w^*}{\partial \theta^2} = 0 \tag{E.34}$$

subject to the following reduced boundary conditions:

$$\tau_w^* (1,\theta) = f(\theta) \tag{E.35}$$

and

$$\left(\frac{\partial \tau_w^*}{\partial R}\right)_{1,\theta} = \frac{q^*}{2} \tag{E.36}$$

The above reduced conduction equation for the metal tube is of the same form as Eq. (E.4) for the glass tube and has similar boundary conditions. The details of solution are omitted for brevity; the final results are given by

$$\tau_w^* (R,\theta) = \alpha_0 + \frac{q^*}{2} \ell n\ R + \sum_{n=1}^{4} \left[\frac{\alpha_n}{2} \left(R^n + R^{-n} \right) \cos\ n\theta \right] \tag{E.37}$$

or, in terms of the nondimensional temperature,

$$\tau_w (R,\theta) = \alpha_0 + \frac{q^*}{2} \ell n\ R + \sum_{n=1}^{4} \left[\frac{\alpha_n}{2} \left(R^n + R^{-n} \right) \cos\ n\theta \right] + q^* \left(\frac{1 - R^2}{4} \right) \tag{E.38}$$

where α's are given by Eq. (E.22).

XI. APPENDIX F:

SAMPLE CALCULATIONS

A. Heat Transfer

Run 25 for ethylene glycol with the metal tube is used to illustrate the details of data reduction procedure for the heat transfer runs

Physical dimensions of tube

Inside tube diameter, d_1 = 0.401 in.

Outside tube diameter, d_2 = 0.441 in.

Total heated length, L_T = 48.0 in.

Length to measuring section, L_S = 11.0 in.

Measured quantities The tube wall thermocouple readings at the measuring section were numbered 1 through 8. These locations were 45° apart starting clockwise from the top of the tube. The two thermocouples placed in the flow at the inlet and outlet sections were numbered 9 and 10. The data are as follows:

e_1 = 5.06 mv	e_6 = 3.73 mv
e_2 = 4.60 mv	e_7 = 4.00 mv
e_3 = 4.02 mv	e_8 = 4.61 mv
e_4 = 3.77 mv	e_9 = 1.035 mv
e_5 = 3.675 mv	e_{10} = 3.04 mv

Flow meter reading, FMR = 80%

Voltage across the test section, V_T = 8.12 v

Voltage across the shunt, V_S = 58.71 v

Mean wall temperature The wall and fluid temperatures were obtained from the corresponding thermocouple readings using NBS circular 561:

$T_{w,o1} = 241.88\ ^{o}F$ $T_{w,o6} = 191.00\ ^{o}F$

$T_{w,o2} = 224.62\ ^{o}F$ $T_{w,o7} = 210.57\ ^{o}F$

$T_{w,o3} = 202.35\ ^{o}F$ $T_{w,o8} = 225.00\ ^{o}F$

$T_{w,o4} = 192.58\ ^{o}F$ $T_{i} = 78.74\ ^{o}F$

$T_{w,o5} = 188.84\ ^{o}F$ $T_{o} = 163.43\ ^{o}F$

The electric current through the test section is obtained from the voltage across the shunt and the shunt calibration (240 amp/100 mv)

$$I = 2.4\ V_s \qquad (F.1)$$

$$= 2.4 \times 58.71 = 140.9 \text{ amp}$$

The metal tube insulation limited the heat loss to about 1.5 percent of the total power generated in the tube wall. Accordingly, the net heat input to the fluid can be calculated as follows:

$$q = 0.985\ V_T\ I \qquad (F.2)$$

$$= 0.985 \times 8.12 \times 140.90 \times 3.4129$$

$$= 3846.3 \text{ Btu/hr}$$

The average heat flux, based on the inside tube surface area, is given by

$$\bar{q}_i'' = \frac{q}{\pi d_1 L_T} \qquad (F.3)$$

$$= \frac{3846.3 \times 144}{\pi \times 0.401 \times 48} = 9159.3 \quad \text{Btu/hr-ft}^2$$

Finally, the rate of volumetric heat generation may be calculated according to the relation

$$q''' = \frac{q}{\pi \left(r_2^2 - r_1^2\right) L_T} \qquad (F.4)$$

$$= \frac{4 \times 3846.3 \times 12^3}{\pi \left[(0.441)^2 - (0.401)^2\right] \times 48}$$

$$= 5.235 \times 10^6 \quad \text{Btu/hr-ft}^3$$

The inside tube wall temperatures were obtained from the solution of the one-dimensional conduction equation for the tube wall

$$\frac{1}{r} \frac{d}{dr} \left(r \frac{dT_w}{dr}\right) + \frac{q'''}{k_w} = 0 \qquad (F.5)$$

subject to the following boundary conditions:

$$T_w (r_1) = T_{w,i}$$

$$T_w\ (r_2) = T_{w,o}$$

$$\left(\frac{dT_w}{dr}\right)_{r_2} = 0$$

Integrating Eq. (F.5) twice with respect to radius yields

$$T_w - T_{w,i} = -\frac{q'''}{4\,k_w}\left(r^2 - r_1^{\,2}\right) + c_1\,\ell n\,\frac{r}{r_1} + c_2$$

which, upon application of the above boundary conditions, reduces to

$$T_w - T_{w,i} = -\frac{q'''}{4\,k_w}\left(r^2 - r_1^{\,2}\right) + \frac{q'''\,r_2^{\,2}}{2\,k_w}\,\ell n\,\frac{r}{r_1} \qquad \text{(F.6)}$$

The temperature drop across the tube wall can then be calculated from Eq. (F.6) as follows:

$$\Delta T_w = \frac{q'''}{2\,k_w}\left[r_2^{\,2}\,\ell n\,\frac{r_2}{r_1} - \frac{1}{2}\left(r_2^{\,2} - r_1^{\,2}\right)\right] \qquad \text{(F.7)}$$

$$= \frac{5.235 \times 10^6}{2 \times 9.4 \times 144 \times 4}\left\{(0.441)^2\,\ell n\left(\frac{0.441}{0.401}\right) - \frac{1}{2}\left[(0.441)^2 - (0.401)^2\right]\right\}$$

$$= 0.80\ ^{o}F$$

The above temperature drop was applied uniformly around the circumference of the tube so as to obtain the following inside wall temperatures:

$T_{w,i1} = 244.08\ ^{o}F$ $\qquad$ $T_{w,i5} = 188.04\ ^{o}F$

$T_{w,i2} = 223.82\ ^{o}F$ $\qquad$ $T_{w,i6} = 190.21\ ^{o}F$

$T_{w,i3} = 201.55\ ^{o}F$ $\qquad$ $T_{w,i7} = 200.78\ ^{o}F$

$T_{w,i4} = 191.78\ ^{o}F$ $\qquad$ $T_{w,i8} = 224.20\ ^{o}F$

The circumferentially averaged inside tube wall temperature was calculated from the above eight values using Simpson's integration:

$$\bar{T}_{w,i} = \frac{1}{12}\left[T_{w,i1} + 2\left(T_{w,i2} + T_{w,i8} + T_{w,i4} + T_{w,i6}\right) + \left(T_{w,i3} + T_{w,i7}\right) + T_{w,i5}\right] \qquad (F.8)$$

$$= 207.62\ ^{o}F$$

Fluid bulk temperature Using the flowmeter calibration curve gives the fluid flow rate

$$\dot{m} = 82.368\ \text{lbm/hr}$$

An energy balance over the tube length from the onset of heating up to the measuring section yields

$$q\,\frac{L_S}{L_T} = \dot{m}\,(i_s - i_i) \qquad (F.9)$$

where i_i and i_s are the fluid enthalphy at inlet and measuring sections, respectively, Eq. (F.9) can then be rearranged to yield

$$i_s = i_i + \frac{q}{\dot{m}} \frac{L_S}{L_T} \qquad \text{(F.10)}$$

$$= 37.93 + \frac{3846.23}{82.368} \times \frac{11}{48}$$

$$= 48.63 \quad \text{Btu/lbm}$$

From the physical properties of ethylene glycol, the fluid bulk temperature, corresponding to i_s, is found to be

$$T_b = 97.58 \ ^{o}F$$

Heat transfer coefficient The circumferentially averaged heat transfer coefficient is defined as

$$h = \frac{\bar{q}''_i}{\bar{T}_{w,i} - T_b} \qquad \text{(F.11)}$$

$$= \frac{9159.3}{207.62 - 97.58}$$

$$= 83.23 \quad \text{Btu/hr-ft}^2 - {}^{o}F$$

Nondimensional parameters The above calculated quantities and

the physical properties of ethylene glycol evaluated at the bulk temperature were used to calculate the following dimensionless parameters:

$$Nu = \frac{h\, d_1}{k} \qquad (F.12)$$

$$= \frac{83.23 \times 0.401}{0.1601 \times 12} = 17.38$$

$$Gr = \frac{g\, \beta\, \rho^2\, d_1^{\,3}}{\mu^2} \left(\overline{T}_{w,i} - T_b \right) \qquad (F.13)$$

$$= \frac{32.2 \times 3.566 \times 10^{-4} \times (68.79)^2 \times (0.401)^3 \times (3.600)^2}{(26.36)^2 \times (12)^3}$$

$$\times (207.62 - 97.58)$$

$$= 4.158 \times 10^3$$

$$Ra = Gr\ Pr \qquad (F.14)$$

$$= 3.95 \times 10^5$$

$$Re = \frac{4\dot{m}}{\pi\, d_1\, \mu} \qquad (F.15)$$

$$= \frac{4 \times 82.368 \times 12}{\pi \times 0.401 \times 26.36} = 119.04$$

$$X = \frac{L_s / d_1}{Re\ Pr} \qquad (F.16)$$

$$= \frac{11}{0.401 \times 119.04 \times 95.36} = 2.416 \times 10^{-3}$$

A listing of the Fortran IV computer program used to facilitate the data reduction is given below; Fig. 31 shows a printing of the output results.

B. Pressure Drop

Run 7 for the pressure drop in the metal tube with ethylene glycol is used to illustrate the calculation procedure for obtaining the friction factor for the heating runs.

Measured quantities As pointed out in the text, the only thermocouple readings recorded during the nonisothermal pressure drop runs were the fluid inlet and outlet thermocouples:

e_9 = 0.994 mv

e_{10} = 2.265 mv

FMR = 90.0%

V_T = 7.0 v

V_S = 51.54 mv

Mercury was used as an indicating fluid in the inclined differential manometer. The differential mercury head is given by

```
C
C      PROGRAM FOR HEAT TRANSFER DATA REDUCTION
C
       REAL NU
       DIMENSION EMF(10),TEMP(10),TWI(10)
       DATA D1,D2,TL1,TL2,TL/0.033417,0.03675,0.91667,3.66667,4.0/,
      1THCTB/9.4/
       DATA PI,GC,PCF /3.141593,32.174,3.4129/
C
     1 READ (5,2,END=500) NR,NS,FLOW,VLT,VLS
     2 FORMAT (2I5,3F10.4)
       AMP      = 2.4*VLS
       RT       = VLT/AMP
       WAT      = 0.985*VLT*AMP
       QTOT     = WAT*PCF
       QPUA     = QTOT/(PI*D1*TL)
       QPUV     = 4.0*QTOT/(PI*(D2*D2-D1*D1)*TL)
       DTW      = QPUV*(C2*D2*ALOG(D2/D1)-(D2*D2-D1*D1)/2.0)/(8.0*THCTB)
C
C      WALL TEMPERATURE
C
       READ (5,5) (EMF(I),I=1,10)
     5 FORMAT (10F8.5)
       CALL THCPL(EMF,TEMP,10)
       DO 10 I = 1,8
    10 TWI(I)   = TEMP(I)-DTW
       TWM      = (TWI(1)+TWI(3)+2.0*(TWI(5)+TWI(6)+TWI(7)+TWI(8))+TWI(2)
      1           +TWI(4))/12.0
C
C      FLUID BULK TEMPERATURE
C
       HFI      = HFL(TEMP(9))
       HFE      = HFL(TEMP(10))
       DHFL     = (HFE-HFI)*FLOW
       TLTC     = TL1
       IF (NS.EQ.2) TLTC = TL2
       QIN      = QTOT*TLTC/TL
```

```
      HFB      = HFI+QIN/FLOW
      TFB      = THL(HFB)
C
C     DIMENSIONLESS PARAMETERS
C
      DTWB     = TWM-TFB
      HTC      = QPUA/DTWB
      NU       = HTC*D1/THCNL(TFB)
      PR       = PRNO(TFB)
      VISC     = VISCL(TFB)
      RE       = 4.0*FLOW/(PI*D1*VISC)
      BETA     = BETAL(TFB)
      VRHO2    = (VISC/RHOL(TFB))**2
      D13      = D1**3
      GR       = GC*BETA*D13*DTWB*3600.0*3600.0/VRHO2
      RA       = GR*PR
      GZ       = TLTC/(D1*RE*PR)
C
      WRITE (6,15) NR,NS,FLOW,VLT,AMP,RT,WAT,QPUA
   15 FORMAT (1H1,9X,60HCOMBINED FORCED AND FREE CONVECTION IN HORIZONTA
     1L METAL TUBE,//,15X,5HRUN: ,I2,33X,9HSECTION: ,I1,//,10X,17HSYSTEM
     2 PARAMETERS,/,10X,17H****************,/,
     315X,27HFLUID FLOW RATE           = ,F10.4,7H LBM/HR,/,
     415X,27HVOLTAGE ACROSS THE TUBE   = ,F10.4,6H VOLTS,/,
     515X,27HCURRENT THROUGH THE TUBE  = ,F10.4,5H AMPS,/,
     615X,27HTUBE ELECTRIC RESISTENCE  = ,E10.4,5H OHMS,/,
     715X,27HELECTRIC POWER INPUT      = ,F10.4,6H WATTS,/,
     815X,27HHEAT FLUX                 = ,F10.4,15H BTU/(HR.SQ.FT),//)
C
      WRITE (6,20) TWI(1),TWI(5),TWI(6),TWI(4),TWI(2),TWI(8),TWI(7),
     1             TWI(3)
   20 FORMAT (10X,36HINSIDE WALL TEMPERATURE DISTRIBUTION,/,10X,36H*****
     1**********************************,//,42X,F10.4,//,31X,F10.4,12X,F10.
     24,//,29X,F10.4,16X,F10.4,//,31X,F10.4,12X,F10.4,//,42X,F10.4,//)
C
      WRITE (6,60) TEMP(9),TEMP(10),TFB,TWM,HTC,QTOT,DHFL,NU,PR,RE,GR,RA
     1             ,GZ
```

```
   60 FORMAT (10X,16HSYSTEM VARIABLES,/,10X,16H****************,/,
     115X,27HFLUID INLET TEMPERATURE   = ,F10.4,2H F,/,
     215X,27HFLUID EXIT TEMPERATURE    = ,F10.4,2H F,/,
     315X,27HFLUID BULK TEMPERATURE    = ,F10.4,2H F,/,
     415X,27HMEAN WALL TEMPERATURE     = ,F10.4,2H F,/,
     515X,27HHEAT TRANSFER COEFF.      = ,F10.4,17H BTU/(HR.SQ.FT.F),//,
     615X,27HTOTAL POWER INPUT         = ,F10.4,7H BTU/HR,/,
     715X,27HTOTAL ENTHALPY CHANGE     = ,F10.4,7H BTU/HR,//,
     815X,27HNUSSELT NUMBER            = ,F10.4,/,
     915X,27HPRANDTL NUMBER            = ,F10.4,/,
     115X,27HREYNOLDS NUMBER           = ,E13.6,/,
     215X,27HGRASHOF NUMBER            = ,E13.6,/,
     315X,27HRAYLEIGH NUMBER           = ,E13.6,/,
     415X,27HGRAETZ NUMBER             = ,E13.6,/)
C
      GO TO 1
  500 STOP
      END
```

```
COMBINED FORCED AND FREE CONVECTION IN HORIZONTAL METAL TUBE

     RUN: 25                                        SECTION: 1

SYSTEM PARAMETERS
*****************
     FLUID FLOW RATE           =     82.3680 LBM/HR
     VOLTAGE ACROSS THE TUBE   =      8.1200 VOLTS
     CURRENT THROUGH THE TUBE  =    140.9040 AMPS
     TUBE ELECTRIC RESISTENCE  = 0.5763E-01 OHMS
     ELECTRIC POWER INPUT      =   1126.9780 WATTS
     HEAT FLUX                 =   9159.2850 BTU/(HR.SQ.FT)


INSIDE WALL TEMPERATURE DISTRIBUTION
************************************

                              241.0780

                    223.8217                  224.2006

                  201.5532                      200.7751

                    191.7791                  190.2054

                              188.0371


SYSTEM VARIABLES
****************
     FLUID INLET TEMPERATURE   =     78.7375 F
     FLUID EXIT TEMPERATURE    =    163.4314 F
     FLUID BULK TEMPERATURE    =     97.5757 F
     MEAN WALL TEMPERATURE     =    207.6213 F
     HEAT TRANSFER COEFF.      =     83.2317 BTU/(HR.SQ.FT.F)

     TOTAL POWER INPUT         =   3846.2630 BTU/HR
     TOTAL ENTHALPY CHANGE     =   4095.3270 BTU/HR

     NUSSELT NUMBER            =     17.3772
     PRANDTL NUMBER            =     95.3620
     REYNOLDS NUMBER           =  0.119045E 03
     GRASHOF NUMBER            =  0.415756E 04
     RAYLEIGH NUMBER           =  0.396473E 06
     GRAETZ NUMBER             =  0.241634E-02
```

Fig. 32. Computer printout of a typical heat transfer run

$\Delta x = 0.115$ in.

Fluid bulk temperature

$T_i = 76.93\ ^{o}F$

$T_o = 131.50\ ^{o}F$

$\dot{m} = 95.16$ lbm/hr

$I = 2.4\ V_S$

$= 2.4 \times 51.54 = 123.696$ amp

$q = 0.985\ I\ V_T$

$= 0.085 \times 123.696 \times 7.0 \times 3.4129$

$= 2910.81$ Btu/hr

$$q_i'' = \frac{q}{\pi\ d_1\ L_T}$$

$$= \frac{2910.81 \times 144}{\pi \times 0.401 \times 48} = 6931.63 \text{ Btu/hr-ft}^2$$

The friction factor was evaluated at an axial location half way along the heated test section. An energy balance over the first half of the heated section yields

$$\frac{q}{2} = \dot{m}\ (i_b - i_i) \qquad \text{(F.17)}$$

where i_b is the fluid enthalpy at the midpoint. Using Eq. (F.17), and

the physical properties of ethylene glycol, one obtains

$$i_b = i_i + \frac{q}{2\,\dot{m}}$$

$$= 36.92 + \frac{2910.81}{2 \times 95.16}$$

$$= 52.21 \quad \text{Btu/lbm}$$

which results in

$$T_b = 103.80\ ^{o}F$$

Mean wall temperature A least squares curve-filling technique was used to obtain the following functional relation for the Nusselt and Rayleigh numbers shown in Fig. 17:

$$Nu = 0.152\ Ra^{0.365} \qquad \text{(F.18)}$$

An iterative procedure which utilizes Eq. (F.18) was used to determine the average wall temperature at the midpoint of the tube. Such a procedure starts by assuming a value for the Rayleigh number, say

$$Ra\ (\text{assumed}) = 2.0 \times 10^{5}$$

which, upon substitution in Eq. (F.18), gives

$$Nu = 13.11$$

The heat transfer coefficient can then be calculated using the value of the Nusselt number and the physical properties of ethylene glycol evaluated at the bulk temperature, as follows:

$$h = \frac{k\ Nu}{d_1}$$

$$= \frac{0.1586 \times 13.11 \times 12}{0.401} = 62.22 \quad \text{Btu/hr-ft}^2\text{-}^\circ\text{F}$$

Using Eq. (F.11) yields the following wall temperature calculation:

$$\bar{T}_{w,i} = T_b + \frac{\bar{q}_i''}{h}$$

$$= 103.80 + \frac{6931.63}{62.22}$$

$$= 215.18\ ^\circ\text{F}$$

A check on the value of $\bar{T}_{w,i}$ is obtained from a calculation of a new value for the Rayleigh number:

$$\text{Gr (calculated)} = \frac{g\ \beta\ \rho^2\ d_1^{\,3}}{\mu^2}\left(\bar{T}_{w,i} - T_b\right)$$

$$= 5.383 \times 10^3$$

Pr (calculated) = 85.48

Ra (calculated) = 4.602×10^5

It is clear that the calculated value of the Rayleigh number is quite different from the assumed one. The iteration procedure was then repeated using the new calculated value of the Rayleigh number to update the assumed value. The procedure was terminated when the following criteria was reached:

$$|\text{Ra (calculated)} - \text{Ra (assumed)}| \leq 50$$

The final results for the iteration process are

$\bar{T}_{w,i} = 192.91\ ^{o}F$

Gr = 4.307×10^3

Pr = 85.48

Ra = 3.681×10^5

Nu = 16.39

Friction factor The Reynolds number at the middle section of the tube is given by

$$Re = \frac{4\dot{m}}{\pi d_1 \mu}$$

$$= \frac{4 \times 95.16 \times 12}{\pi \times 0.401 \times 23.32} = 155.45$$

From the isothermal pressure drop data shown in Fig. 26, the friction factor is found to have the following functional dependence on the Reynolds number:

$$f_o = \frac{61}{Re} \tag{F.19}$$

The pressure taps on the metal tube are 50 in. apart, 1 in. on other side of the 48-in. heated length. It is necessary, therefore, to calculate the isothermal pressure drop, using Eq. (F.19) for both of these segments. This pressure drop is subtracted from the total measured pressure drop to yield the pressure drop across the heated section. Using the inlet and outlet fluid temperatures, one can calculate the Reynolds numbers at inlet and outlet section as follows:

$$Re_i = \frac{4 \times 95.16 \times 12}{\pi \times 0.401 \times 41.13}$$

$$= 88.16$$

$$Re_o = \frac{4 \times 95.16 \times 12}{\pi \times 0.401 \times 14.65}$$

$$= 247.41$$

The corresponding friction factors are given by

$$f_{o,i} = \frac{61}{88.158} = 0.692$$

$$f_{o,o} = \frac{61}{247.41} = 0.247$$

The isothermal pressure drop across the unheated inlet and outlet segment can be calculated according to the following equation:

$$\Delta p_i = \frac{g}{g_c} \frac{f_{o,i}}{d_1} \Delta L_i \frac{\rho u_i^2}{2g} \qquad \text{(F.20)}$$

$$= \frac{0.692 \times 1 \times 69.29 \times (1.566 \times 10^3)^2}{32.2 \times 0.401 \times 2 \times (3600)^2 \times 12}$$

$$= 2.44 \times 10^{-3} \text{ psi}$$

$$\Delta p_o = \frac{0.247 \times 1 \times 67.98 \times (1.596 \times 10^3)^2}{32.2 \times 0.401 \times 2 \times (3600)^2 \times 12}$$

$$= 0.8866 \times 10^{-4} \text{ psi}$$

The total measured pressure drop, as calculated from the differential mercury head, is given by

$$\Delta p_t = \frac{g}{g_c} \Delta x \left(\rho_{Hg} - \rho_{Eg} \right) \qquad \text{(F.21)}$$

$$= 0.115 \times \frac{(874.12 - 69.34)}{1728}$$

$$= 0.05356 \text{ psi}$$

Finally, the pressure drop across the heated section can be calculated as

$$\Delta p_h = \Delta p_t - \Delta p_i - \Delta p_o \qquad \text{(F.22)}$$

$$= 0.05356 - 2.44 \times 10^{-3} - 8.866 \times 10^{-4}$$

$$= 0.05023 \quad \text{psi}$$

which yields

$$f = \frac{2 g_c \, d_1 \, \Delta p_h}{L_T \, \rho \, u^2}$$

$$= \frac{2 \times 32.2 \times 0.401 \times 0.05023 \times (3600)^2 \times 144}{48 \times 68.63 \times (1.581 \times 10^3)^2}$$

$$= 0.2938$$

and

$$f/f_o = 0.7489$$

A listing of the Fortran IV computer program used to facilitate the data reduction for the pressure drop runs is given below. The computer output for example Run 7 is shown in Fig. 33.

```
C
C       PROGRAM FOR PRESSURE DROP DATA REDUCTION
C
        REAL NU
        DATA D1,D2,TL1,TL2,TL/0.033417,0.03675,0.916667,3.666667,4.0/,
       1THCTB/9.4/
        DATA RHOHG,RHOFL/874.12,69.34/
        DATA PI,GC,PCF /3.141593,32.174,3.4129/
        DIMENSION EMF(2),TEMP(2)
C
        AREA    = PI*D1*D1/4.0
      1 READ (5,2,END=500) NR,FLOW,VLT,VLS,HP,(EMF(I),I=1,2)
      2 FORMAT (I5,6F10.4)
        AMP     = 2.4*VLS
        WAT     = 0.985*VLT*AMP
        QTOT    = WAT*PCF
        QPUA    = QTOT/(PI*D1*TL)
        CALL THCPL(EMF,TEMP,2)
        DPFL    = HP*(RHOHG-RHOFL)/1728.0
C
C       FLUID BULK TEMPERATURE
C
        HFI     = HFL(TEMP(1))
        QIN     = QTOT/2.0
        HFB     = HFI+QIN/FLOW
        TFB     = THL(HFB)
C
        HFO     = HFI+QTOT/FLOW
        TFO     = THL(HFO)
C
C       WALL TEMPERATURE
C
        RAA     = 2.0E05
     10 NU      = EXP(0.3653*ALOG(RAA)-1.8855)
        HTC     = NU*THCNL(TFB)/D1
        TWM     = TFB+QPUA/HTC
        DTWB    = TWM-TFB
```

```
      PR       = PRNO(TFB)
      VISC     = VISCL(TFB)
      BETA     = BETAL(TFB)
      RHO      = RHOL(TFB)
      VRHO2    = (VISC/RHO)**2
      D13      = D1**3
      GR       = GC*BETA*D13*DTWR*3600.0*3600.0/VRHO2
      RA       = GR*PR
C
      IF (ABS(RA-RAA) .LT. 50.0) GO TO 20
      RAA      = RA
      GO TO 10
   20 RE       = 4.0*FLOW/(PI*D1*VISC)
      FRI      = 61.0/RE
C
C     MEASURED FRICTION FACTOR
C
      RHOI     =RHOL(TEMP(1))
      VELI     = FLOW/(RHOI*AREA)
      REI      = 4.0*FLOW/(PI*D1*VISCL(TEMP(1)))
      FRIN     = 61.0/REI
      DPI      = FRIN*RHOI*VELI*VELI/(D1*GC*2.0*3600.0*3600.0*1728.0)
C
      RHOO     =RHOL(TFO)
      VELO     = FLOW/(RHOO*AREA)
      REO      = 4.0*FLOW/(PI*D1*VISCL(TFO))
      FRO      = 61.0/REO
      DPO      = FRO*RHOO*VELO*VELO/(D1*GC*2.0*3600.0*3600.0*1728.0)
C
      VEL      = FLOW/(RHO*AREA)
      DPH      = DPFL-DPI-DPO
      FR       = 288.0*3600.0*3600.0*GC*D1*DPH/(TL*RHO*VEL*VEL)
      FRR      = FR/FRI
C
      WRITE (6,30) NR,FLOW,VLT,AMP,WAT,QPUA
   30 FORMAT (1H1,9X,60HCOMBINED FORCED AND FREE CONVECTION IN HORIZONTA
     1L METAL TUBE,//,35X,13HPRESSURE DROP,//,15X,5HRUN: ,I2,//,10X,17HS
```

```
     2YSTEM PARAMETERS,/,10X,17H*****************,//,
     315X,27HFLUID FLOW RATE           = ,F10.4,7H LBM/HR,/,
     415X,27HVOLTAGE ACROSS THE TUBE   = ,F10.4,6H VOLTS,/,
     515X,27HCURRENT THROUGH THE TUBE  = ,F10.4,5H AMPS,/,
     615X,27HELECTRIC POWER INPUT      = ,F10.4,6H WATTS,/,
     715X,27HHEAT FLUX                 = ,F10.4,15H BTU/(HR.SQ.FT),//)
C
      WRITE (6,35) TEMP(1),TEMP(2),TFB,TWM,HTC,DPH,NU,PR,RE,GR,RA,FR,
     1             FF , FRR
   35 FORMAT (10X,16HSYSTEM VARIABLES,/,10X,16H***************,//,
     115X,27HFLUID INLET TEMPERATURE   = ,F10.4,2H F,/,
     215X,27HFLUID EXIT TEMPERATURE    = ,F10.4,2H F,/,
     315X,27HFLUID BULK TEMPERATURE    = ,F10.4,2H F,/,
     415X,27HMEAN WALL TEMPERATURE     = ,F10.4,2H F,/,
     515X,27HHEAT TRANSFER COEFFI.     = ,F10.4,17H BTU/(HR.SQ.FT.F),/,
     615X,27HPRESSURE DROP             = ,F10.4,4H PSI,//,
     715X,27HNUSSELT NUMBER            = ,F10.4,/,
     815X,27HPRANDTL NUMBER            = ,F10.4,/,
     915X,27HREYNOLDS NUMBER           = ,E13.6,/,
     115X,27HGRASHOF NUMBER            = ,E13.6,/,
     215X,27HRAYLEIGH NUMBER           = ,E13.6,//,
     315X,27HFRICTION FACTOR           = ,E13.6,/,
     415X,27HISOTHERMAL FR. FACTOR     = ,E13.6,/,
     515X,27HFRICTION FACTORS RATIO    = ,E13.6)
C
      GO TO 1
  500 STOP
      END
```

COMBINED FORCED AND FREE CONVECTION IN HORIZONTAL METAL TUBE

PRESSURE DROP

RUN: 7

SYSTEM PARAMETERS
****

FLUID FLOW RATE	=	95.1600	LBM/HR
VOLTAGE ACROSS THE TUBE	=	7.0000	VOLTS
CURRENT THROUGH THE TUBE	=	123.6960	AMPS
ELECTRIC POWER INPUT	=	852.8833	WATTS
HEAT FLUX	=	6931.6320	BTU/(HR.SQ.FT)

SYSTEM VARIABLES
****

FLUID INLET TEMPERATURE	=	76.9346	F
FLUID EXIT TEMPERATURE	=	131.5013	F
FLUID BULK TEMPERATURE	=	103.7997	F
MEAN WALL TEMPERATURE	=	192.9226	F
HEAT TRANSFER COEFFI.	=	77.7761	BTU/(HR.SQ.FT.F)
PRESSURE DROP	=	0.0502	PSI
NUSSELT NUMBER	=	16.3847	
PRANDTL NUMBER	=	85.4783	
REYNOLDS NUMBER	=	0.155452E	03
GRASHOF NUMBER	=	0.430741E	04
RAYLEIGH NUMBER	=	0.368190E	06
FRICTION FACTOR	=	0.293805E	00
ISOTHERMAL FR. FACTOR	=	0.392403E	00
FRICTION FACTORS RATIO	=	0.748733E	00

Fig. 33. Computer printout of a typical pressure drop run

XII. APPENDIX G:

TABULATION OF EXPERIMENTAL RESULTS

Table 5. Heat transfer results for water with glass tube

Run	$\dot{m}$	$\bar{q}''_i$	T_b	$\bar{T}_{w,i}$	Nu	Ra	Pr	Re
	$\left(\frac{lbm}{hr}\right)$	$\left(10^3 \frac{Btu}{hr\text{-}ft^2}\right)$	(^oF)	(^oF)		(10^5)		
1	74.87	0.5094	65.53	72.57	7.273	0.6266	7.227	1087.3
2	47.91	0.5094	70.22	76.84	7.680	0.6918	6.735	741.3
3	74.87	0.6368	66.38	74.79	7.605	0.7710	7.134	1100.0
4	74.87	0.7642	67.01	76.65	7.947	0.9041	7.067	1109.5
5	47.91	0.7642	71.48	80.68	8.275	1.0014	6.611	753.8
6	74.87	1.0189	69.01	80.88	8.586	1.1913	6.857	1139.9
7	47.91	1.0189	73.62	85.07	8.842	1.3328	6.408	775.3
8	62.01	1.2736	67.19	81.51	8.915	1.3512	7.048	921.1
9	74.87	1.2736	68.93	83.59	8.691	1.4673	6.865	1138.7
10	62.01	1.2736	69.01	83.69	8.676	1.4735	6.857	944.1
11	74.87	1.5283	72.18	88.92	9.087	1.8633	6.544	1188.9
12	47.91	1.5283	75.48	91.86	9.244	2.0179	6.239	794.1
13	62.01	2.0378	68.79	89.79	9.706	2.0923	6.880	941.3
14	47.91	1.7830	77.62	96.03	9.573	2.4145	6.052	816.1
15	74.87	2.0378	74.01	95.07	9.609	2.4811	6.372	1217.7
16	74.87	2.5472	73.00	98.89	9.786	2.9556	6.466	1201.8
17	62.01	2.5472	74.90	99.97	10.078	3.0340	6.291	1020.2
18	47.91	2.2925	80.14	102.52	10.089	3.1533	5.843	842.4
19	47.91	2.8019	81.77	107.95	10.518	3.8583	5.714	859.6
20	62.01	3.8208	73.04	107.43	11.046	3.9322	6.462	995.9
21	74.87	3.8208	79.12	113.36	11.006	4.6878	5.927	1299.8
22	47.91	3.3114	84.96	114.62	10.924	4.7580	5.473	893.6
23	62.01	3.8208	80.96	114.38	11.247	4.8172	5.778	1101.5
24	47.91	4.0755	88.73	123.71	11.351	6.1724	5.206	034.8
25	74.87	5.0944	85.37	128.71	11.497	7.0261	5.443	1403.5
26	62.01	5.0944	87.38	130.19	11.610	7.3052	5.300	1190.7
27	47.91	4.5849	91.25	130.44	11.361	7.3527	5.040	962.7
28	62.01	6.6227	79.32	133.19	12.120	7.4188	5.910	1079.3
29	74.87	5.6038	85.87	132.61	11.720	7.6753	5.407	1412.0
30	74.87	6.6227	91.66	143.87	12.311	9.8922	5.013	1511.6
31	62.01	6.6227	93.44	144.30	12.609	10.0485	4.902	1277.7

Table 6. Heat transfer results for water with metal tube

Run	$\dot{m}$	$\bar{q}''_i$	T_b	$\bar{T}_{w,i}$	Nu	Ra	Pr	Re
	$\left(\frac{lbm}{hr}\right)$	$\left(10^3 \frac{Btu}{hr\text{-}ft^2}\right)$	(^oF)	(^oF)		(10^5)		
1	62.01	0.8466	58.99	69.70	7.678	0.6500	8.004	858.4
2	47.91	0.8264	60.37	71.06	7.491	0.6863	7.831	676.3
3	62.01	0.8466	62.94	73.43	7.791	0.7441	7.522	907.8
4	47.91	0.8264	65.35	75.43	7.887	0.7815	7.247	725.2
5	74.87	1.2649	59.30	73.43	8.691	0.8687	7.964	1041.1
6	74.87	1.2649	64.19	78.05	8.793	1.0301	7.378	1115.2
7	62.01	1.6909	59.99	77.95	9.130	1.1355	7.878	870.8
8	74.87	1.6833	60.96	78.53	9.276	1.1548	7.758	1065.9
9	62.01	1.6909	67.87	84.23	9.907	1.3852	6.975	971.5
10	74.87	1.6833	67.46	84.44	9.508	1.4176	7.019	1166.4
11	62.01	2.4735	62.91	86.23	10.240	1.6522	7.526	907.3
12	47.91	2.4751	64.62	87.86	10.258	1.7544	7.329	717.9
13	62.01	3.1744	64.40	92.54	10.867	2.1074	7.354	926.4
14	74.87	3.2846	63.47	92.88	10.775	2.1278	7.460	1104.1
15	62.01	2.4735	74.44	95.89	10.953	2.2441	6.333	1059.6
16	47.91	2.4886	79.55	100.04	11.399	2.4886	5.891	873.8
17	62.01	4.1192	66.31	99.92	11.774	2.6959	7.142	951.1
18	74.87	3.2846	76.15	102.83	11.664	2.9391	6.180	1307.9
19	47.91	4.1121	68.85	102.50	11.699	2.9448	6.874	760.5
20	62.01	3.1744	79.19	104.40	11.886	3.0314	5.921	1125.9
21	74.87	4.9180	64.90	104.38	11.993	3.0108	7.297	1126.2
22	62.01	4.7864	67.08	105.03	12.105	3.1265	7.059	961.1
23	62.01	5.6630	69.25	111.33	12.873	3.7325	6.833	989.6
24	74.87	6.4735	67.80	114.20	13.374	3.9189	6.983	1171.7
25	47.91	5.6630	72.10	113.83	12.931	4.0609	6.551	794.1
26	62.01	4.1192	85.51	115.17	12.999	4.2306	5.432	1216.7
27	62.01	6.5297	70.06	116.43	13.456	4.2243	6.751	1000.4
28	74.87	4.9180	83.89	119.44	12.974	4.8607	5.552	1440.5
29	74.87	8.0561	70.05	124.18	14.223	4.9304	6.751	1207.8
30	47.91	4.1121	93.66	122.92	13.022	5.0935	4.888	1034.1
31	62.01	7.6899	71.86	124.29	13.980	5.0628	6.574	1024.6
32	62.01	4.7864	89.39	122.73	13.372	5.2423	5.162	1274.1
33	62.01	5.6630	95.64	132.38	14.252	6.6909	4.768	1368.9
34	74.87	6.4735	92.79	133.70	14.679	6.9772	4.942	1600.0
35	62.01	6.5297	100.49	139.95	15.212	7.9971	4.493	1444.3
36	47.91	5.6630	106.27	141.88	14.526	8.1334	4.197	1186.8
37	74.87	8.0561	101.16	148.69	15.570	9.7698	4.458	1756.4
38	62.01	7.6899	107.70	151.99	15.836	10.4074	4.129	1559.3

Table 7. Heat transfer results for ethylene glycol with glass tube

Run	$\dot{m}$	$\bar{q}''_i$	T_b	$\bar{T}_{w,i}$	Nu	Ra	Pr	Re
	$\left(\frac{lbm}{hr}\right)$	$\left(10^3 \frac{Btu}{hr\text{-}ft^2}\right)$	(^oF)	(^oF)		(10^5)		
1	110.44	0.5094	67.88	82.70	7.194	0.2937	172.77	78.91
2	82.37	0.5094	73.20	88.25	7.130	0.3437	153.92	66.91
3	82.37	0.6368	72.08	90.38	7.325	0.4056	157.64	65.16
4	110.44	0.7642	69.08	90.17	7.596	0.4317	168.26	81.27
5	56.50	0.7642	78.49	99.28	7.805	0.5433	137.74	51.92
6	110.44	1.0189	70.95	97.67	8.010	0.5750	161.55	85.02
7	82.37	0.8915	76.03	99.57	8.016	0.5780	144.95	71.52
8	82.37	1.0189	74.48	100.99	8.115	0.6256	149.76	68.98
9	110.44	1.3169	73.85	106.77	8.440	0.7643	151.77	91.12
10	82.37	1.3169	77.11	110.16	8.444	0.8343	141.73	73.32
11	56.50	1.2736	82.05	113.24	8.715	0.8907	128.11	56.27
12	82.37	1.5283	78.19	114.32	8.979	0.9371	138.60	75.16
13	110.44	2.0378	76.39	121.81	9.497	1.1257	143.89	96.68
14	82.37	1.7830	81.46	121.64	9.463	1.1307	129.65	80.95
15	56.50	1.7830	87.35	126.65	9.753	1.2759	115.41	63.19
16	82.37	2.2925	82.52	130.65	10.171	1.3903	126.92	82.88
17	110.44	2.5778	81.73	134.74	10.372	1.5020	128.94	109.19
18	82.37	2.5778	85.28	137.55	10.572	1.6147	120.17	88.07
19	110.44	3.3114	83.64	145.62	11.426	1.8401	124.12	113.91
20	82.37	3.0566	86.83	145.24	11.243	1.8729	116.57	91.09
21	56.50	2.5778	93.63	144.79	10.929	1.9231	102.48	72.12
22	82.37	3.3114	89.21	150.07	11.729	2.0645	111.36	95.85
23	56.50	3.3114	99.64	158.38	12.334	2.5277	91.92	81.43
24	82.37	3.8666	93.96	161.79	12.372	2.5687	101.86	105.85
25	56.50	3.8666	103.89	169.12	13.050	3.0802	85.35	88.49
26	95.16	5.0944	96.25	179.20	13.373	3.3092	97.67	128.16
27	41.21	3.8666	111.27	176.60	13.171	3.6069	75.44	74.16
28	82.37	5.0944	101.40	182.89	13.713	3.6452	89.11	122.91
29	70.36	5.0944	103.59	185.38	13.707	3.8372	85.79	109.55
30	95.16	6.3680	102.62	196.94	14.837	4.3332	87.23	145.43
31	56.50	5.0944	114.25	192.69	14.514	4.6049	71.92	107.33
32	82.37	6.3680	110.08	201.71	15.440	4.9348	76.92	145.00
33	70.36	6.3680	112.05	204.26	15.387	5.1736	74.49	128.43
34	41.21	5.0944	123.75	201.66	14.821	5.5292	62.16	92.44
35	110.44	7.6416	110.61	215.42	16.209	5.7077	76.26	196.32

Table 8. Heat transfer results for ethylene glycol with metal tube

Run	$\dot{m}$	$\bar{q}''_i$	T_b	$\bar{T}_{w,i}$	Nu	Ra	Pr	Re
	$\left(\frac{lbm}{hr}\right)$	$\left(10^3 \frac{Btu}{hr\text{-}ft^2}\right)$	(^oF)	(^oF)		(10^5)		
1	82.37	0.4181	74.51	87.76	6.377	0.2743	149.66	72.12
2	56.50	0.7762	79.57	99.56	7.902	0.4706	134.73	55.59
3	110.44	0.8254	76.82	98.82	7.606	0.4832	142.59	102.04
4	82.37	1.2330	83.69	111.47	9.086	0.7238	123.99	88.87
5	56.50	1.6486	74.71	110.80	9.235	0.7509	149.03	49.71
6	82.37	1.6250	88.88	121.93	10.140	0.9751	112.05	99.46
7	56.50	1.6486	89.63	123.48	10.052	1.0166	110.47	69.31
8	56.50	2.4135	79.45	126.15	10.515	1.0961	135.05	55.45
9	82.37	3.1497	81.54	136.81	11.629	1.3663	129.45	84.72
10	56.50	3.1718	81.52	137.94	11.473	1.3940	129.49	58.10
11	56.50	2.4135	101.11	142.55	12.224	1.6145	89.56	87.60
12	110.44	3.1866	96.77	149.17	12.681	1.8544	96.75	157.05
13	82.37	3.1491	100.91	151.58	13.042	1.9656	89.87	127.21
14	82.37	4.7631	85.96	158.83	13.423	2.0059	118.56	93.41
15	56.50	4.7376	87.98	161.24	13.318	2.1161	114.02	66.92
16	110.44	5.4843	85.01	164.59	14.132	2.1413	120.80	122.66
17	56.50	3.1718	109.84	159.82	13.488	2.3478	77.22	103.47
18	82.37	6.2379	90.08	176.74	14.868	2.6303	109.52	102.03
19	56.50	6.2201	97.17	181.49	15.393	3.0104	96.06	81.00
20	110.44	7.7424	90.22	190.01	16.029	3.0387	109.24	137.18
21	82.37	7.7424	93.60	192.50	16.252	3.2565	102.53	109.80
22	82.37	4.7631	115.00	178.98	15.942	3.3432	71.06	165.71
23	110.44	5.4843	110.02	183.82	15.799	3.4796	77.00	202.91
24	56.50	7.5639	99.65	195.95	16.559	3.6334	91.89	85.12
25	82.37	9.1593	97.58	207.62	17.377	3.9647	95.36	119.04
26	56.50	4.7376	129.74	192.23	16.594	4.3630	56.99	146.33
27	82.37	6.2379	127.80	201.80	18.397	4.9788	58.59	206.61
28	110.44	7.7424	125.17	214.79	18.782	5.7319	60.86	265.15
29	82.37	7.7424	140.04	222.28	20.933	6.9533	49.54	251.25
30	82.37	9.1593	152.07	241.36	23.238	9.3486	42.63	300.51
31	56.50	7.5639	164.77	239.26	23.468	9.6782	36.92	245.91

Table 9. Isothermal pressure drop results for water with glass tube

Run	$\dot{m}$ $\left(\frac{lbm}{hr}\right)$	T_b $\left(^oF\right)$	Δp $\left(psi\right)$	Re	f_o
1	32.15	54.99	0.0032	416.8	0.1519
2	40.26	52.74	0.0041	504.8	0.1240
3	47.91	52.74	0.0049	600.7	0.1055
4	47.91	56.33	0.0049	633.4	0.1043
5	55.14	52.74	0.0053	691.4	0.0849
6	62.01	52.74	0.0061	777.5	0.0778
7	62.01	53.64	0.0060	788.0	0.0772
8	68.57	52.74	0.0064	859.8	0.0674
9	68.57	55.88	0.0068	900.7	0.0710
10	74.87	52.74	0.0073	038.8	0.0636
11	74.87	55.88	0.0071	983.4	0.0622
12	62.01	85.53	0.0045	1207.9	0.0576
13	68.57	84.22	0.0049	1314.7	0.0505
14	74.87	89.45	0.0049	1527.9	0.0430
15	74.87	96.39	0.0051	1654.3	0.0446

Table 10. Isothermal pressure drop results for ethylene glycol with glass tube

Run	$\dot{m}$ $\left(\frac{lbm}{hr}\right)$	T_b (^oF)	Δp (psi)	Re	f_o
1	41.21	66.06	0.0289	28.15	1.644
2	41.21	69.72	0.0317	30.80	1.801
3	56.50	69.21	0.0424	41.71	1.282
4	56.50	69.46	0.0414	41.96	1.254
5	70.36	69.11	0.0550	51.80	1.072
6	82.37	65.13	0.0675	54.97	0.972
7	82.37	65.17	0.0685	55.02	0.985
8	82.37	67.98	0.0661	59.00	0.942
9	82.37	68.90	0.0657	60.34	0.935
10	95.16	65.05	0.0792	63.37	0.846
11	95.16	66.14	0.0787	65.12	0.848
12	95.16	68.51	0.0764	69.05	0.915
13	110.44	64.69	0.0931	72.89	0.746
14	110.44	68.18	0.0876	79.49	0.694
15	110.44	68.84	0.0876	80.79	0.694
16	110.44	77.80	0.0722	99.88	0.570
17	82.37	100.14	0.0368	119.90	0.518
18	95.16	98.69	0.0428	134.60	0.452
19	110.44	96.24	0.0512	148.70	0.402
20	82.37	118.01	0.0279	167.29	0.391
21	95.16	115.19	0.0331	183.85	0.347
22	110.44	115.62	0.0382	215.02	0.298
23	82.37	138.76	0.0205	235.73	0.285
24	95.16	139.26	0.0242	274.47	0.252
25	110.44	131.07	0.0321	279.75	0.249

Table 11. Isothermal pressure drop results for ethylene glycol with metal tube

Run	$\dot{m}$ $\left(\frac{lbm}{hr}\right)$	T_b $\left(^oF\right)$	Δp $\left(psi\right)$	Re	f_o
1	24.95	75.50	0.0335	22.36	2.766
2	41.21	73.91	0.0550	35.58	1.663
3	41.21	79.65	0.0470	40.63	1.420
4	56.50	71.17	0.0792	45.69	1.276
5	56.50	74.16	0.0754	49.07	1.214
6	70.36	73.11	0.0969	59.59	1.006
7	82.37	68.01	0.1220	61.68	0.926
8	56.50	85.60	0.0568	63.57	0.911
9	82.37	71.10	0.1178	66.50	0.893
10	82.37	73.23	0.1164	69.98	0.882
11	95.16	70.60	0.1388	75.90	0.789
12	95.16	73.20	0.1355	80.78	0.769
13	82.37	83.56	0.0904	88.62	0.682
14	110.44	73.06	0.1537	93.44	0.648
15	110.44	74.78	0.1523	97.30	0.641
16	110.44	85.71	0.1160	124.56	0.487
17	82.37	108.15	0.0536	146.16	0.401
18	82.37	119.50	0.0452	179.45	0.337
19	110.44	105.48	0.0745	186.31	0.310
20	110.44	115.16	0.0633	222.82	0.263

Table 12. Nonisothermal pressure drop results for ethylene glycol with glass tube

Run	$\dot{m}$	$\bar{q}''_i$	T_b	$\bar{T}_{w,i}$	Δp	Re	f	f/f_o	Ra
	$\left(\frac{lbm}{hr}\right)$	$\left(10^3 \frac{Btu}{hr\text{-}ft^2}\right)$	$\left(^oF\right)$	$\left(^oF\right)$	$\left(psi\right)$				$\left(10^5\right)$
1	95.16	0.8829	69.92	93.71	0.0577	71.46	0.7005	0.8797	0.4980
2	95.16	1.1352	71.21	99.99	0.0555	73.73	0.6734	0.8688	0.6234
3	110.44	1.2613	69.23	100.77	0.0657	81.51	0.5919	0.8328	0.6483
4	82.37	1.2613	71.40	102.62	0.0468	64.11	0.7585	0.8742	0.6797
5	95.16	1.5136	72.91	108.65	0.0515	76.78	0.6240	0.8336	0.8097
6	82.37	1.6397	72.27	110.44	0.0432	65.46	0.6988	0.8139	0.8503
7	82.37	2.1442	74.88	121.38	0.0396	69.62	0.6409	0.7870	1.1086
8	110.44	2.5226	73.37	126.48	0.0544	90.09	0.4901	0.7511	1.2176
9	82.37	2.5226	77.20	129.40	0.0393	73.48	0.6354	0.8173	1.3207
10	82.37	3.0271	78.78	138.58	0.0352	76.20	0.5687	0.7548	1.5745
11	110.44	3.5317	76.86	144.90	0.0492	97.75	0.4421	0.7269	1.7066
12	82.37	3.5317	80.67	147.63	0.0348	140.30	0.5624	0.7744	1.8482
13	82.37	4.0362	82.64	156.28	0.0317	83.11	0.5111	0.7309	2.1338
14	110.44	5.0452	80.72	169.18	0.0425	106.75	0.3813	0.6762	2.4447
15	82.37	5.0452	85.66	172.25	0.0299	88.81	0.4825	0.7304	2.6997
16	110.44	6.5588	8575	192.00	0.0382	119.29	0.3420	0.6674	3.3196
17	82.37	6.0543	90.62	188.48	0.0269	98.76	0.4328	0.7180	3.4312
18	82.37	7.5679	95.74	209.98	0.0243	109.77	0.3898	0.7082	4.5051
19	110.44	8.5769	92.29	219.97	0.0334	137.11	0.2988	0.6573	4.6536

Table 13. Nonisothermal pressure drop results for ethylene glycol with metal tube

Run	$\dot{m}$	$\bar{q}''_i$	T_b	$\bar{T}_{w,i}$	Δp	Re	f	f/f_o	Ra
	$\left(\frac{lbm}{hr}\right)$	$\left(10^3 \frac{Btu}{hr\text{-}ft^2}\right)$	$\left(^oF\right)$	$\left(^oF\right)$	$\left(psi\right)$				$\left(10^5\right)$
1	82.37	0.8012	74.01	95.46	0.0881	71.27	0.6954	0.8125	0.4383
2	95.16	0.7989	75.05	96.33	0.1025	84.39	0.6055	0.8376	0.4466
3	56.50	0.8165	77.54	98.85	0.0572	53.08	0.9577	0.8333	0.4766
4	110.44	0.8321	74.51	96.50	0.1188	96.69	0.5213	0.8264	0.4552
5	82.37	1.2167	75.68	104.53	0.0804	74.11	0.6337	0.7699	0.6155
6	82.37	1.6320	79.54	114.54	0.0742	80.99	0.5841	0.7756	0.8232
7	95.16	1.6150	81.11	115.54	0.0863	96.95	0.5089	0.8089	0.8421
8	82.37	1.9943	80.74	121.01	0.0701	83.22	0.5515	0.7524	0.9759
9	95.16	2.4275	83.19	129.07	0.0776	101.55	0.4572	0.7611	1.1811
10	110.44	2.4283	82.10	128.27	0.0950	115.04	0.4156	0.7838	1.1572
11	82.37	2.6674	83.99	132.94	0.0637	89.47	0.5012	0.7351	1.2859
12	56.50	2.4174	89.15	133.52	0.0446	68.62	0.7446	0.8376	1.3174
13	82.37	3.1703	89.52	143.50	0.0604	100.82	0.4739	0.7833	1.6170
14	110.44	4.0192	89.18	153.47	0.0806	134.21	0.3521	0.7746	1.9104
15	82.37	3.9303	91.75	154.19	0.0558	105.66	0.4375	0.7578	1.9702
16	56.50	3.9969	101.02	161.34	0.0333	87.43	0.5533	0.7931	2.3454
17	110.44	5.5402	95.77	174.44	0.0694	153.90	0.3024	0.7628	2.7214
18	95.16	6.2153	101.31	184.56	0.0530	148.12	0.3101	0.7529	3.2581
19	82.37	6.2417	105.13	187.14	0.0442	138.02	0.3449	0.7804	3.4862
20	56.50	5.4628	111.42	183.69	0.0284	106.53	0.4695	9.8198	3.5085
21	110.44	6.9811	101.19	191.89	0.0576	171.49	0.2502	0.7035	3.5401
22	95.16	6.9316	103.80	192.91	0.0502	155.45	0.2938	0.7487	3.6813
23	82.37	7.7173	112.04	204.86	0.0397	157.07	0.3090	0.7956	4.5643
24	95.16	8.4514	110.53	210.49	0.0453	176.40	0.2644	0.7650	4.7638

XIII. BIBLIOGRAPHY

1. Sabersky, R. H. "Heat Transfer in the Seventies." International Journal of Heat and Mass Transfer 14 (1971): 1927-49.

2. Porter, J. E. "Heat Transfer at Low Reynold Number (Highly Viscous Liquids in Laminar Flow), Industrial Research Fellow Report." Trans. IChE 49 (1971): 1-29.

3. Hallman, R. M. "Experimental Study of Combined Forced and Free Laminar Convection in a Vertical Tube." NASA TN D-1104 (1961).

4. Graetz, L. "Über die Wärmeleitungsfähigkeit von Flüssigkeiten." Ann. d. Physik 18 (1883): 79-94.

5. Siegel, R.; Sparrow, E. M.; and Hallman, T. M. "Steady Laminar Heat Transfer in a Circular Tube with Prescribed Wall Heat Flux." Applied Scientific Research 7, Section A (1958): 386-92.

6. Morton, B. R. "Laminar Convection in Uniformly Heated Horizontal Pipes at Low Rayleigh Numbers." Quarterly Journal of Mechanics and Applied Mathematics 12 (1959): 410-20.

7. Iqbal, M. and Stachiewicz, J. W. "Influence of Tube Orientation on Combined Free and Forced Laminar Convection Heat Transfer." Journal of Heat Transfer 88 (1966): 109-6.

8. Iqbal, M. "Free-Convection Effects Inside Tubes of Flat-Plate Solar Collectors." Solar Energy 10 (1966): 207-11.

9. Faris, G. N. and Viskanta, R. "An Analysis of Laminar Combined Forced and Free Convection Heat Transfer in a Horizontal Tube." International Journal of Heat and Mass Transfer 12 (1969): 1295-1309.

10. Mikesell, R. D. "The Effect of Heat Transfer on the Flow in a Horizontal Pipe." Ph.D. dissertation, University of Illinois, 1963.

11. Siegwarth, D. P.; Mikesell, R. D.; Readal, T. C.; and Hanratty, T. J. "Effect of Secondary Flow on the Temperature Field and Primary Flow in a Heated Horizontal Tube." International Journal of Heat and Mass Transfer 12 (1969): 1535-52.

12. Mori, Y., and Futagami, K. "Forced Convective Heat Transfer in Uniformly Heated Horizontal Tubes, 2nd Report--Theoretical Study." International Journal of Heat and Mass Transfer 10 (1967): 1801-13.

13. Hwang, G. J., and Cheng, K. C. "Boundary Vorticity Method for Convective Heat Transfer with Secondary Flow--Application to the Combined Free and Forced Laminar Convection in Horizontal Tubes." Heat Transfer 1970 4, Paper No. NC3.5. Amsterdam: Elsevier Publishing Company, 1970.

14. Cheng, K. D.; Hwang, G. J.; and Akiyama, M. "On a Simple Correlation for Prandtl Number Effect on Forced Convective Heat Transfer with Secondary Flow." International Journal of Heat and Mass Transfer 15 (1972): 172-5.

15. Newell, P. H., Jr., and Bergles, A. E. "Analysis of Combined Free and Forced Convection for Fully Developed Laminar Flow in Horizontal Tubes." Journal of Heat Transfer 92 (1970): 83-89.

16. Siegwarth, D. P., and Hanratty, T. J. "Computational and Experimental Study of the Effect of Secondary Flow on the Termperature Field and Primary Flow in a Heated Horizontal Tube." International Journal of Heat and Mass Transfer 13 (1970): 27-42.

17. Ede, A. J. "The Heat Transfer Coefficient for Flow in a Pipe." International Journal of Heat and Mass Transfer 4 (1961): 105-10.

18. McComas, S. T., and Eckert, E. R. G. "Combined Free and Forced Convection in a Horizontal Circular Tube." Journal of Heat Transfer 88 (1966): 147-53.

19. Mori, Y.; Futagami, K.; Tokuda, S.; and Nakamura, M. "Forced Convective Heat Transfer in Uniformly Heated Horizontal Tubes, 1st Report-Experimental Study on the Effect of Buoyancy." International Journal of Heat and Mass Transfer 12 (1969): 1535-52.

20. Petukhov, B. S., and Polyakov, A. F. "Experimental Investigation of Viscogravitational Fluid Flow in a Horizontal Tube." High Temperature 5 (1967): 75-81.

21. Petukhov, B. S., and Polyakov, A. F. "Effect of Free Convection on Heat Transfer During Forced Flow in a Horizontal Pipe." High Temperature 5 (1967): 348-51.

22. Petukhov, B. S.; Polyakov, A. F.; and Strigin, B. K. "Heat Transfer in Tubes with Viscous-gravity Flow." Heat Transfer-Soviet Research 1 (1969): 24-31.

23. Shannon, R. L., and Depew, C. A. "Combined Free and Forced Laminar Convection in a Horizontal Tube with Uniform Heat Flux." Journal of Heat Transfer 90 (1968): 353-7.

24. Shannon, R. L., and Depew, C. A. "Forced Laminar Flow Convection in a Horizontal Tube with Variable Viscosity and Free-Convection Effects." Journal of Heat Transfer 91 (1969): 251-8.

25. Hussain, N. A., and McComas, S. T. "Experimental Investigation of Combined Convection in a Horizontal Circular Tube with Uniform Heat Flux." Heat Transfer 1970 4, Paper No. NC3.4. Amsterdam: Elsevier Publishing Company, 1970.

26. Lichtarowicz, A. "Combined Free and Forced Convection Effects in Fully Developed Laminar Flow in Horizontal Tubes." Heat and Mass Transfer by Combined Forced and Free Convection, Paper No. C114/71. London: Institution of Mechanical Engineers, 1972.

27. Bergles, A. E., and Simonds, R. R. "Combined Forced and Free Convection for Laminar Flow in Horizontal Tubes with Uniform Heat Flux." International Journal of Heat and Mass Transfer 14 (1971): 1989-2000.

28. del Casal, E., and Gill, W. N. "A Note on Natural Convection Effects in Fully Developed Horizontal Tube Flow." AIChE Journal 8 (1962): 570-4.

29. Iqbal, M., and Stachiewicz, J. W. "Variable Density Effects in Combined Free and Forced Convection in Inclined Tubes." International Journal of Heat and Mass Transfer 10 (1967): 1625-9.

30. Sparrow, E. M., and Lin, S. H. "Turbulent Heat Transfer in a Tube with Circumferential Varying Temperature or Heat Flux." International Journal of Heat and Mass Transfer 6 (1963): 866-7.

31. Rapier, A. C. "Forced Convection Heat Transfer in a Circular Tube with Non-Uniform Heat Flux Around the Circumference." International Journal of Heat and Mass Transfer 15 (1972): 527-37.

32. Reynolds, W. C. "Heat Transfer to Fully-Developed Laminar Flow in a Circular Tube with Arbitrary Circumferential Heat Flux." Journal of Heat Transfer 82 (1960): 108-12

33. Reynolds, W. C. "Turbulent Heat Transfer in a Circular Tube with Variable Circumferential Heat Flux." International Journal of Heat and Mass Transfer 6 (1963): 445-54.

34. Luikov, A. V.; Martynenko, O. G.; and Kolpashchikov, V. L. "Prediction of Local Heat Transfer in Compact Tubular Heat Exchangers with Various Body Forces." Paper presented at the 1972 International Seminar, Trogir, Yugaslavia, August 30 - September 6, 1972.

35. Luikov, A. V.; Aleksashenko, V. A.; and Aleksashenko, A. A. "Analytical Methods of Solution of Conjugated Problems in Convective Heat Transfer." International Journal of Heat and Mass Transfer 14 (1971): 1047-56.

36. Colburn, A. P. "A Method of Correlating Forced Convection Heat Transfer Data and a Comparison with Fluid Friction." Trans. AIChE 29 (1933): 174-210.

37. Sieder, E. N., and Tate, G. E. "Heat Transfer and Pressure Dorp of Liquids in Tubes." Industrial and Engineering Chemistry 28 (1936): 1429-35.

38. Deissler, R. G. "Analytical Investigation of Fully Developed Laminar Flow in Tubes with Heat Transfer with Fluid Properties Variable Along the Radius." NACA TN 2410 (1951).

39. Fand, R. M., and Keswani, K. K. "The Influence of Property Variation on Forced Convection Heat Transfer to Liquids." International Journal of Heat and Mass Transfer 15 (1972): 1515-36.

40. Iqbal, M.; Aggarwala, B. D.; and Khatry, A. K. "On the Conjugate Problem of Laminar Combined Free and Forced Convection Through Vertical Non-Circular Ducts." Journal of Heat Transfer 94 (1972): 52-6.

41. Shah, R. K., and London, A. L. "Thermal Boundary Conditions for Laminar Duct Flow Forced Convection Heat Transfer." ASME Paper No. 72-WA/HT-54 (1972).

42. Mischke, C. R., and Hall, J. L. "Computer Subroutine ME0226." Iowa Cadet Algorithm, Mechanical Engineering Department, Iowa State University, 1972.

43. A.S.M.E. Steam Tables. New York: Author, 1967.

44. Curme, G. O., Jr., and Johnston, F., eds. Glycols. New York: Reinhold Publishing Corporation, 1952.

45. Union Carbide Corporation. Glycols. New York: Author, 1971.

46. McAdams, W. H. Heat Transmission. New York: McGraw-Hill Book Company, Inc., 1954.

47. Hildebrand, F. B. Advanced Calculus for Applications. Englewood Cliffs, New Jersey: Prentice-Hall, Inc., 1962.

48. Hildebrand, F. B. Introduction to Numerical Analysis. New York: McGraw-Hill Book Company, Inc., 1956.

49. Black, A. W., and Sparrow, E. M. "Experiments on Turbulent Heat Transfer in a Tube with Circumferentially Varying Thermal Boundary Conditions." Journal of Heat Transfer 89 (1967): 258-68.